eman ta zabal zazu

Universidad del País Vasco
Euskal Herriko Unibertsitatea

Departamento de Ingeniería de Comunicaciones
Komunikazioen Ingenieritza Saila
Department of Communications Engineering

Ph.D. Thesis

Human Exposure to Electromagnetic Fields from WLANs and WBANs in the 2.4 GHz Band

Author: Marta Fernández Andrés

Supervisors: Dra. Amaia Arrinda Sanzberro
Dr. Iván Peña Valverde

May 2018

Human Exposure to Electromagnetic Fields from WLANs and WBANs in the 2.4 GHz Band.

Resumen en castellano.

Introducción

En los últimos años, el masivo crecimiento de las comunicaciones inalámbricas ha incrementado la preocupación acerca de la exposición humana a los campos electromagnéticos debido a los posibles efectos sobre la salud. Esta tesis surge de la necesidad de proporcionar información acerca de este tipo de exposición. Se requiere un mayor conocimiento acerca de las emisiones de radiofrecuencia por dos motivos: para asegurar la protección humana frente a dichas emisiones, pero sin reducir los beneficios de la tecnología debido a normativas de despliegue excesivamente restrictivas, y para dar respuesta a la preocupación pública que normalmente está acentuada por la falta de conocimiento.

La exposición a campos electromagnéticos causada tanto por los dispositivos de usuario como por las estaciones base se evalúa generalmente para comprobar el cumplimiento con la regulación vigente. Dado que la medida de la exposición en campo cercano es compleja, y en algunos casos inviable, las señales de radiofrecuencia se miden normalmente en la región de campo lejano para evaluar los niveles de exposición en distintos entornos. Sin embargo, para validar los dispositivos de usuario es esencial la evaluación de la exposición en campo cercano. En esta tesis se ha estudio la exposición humana a emisiones de radiofrecuencia en ambas regiones.

Uno de los principales inconvenientes cuando se miden señales en el campo lejano se debe a la falta de un procedimiento estandarizado para la toma de muestras de campos electromagnéticos, especialmente agravado cuanto se trata de señales transmitidas en forma de ráfagas, como es el caso del WiFi, ya que la instrumentación de medida puede tener gran influencia en los resultados. Esta tesis incluye una nueva metodología de medida para evaluar la exposición debida a este tipo de señales.

Por otra parte, uno de los aspectos claves a considerar a la hora de diseñar dispositivos que transmiten señales cerca del cuerpo es la interacción entre el cuerpo y la antena. En esta tesis se presentan dos antenas 'wearables' adecuadas

para reducir dicha interacción, junto con un análisis detallado de la potencia absorbida por el cuerpo humano debido a estas antenas.

En general, el objetivo de este trabajo consiste en presentar varias soluciones para mejorar la evaluación de la exposición a campos electromagnéticos, así como aumentar el conocimiento en cuanto a niveles de exposición. Para realizar esta investigación se han seleccionado dos tipos de fuentes de radiación, en la región de campo lejano se han estudiado las señales WiFi transmitidas en redes de área local inalámbricas y se han seleccionado las antenas 'wearables' como dispositivos transmitiendo en campo cercano.

Objetivos

Teniendo en cuenta la necesidad de aumentar el conocimiento en el área de la evaluación de la exposición a campos electromagnéticos, así como las carencias e inconvenientes detectados en los procedimientos de medida, evaluación o diseño de dispositivos orientados a reducir la potencia absorbida por el cuerpo, se plantea una serie de objetivos para esta tesis. Más concretamente, este trabajo está basado en el análisis de señales procedentes de dos tipos de fuentes de radiación: dispositivos 'wearables' adecuados para formar parte de redes de área corporales inalámbricas (WBANs, del inglés *Wireless Body Area Networks*), y señales WiFi transmitidas en redes de área local inalámbricas (WLANs, del inglés *Wireless Local Area Networks*), todas ellas transmitiendo en la banda de frecuencias de 2.4 GHz. Como la evaluación de la exposición electromagnética se realiza de manera diferente en función de la región de campo en la que se haga el estudio, los objetivos de este trabajo se pueden agrupar en dos partes:

1) Exposición en la región de campo lejano:

En esta región de campo, se han analizado las señales WiFi y se propone como finalidad la obtención de una metodología de medida que permita estimar con exactitud los niveles de exposición a señales WiFi en WLANs, así como contribuir a aumentar el conocimiento de los niveles de radiación producidos por este tipo de señales. Los objetivos parciales para lograr dicha finalidad se mencionan a continuación:

- Identificar inconvenientes y beneficios de metodologías de medida existentes y, en base a ello, seleccionar la instrumentación más apropiada para adquirir muestras de señal WiFi que permitan obtener niveles de campos electromagnéticos precisos en todo momento.

- Caracterizar las señales WiFi en la banda de 2.4 GHz en diferentes situaciones, en el dominio del tiempo y de la frecuencia.
- Definir el procedimiento adecuado y los criterios seguidos para establecer la configuración del equipo de medida, así como determinar y validar la metodología de medición de señales WiFi basada en dicha configuración.
- Evaluar detalladamente la exposición de este tipo de señales en el interior de entornos públicos. Para ello se deben definir las campañas de medida basadas en el procedimiento previamente establecido. Una vez tomadas las muestras, se deben examinar con detalle y seleccionar los estadísticos adecuados para presentar los resultados.
- Comparar los niveles obtenidos en estas campañas de medida con los adquiridos por otros autores, para ello es necesaria una búsqueda bibliográfica en la literatura científica.

2) Exposición en la región de campo cercano:

En la región de campo cercano se ha realizado una evaluación exhaustiva de la potencia absorbida por el cuerpo humano debido a dos tipos de antenas 'wearables'. Además, se han convertido los valores de medidas de WiFi realizadas en la región de campo lejano a niveles en campo cercano, pudiendo comparar de este modo las diferentes fuentes de radiación. Los objetivos parciales de esta segunda parte del estudio se detallan a continuación:

- Diseñar antenas 'wearables' apropiadas para formar parte de una WBAN, de manera que la potencia radiada en el cuerpo sea la mínima posible.
- Fabricar las antenas y validarlas colocándolas en el cuerpo de personas reales. Analizar el efecto de las antenas en el cuerpo, así como el efecto del cuerpo en el funcionamiento de la antena.
- Llevar a cabo un análisis detallado, basado en simulaciones, de la potencia absorbida en el cuerpo humano. Para ello, seleccionar diferentes modelos de cuerpo y realizar las simulaciones con las antenas colocadas en diversas partes del cuerpo.
- Convertir los valores obtenidos de las medidas WiFi a valores en campo cercano y comparar éstos con los valores obtenidos en las simulaciones de las antenas.

Principales contribuciones de la tesis

Las contribuciones de esta tesis dan respuesta a los objetivos previamente definidos. En este apartado se resumen las contribuciones más relevantes de este trabajo de investigación:

- **Establecer una metodología de medición apropiada para obtener niveles de señal WiFi precisos en todo momento.**

Esta aportación se recoge en el tercer capítulo de la tesis. El primer paso para determinar la metodología de medida consiste en definir la configuración adecuada del analizador de espectros. Para ello se definió un procedimiento que consiste en tres fases: adquisición de niveles de referencia, estudio de la influencia de los parámetros del analizador en los valores medidos e identificación de la configuración óptima de medida. La Tabla 1 muestra las configuraciones del analizador de espectros seleccionadas como las más adecuadas para la toma de muestras en un canal y en toda la banda WiFi de 2.4 GHz.

Tabla 1. Configuración del analizador de espectros para realizar medidas en un canal y en toda la banda WiFi de 2.4GHz.

Parameter	Value One channel	Value 2.4 GHz WiFi band
f_c	Central frequency of the channel	2441.75 MHz
Span	20 MHz	83.5 MHz
RBW	0.3 MHz	1 MHz
VBW	1 MHz	3 MHz
SWT	2.5 ms	2.5 ms
SWP	501 points	501 points
Detector	RMS	RMS
Trace Mode	clear/write	clear/write

A partir de estas configuraciones, se detalla en el capítulo 3 de la tesis la metodología de medida de exposición a señales WiFi.

- **Evaluar la exposición a señales WiFi en un entorno público interior.**

Utilizando la metodología definida en el punto anterior, se realizaron campañas de medida para estimar la evaluación a este tipo de exposición en diferentes lugares dentro de la Universidad del País Vasco UPV/EHU. Estas

tareas y los resultados correspondientes están especificados en el capítulo 4 de esta tesis doctoral. Se realizó un análisis de los estadísticos adecuados para describir la exposición a señales WiFi en la banda de 2.4 GHz y su variabilidad espacial y temporal. Además, se realizó una comparación con los niveles obtenidos en otras campañas de medida. Dicha comparación se muestra en la Tabla 2.

Tabla 2. Niveles de campo eléctrico (V/m) obtenidos en diferentes campañas de medida

Ref	***Mean***	***Median***	***Range***	***Description***
(Sagar 2018)	0.01-0.03	-	-	Eme Spy 201 ExpoM-RF
(Joseph 2010a)	0.019-0.082	-	-	Eme Spy 120/ 121
(Joseph 2010c)	0.020	-	0.006-0.1	Weighting factor
(Röösli 2008) ROS	0.05	0.02	NA-0.23	Eme Spy 120
(Röösli 2008) Naïve	0.06	0.05	0.05-0.22	Eme spy 120
(Karipidis 2017)	0.060-0.114	-	-	Radiation Meter
(Tomitsch 2015)	0.077-0.118	0.000-0.013	-	Max-hold
Our work	0.005	0.005*	0.004-0.408	Analyzer 24 h
Our work	0.005	0.005*	0.005*-0.269	Analyzer 1 h
Our work	0.031	0.029	0.005-0.242	Eme Spy 200 1 h

* The calculated values were between 0.0045 and 0.0049 V/m, but when rounding to the nearest third decimal a value of 0.005 V/m was set.

- **Diseño e implementación de dos antenas 'wearables'.**

En el capítulo 5 de esta tesis se detalla el proceso de diseño y fabricación de ambas antenas. Una de ellas está diseñada para su uso en comunicaciones entre el cuerpo y un dispositivo exterior (off-body) y la otra consiste en una antena que se coloca en el cuerpo humano y puede comunicarse con un dispositivo situado en el interior (in-body). Ambas antenas fueron diseñadas con el objetivo de reducir la interacción entre el cuerpo y la antena. El diseño en 3D de las antenas se puede ver en la Figura 1. A la izquierda se encuentra el modelo diseñado para comunicaciones 'off-body', siendo las dimensiones de esta antena 56×33×11 mm. A partir de este diseño se obtuvo la antena apropiada para comunicaciones 'in-body', ésta tiene un tamaño menor, siendo sus dimensiones 33×33×11 mm. Como se observa, ambas tiene una ranura por donde se genera la mayor parte de la radiación. En el caso de la antena 'in-body', esta ranura estará en contacto con la piel.

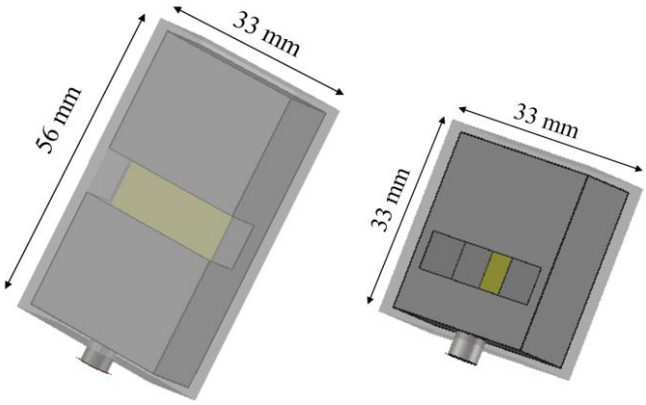

Figura 1. Modelos de antenas diseñadas en esta tesis. Una de ellas diseñada para comunicaciones 'off-body' (izquierda), y la otra para comunicaciones 'in-body' (derecha).

Ambas antenas fueron fabricadas y su funcionamiento se validó cuando estaban colocadas en diferentes posiciones del cuerpo de personas reales.

- **Análisis de la exposición en campo cercano**

El capítulo 6 de esta tesis muestra la evaluación de la exposición realizada en la región de campo cercano. Primero se llevó a cabo el análisis de la potencia absorbida y de la Tasa de Absorción Específica (SAR, del inglés *Specific Absorption Rate*) debido a las dos antenas previamente mostradas. Para ello se realizaron diversas simulaciones seleccionando un modelo de cuerpo de mujer y otro de hombre. Finalmente, se convirtieron niveles obtenidos en medidas WiFi a valores en capo cercano, concretamente se calcularon niveles de SAR_{WB} del inglés, Whole-body SAR, que se refiere a la potencia absorbida por el cuerpo dividida por la masa de éste. Para realizar esta conversión se realizó una búsqueda en la literatura científica y se eligieron tres métodos definidos por diferentes autores. De manera que las diferencias debidas a la utilización de un método u otro fueron analizadas. También se calcularon estos resultados para los valores de potencia más altos obtenidos para cada una de las antenas 'wearables'. Los resultados obtenidos en el campo cercano pueden verse en la Tabla 3.

Tabla 3. Niveles de SARWB (nW/kg) calculados a partir de las medidas de WiFi en cammpo lejano y obtenidos a partir de las simulaciones de las antenas 'wearables'.

SAR_{WB} (nW/kg)								
		Converted data from EMF measurements						
		Method 1	**Method 2**				**Method 3**	
	Position	**10 kg**	**10 kg**	**70 kg**	**DMC 10 kg**	**DMC 70 kg**	**10 kg**	**70 kg**
Lab 1	1	31.49	20.84	9.59	31.68	14.57	21.07	11.84
	2	40.61	26.87	12.36	64.50	29.67	27.17	15.26
	3	31.96	21.15	9.73	25.38	11.67	21.38	12.01
	4	31.72	20.99	9.66	41.98	19.31	21.22	11.92
	5	24.88	16.47	7.57	35.57	16.36	16.65	9.35
Classroom 1	5	553	366	184	556	280	370	208
Lab 2	Morning	9.89	6.54	3.01	9.95	4.58	6.62	3.72
	Afternoon	5.18	3.42	1.58	5.21	2.39	3.46	1.95
	Night	2.91	1.92	0.88	2.92	1.34	1.94	1.09
Wearable antennas								
Off-Body Max Level		$61.42 \cdot 10^3$						
In-Body Max Level		$115.30 \cdot 10^3$						

eman ta zabal zazu

Universidad del País Vasco
Euskal Herriko Unibertsitatea

Departamento de Ingeniería de Comunicaciones
Komunikazioen Ingenieritza Saila
Department of Communications Engineering

Ph.D. Thesis

Human Exposure to Electromagnetic Fields from WLANs and WBANs in the 2.4 GHz Band

Author: Marta Fernández Andrés

Supervisors: Dra. Amaia Arrinda Sanzberro
Dr. Iván Peña Valverde

May 2018

A mi madre, gracias por todo.

Después de estos años de doctorado que se han pasado volando, ya estoy delante de la última hoja que me queda de escribir, que es a la vez, la hoja en blanco del documento que más tiempo he estado mirando.

En primer lugar me gustaría dar las gracias a Iratxe y Amaia, con quienes empecé en este mundo de la investigación y quienes tienen gran parte de culpa de que decidiera seguir. Gracias Amaia por haberme dado esta oportunidad y haber hecho que este camino sea tan ameno.

Gracias Iván y David por todo vuestro esfuerzo y ayuda durante la realización de esta tesis.

En realidad, tengo que agradecer a todos los miembros de TSR por haberme ofrecido esta oportunidad de poder realizar la tesis y pasar los momentos que ello conlleva, muchas gracias.

Empezando con mis compañeros del laboratorio, las que ya no están Cris, Laura, Jon B. muchas gracias por vuestra ayuda y buenos ratos fuera y dentro de la Uni, se os echa de menos. A Itzi y Jon M., donde quienes acudo para resolver cualquier duda, ya sea de la tesis o de la vida ;-), gracias por todos vuestros valiosos consejos. Gracias Bea por las conversaciones y ratillos de desconexión, y a Iker, quien siempre aporta un toque de humor. Teresa, muchas gracias por toda tu ayuda, no sé qué haríamos por aquí arriba sin ti. Gracias Unai, aunque ya no estás por aquí arriba, gracias por los buenos momentos que seguimos teniendo en los cafés. A Eneko, aunque últimamente coincidimos menos, mucho ánimo que igual en unos añitos estás tú en esta situación, aprovecha el tiempo que pasa muy rápido! A Christopher, gracias por la compañía en el despacho y espero que te sea útil esta tesis!

Muchas gracias al resto de profesores de TSR, porque todos me habéis ayudado en algún momento y de todos he podido aprender algo nuevo. Gracias a Pablo, David de la Vega, Igor, Iñaki, Manolo y Juan Luis.

Thanks to all my workmates at Griffith University, because they helped me a lot, made me feel at home and because of all the good moments we had in and outside the lab. Specially, thanks to David and Hugo for giving me the opportunity to work there and learn from you.

Gracias a mis amigos de Zurbaran, por los momentos que hemos pasado juntos… y los que están por venir! Gracias a Jani y Alba por todos los momentos vividos durante todos estos años.

También a los amigos que he hecho durante mis años de universidad, especialmente a 'Friends', que aunque cada vez es más difícil coincidir todos a la vez, sigue siendo genial pasar una tarde, mañana o noche con vosotros.

Gracias a mis padres y a mis hermanos, Sheila y Adrián, y gracias a Roberto, por haberme apoyado y ayudado y por el esfuerzo que habéis hecho por mí.

A Alvaro, gracias por estar siempre ahí. Unas líneas se quedan cortas para agradecerte todo lo que siento, gracias por ser como eres.

Summary

In the last years, the massive growth of wireless communications has raised concerns about human exposure to electromagnetic fields due to possible adverse health effects. This thesis arose from the need of providing scientific information regarding this type of exposure. A wider knowledge about radiofrequency emissions is necessary because of two main reasons, ensure people protection against these emissions, but without reducing the benefits of technology due to overly restrictive deployment policies, and give response to public concern, which is usually caused due to the lack of knowledge.

Exposure to electromagnetic fields from both user devices and base stations is usually assessed in order to check compliance with regulations. As the assessment of exposure in the near field is complex and in some cases infeasible, radiofrequency signals are usually measured in the far field region for assessing exposure levels in different environments. However, in order to validate user devices, near field exposure assessment is essential. In this thesis human exposure to radiofrequency emissions in the two regions has been studied.

When measuring signals in the far field region, one of the main drawbacks is the lack of a standardized procedure for taking samples of electromagnetic field levels. This is especially problematic in the case of signals transmitted in the form of bursts or pulses, such as in the case of WiFi, because the measurement instrumentation can have huge influence on the results. This thesis includes a novel measurement methodology for assessing exposure due to WiFi signals, as well as an evaluation of exposure levels due to these signals.

Moreover, one of the key aspects to consider when designing devices that operate close to the body is the interaction between the antenna and the human body. In this thesis, two different wearable antennas appropriate for reducing that interaction are presented, and a comprehensive analysis of the power absorbed in the human tissues has been conducted.

The main objective of this work is to present several solutions for improving exposure assessment, as well as enhance knowledge regarding electromagnetic field exposure levels. Specifically, two types of radiation sources were selected for the research, WiFi signals from Wireless Local Area Networks as sources in the far field region and wearable antennas as devices transmitting in the near field.

Resumen

En los últimos años, el masivo crecimiento de las comunicaciones inalámbricas ha incrementado la preocupación acerca de la exposición humana a los campos electromagnéticos debido a los posibles efectos sobre la salud. Esta tesis surge de la necesidad de proporcionar información acerca de este tipo de exposición. Se requiere un mayor conocimiento acerca de las emisiones de radiofrecuencia por dos motivos: para asegurar la protección humana frente a dichas emisiones, pero sin reducir los beneficios de la tecnología debido a normativas de despliegue excesivamente restrictivas, y para dar respuesta a la preocupación pública que normalmente está acentuada por la falta de conocimiento.

La exposición a campos electromagnéticos causada tanto por los dispositivos de usuario como por las estaciones base se evalúa generalmente para comprobar el cumplimiento con la regulación vigente. Dado que la medida de la exposición en campo cercano es compleja, y en algunos casos inviable, las señales de radiofrecuencia se miden normalmente en la región de campo lejano para evaluar los niveles de exposición en distintos entornos. Sin embargo, para validar los dispositivos de usuario es esencial la evaluación de la exposición en campo cercano. En esta tesis se ha estudio la exposición humana a emisiones de radiofrecuencia en ambas regiones.

Uno de los principales inconvenientes cuando se miden señales en el campo lejano se debe a la falta de un procedimiento estandarizado para la toma de muestras de campos electromagnéticos, especialmente agravado cuanto se trata de señales transmitidas en forma de ráfagas, como es el caso del WiFi, ya que la instrumentación de medida puede tener gran influencia en los resultados. Esta tesis incluye una nueva metodología de medida para evaluar la exposición debida a este tipo de señales.

Por otra parte, uno de los aspectos claves a considerar a la hora de diseñar dispositivos que transmiten señales cerca del cuerpo es la interacción entre el cuerpo y la antena. En esta tesis se presentan dos antenas 'wearables' adecuadas para reducir dicha interacción, junto con un análisis detallado de la potencia absorbida por el cuerpo humano debido a estas antenas.

En general, el objetivo de este trabajo consiste en presentar varias soluciones para mejorar la evaluación de la exposición a campos electromagnéticos, así como aumentar el conocimiento en cuanto a niveles de exposición. Para realizar esta investigación se han seleccionado dos tipos de fuentes de radiación, en la región

de campo lejano se han estudiado las señales WiFi transmitidas en redes de área local inalámbricas y se han seleccionado las antenas 'wearables' como dispositivos transmitiendo en campo cercano.

Laburpena

Azken urte hauetan, hari gabeko komunikazioen hazkundea nabaria izan da eta jendea eremu elektromagnetikoen esposizioaz arduratuta dago, osasunerako efektu potentzialengatik. Tesi hau sortu da mota honetako esposizioari buruzko informazioa emateko beharragatik. Irrati frekuentziako emisioen ezaguera handiagoa izatea beharrezkoa da bi arrazoiengatik. Bata da teknologiaren abantailak murriztu gabe gizakiak eremu elektromagnetikoengatik babesteko. Bigarrena biztanleei zientzian oinarritutako erantzunak ematea da, modu honetan ardurak gutxitzeko.

Erabiltzaileek dauzkaten gailu elektronikoek, adibidez telefono mugikorrek, edo oinarri-estazioek eragiten dituzte irrati frekuentziako esposizioa. Normalean, eremu elektromagnetikoen esposizio mailak neurtzen dira, araudiak betetzen diren egiaztatzeko. Neurketa-prozedura desberdina da erradiazio-iturriak gizakiarengandik hurbil edo urrun badaude. Erradiazioa sortzen duten antenak hurbil badaude, zailagoa da eremu elektromagnetikoak neurtzea eta, batzuetan bideraezina da. Beraz, normalean esposizioaren estimazioa erradiazio-iturritik urrun egiten da. Teknika hauek oso baliagarriak dira eremu elektromagnetikoen mailak ezagutzeko. Hala ere, gailu batzuen erradiazioak estimatzeko, adibidez telefono mugikorren, tableten edo soinean eramateko gailuen (ingelesez, 'wearable devices'), hargailua gailuaren ondoan egon behar da. Tesi honetan, eremu elektromagnetikoen esposizioari buruzko ikerketa egin da bi egoeretetan erradiazio-iturritik urrun eta erradiazio-iturritik hurbil.

Eremu elektromagnetikoen mailak neurtzen direnean, arazo nagusietako bat neurri-metodologiarekin erlazionatuta dago. Nahiz eta araudi ofizial batzuk argitaratuta egon, ez dago metodologia zehatz bat esposizioa estimatzeko. Dokumentu ofizial hauek, azalpen orokorrak eta jarraibideak ematen dituzte, baina ezin dute prozesua zehatz-mehatz deskribatu, kasuaren arabera instrumentu edo metodo desberdinak behar direlako. Adibidez, pultsuz transmititzen diren seinaleak neurtzeko, instrumentuek neurketetan eragina daukatela kontuan izan behar da. Tesi honetan, WiFi seinaleak neurtzeko metodologia bat proposatzen da eta hari gabeko sare lokalek sortzen duten esposizio mailak neurtu dira.

Bestalde, gorputzaren ondoan jartzeko gailuak garatzen direnean, oso inportantea da gailuaren eta gorputzaren interakzioa ikertzea. Gorputzak gailuaren errendimendua murriztu ahal du eta bestalde gorputzean erradiatutako energiaren absortzioa kontuan hartu behar da ere. Tesi honetan gorputz-

hedadurako sare batean parte izan daitezken bi antena ‘wearable’- k aurkezten dira. , gailuaren eta gorputzaren interakzioa gutxitzeko oso egokiak direnak. Gainera, gorputzean energiaren absortzioari buruzko ikerketa ere egin da.

INDEX

FIGURE INDEX

TABLE INDEX

CHAPTER 1: INTRODUCTION AND THESIS OBJECTIVES

This chapter includes a brief introduction as well as the motivation and main objectives of this thesis. Also, the organization of the thesis contents is described in the last section.

1. INTRODUCTION

Human exposure to radiofrequency (RF) fields is nowadays a matter on the spotlight of our society due to the current massive use of this type of communications. Several standards and regulations have been defined by regulatory bodies to protect people against these emissions (ICNIRP 1998), (IEEE 2005). Some of these standards include limits for human exposure to electromagnetic fields (EMFs) and others provide guidance on the measurement methods and procedures that should be carried out in order to check compliance with the exposure limits. Data collection by means of robust methods is a need in order to quantify the exposure levels and its variability. The good knowledge of the exposure distribution can contribute to an efficient deployment of networks taking into account emissions levels.

Different types of sources of EMFs are present in everyday life, and the services provided by many of them have become essential for people, since they improve the quality of life of individuals. Figure 1.1 illustrates some of the most common sources of RF fields. As shown, some devices are transmitting close to the body, this is the case of mobile phones, tablets or wearable devices, such as smart watches.

Figure 1.1. Different sources of RF fields in everyday life.

Base stations are usually located at longer distances. For example, mobile communication base stations can be placed on the roof of a building and radio

or television transmitters can be located on the outskirts of a city or town. However, in the case of Wireless Local Area Networks (WLANs) using WiFi technology, the access points are situated at closer distances. In indoor environments, these transmitters are usually located inside buildings at few meters from people, or even closer. This is one of the main reasons why there is special concern about WiFi networks.

When assessing EMF exposure, it is important to note that the procedures for evaluating the emissions coming from transmitters in the vicinity of the human body (near field), such as devices that are part of Wireless Body Area Networks (WBANs), are different than those methods applied for sources located at further distances (far field), such as WiFi access points or other base stations.

The work developed during this thesis can be divided into two parts.

- The first one includes the tasks carried out for improving the assessment and analysis of EMF exposure in the far field region. Specifically, WiFi signals at 2.4 GHz were analyzed. For this purpose, several measurement campaigns were carried out.

- The second part of this thesis involves the tasks performed for improving the methods and knowledge in the near field. In this case, two wearable antennas working at 2.4 GHz were designed and the power absorbed in the body due to these devices was evaluated. The antennas were also fabricated to validate their performance on real humans. The evaluation of the power absorbed was done by means of simulations. In addition, measured WiFi electric field strength was converted to power absorbed in the body using different methods.

Finally, it is worth highlighting that the design of the antennas and the first works related to the evaluation of the power absorbed in the human body were performed during a research stay of 8 months at Griffith University in Brisbane, Australia, under the supervision of the Professor David V. Thiel. His experience and the support of his research group have been very valuable to obtain many of the results that will be described in the following chapters.

2. MOTIVATION

There is a need of providing scientific information regarding exposure to EMFs for two main reasons, ensure people's protection against these emissions but without reducing the technological benefits because of overly restrictive deployment policies, and give response to public concern, usually caused due to the lack of knowledge. In this regard, two types of studies regarding RF exposure are of interest, those aimed at characterizing RF emissions in specific scenarios and those based on quantify personal exposure due to different sources.

Although several standards and guidelines have been proposed with the objective of protecting people from potential adverse effects, several disparities can be found in different official documents. One of the main problems lies in the disagreements on the established exposure limitations and the second one, in the lack of a standardized procedure for evaluating exposure levels, necessary for checking compliance with regulations and for having more knowledge about this type of radiation.

In particular, the starting motivation of this thesis was to provide an alternative for the measurement methodologies used for measuring pulsed signals, since in the case of these emissions, substantial overestimation of the results is produced when applying usual measuring techniques. Specifically, the exposure to WiFi signals was investigated because of their nature, since they are transmitted in the form of pulses of short duration, and due to the public concern raised in the last years about WLANs.

The second part of the thesis is focused on the assessment of personal exposure due to devices emitting close to the body. In this part, special attention has been paid to consider exposure reduction when designing wearable antennas, obtaining final antenna models suitable for reducing the interaction between the human body and the antenna. These types of devices are part of emerging technologies and systems useful for contributing to the progress in many areas, such as in medical applications. However, several factors including the exposure to EMFs can slow down their deployment. For this reason, research into power absorption and distribution due to wearable antennas is indeed essential.

As, in general, emissions from base stations cause greater concern than signals from user devices, a comparison of the exposure levels produced by both types of sources was carried out to complete this thesis. Due to the different distance from each type of these sources to the people exposed, exposure levels are characterized using different quantities. Thus, a proper comparison has

required a literature review to investigate methods for converting WiFi signal levels to exposure values in terms of power absorbed, so as to compare the exposure levels produced by the different sources analyzed in this thesis. These methods can also be applicable to other technologies.

3. OBJECTIVES

The thesis aims to contribute to enhance the scientific knowledge of human exposure to EMFs in the 2.4 GHz frequency band. Specifically, two types of radiation sources were selected for the research, WiFi signals from WLANs as sources in the far field region and wearable antennas as devices transmitting in the near field. As the assessment of EMFs exposure differs significantly depending on the field region, the objectives can be grouped into two different areas:

Exposure in the far field region

The objectives about human exposure to WiFi signals are focused on determining the proper measurement methodology to accurately assess exposure in WLANs, as well as on contributing to enhance the knowledge of the EMF levels caused by this type of signals. Specifically, these objectives are:

- Establish a measurement methodology suitable for recording accurate and actual WiFi signal samples in the far field region. This methodology aims at improving the accuracy on the measured levels in comparison to the existing methodologies, saving measuring time and reducing the complexity of work of those new techniques that try to provide accurate levels. In order to define the proper methodology for acquiring WiFi signal samples, the following goals have to be achieved.

  - Identify the drawbacks and benefits from previous measurement methodologies.
  - Select the appropriate instrumentation that allows the acquisition of robust, accurate and actual signal levels in WLANs.
  - Characterize WiFi signals in different situations in the time and frequency domain, theoretically and by means of experimental tests.
  - Define the procedure to be followed and the criteria for establishing the proper configuration of the measurement equipment once it has been selected.
  - Determine and validate the measurement methodology based on the previously defined configuration.

- Assess human exposure to WiFi signals in public indoor environments, providing in this way specific information needed for enhancing scientific knowledge of EMF exposure.

  - Define the measurement campaigns based on the methodology previously proposed.
  - Perform the measurements of WiFi signal levels.
  - Examine in detail the obtained results and determine the appropriate statistics and criteria for presenting the values.
  - Assess WiFi exposure values, compare with the limitations given in the standards and regulations, and analyze the spatial and temporal variability of WiFi emissions in the selected environment.

Exposure in the near field region

The objectives related to human exposure assessment in the near field region are focused on the contribution towards understanding and gaining knowledge about radiation assessment and analysis from wearable antennas, as well as comparing these values with the exposure measurements in the far field region.

- Propose and implement wearable devices suitable for different applications while ensuring human protection against electromagnetic radiation. The antennas performance was analyzed through simulations and measurements, while the exposure evaluation was conducted by means of simulations.

  - Evaluate the literature review of the wearable antenna models in order to select suitable antenna designs for achieving the goal of satisfying user's demands while maintaining low power absorption.
  - Design antenna models and fabricate them in order to validate the designs on real human bodies. Analyze the effect of the antenna on the body together with the effect of the body on the antenna performance.

- Conduct a comprehensive study of the electromagnetic field absorption in human bodies.

  - Define the simulation scenarios appropriate for evaluating exposure levels due to wearable antennas, select suitable body models, measurement locations, exposure analysis parameters.

- Analyze exposure levels from wearable antennas and compare these results with those obtained from the WiFi measurements. To do that, a previous conversion from the recorded WiFi signal levels to near field values is required. A research of the methods proposed in the literature for undertaking this conversion has to be conducted.

4. THESIS ORGANIZATION

This thesis will provide technical solutions and knowledge for the assessment and analysis of human exposure to electromagnetic fields in both the near and far field regions.

This thesis is organized in 7 chapters. The second chapter shows the context of this work. Following, there are two chapters dedicated to the exposure in the far field region and another two focused on the exposure in the near field. Finally, the last chapter summarizes the main contributions of the thesis, the results dissemination and some future lines.

Chapter 1. A brief introduction to the topic of this thesis, the motivation and the main objectives of this work are explained in this first chapter.

Chapter 2. The context of the research is presented by means of a description of the regulations and standards involved in defining exposure limits and procedures for checking compliance with these limitations. A scientific literature review of studies related to exposure assessment is provided and finally, the two types of networks involved in this thesis are described (WLAN and WBAN).

Chapter 3. This chapter describes the drawbacks of the existing techniques for measuring WiFi signals in order to assess WiFi exposure levels. A new measurement methodology is proposed and the procedure followed to identify this methodology is described in detail.

Chapter 4. An evaluation of the WiFi exposure levels and its variability in an indoor public environment is presented. The measurement campaigns carried out to record the signal samples and the procedure for analyzing these data are described. Moreover, a comparison between WiFi levels acquired in different measurement campaigns is made.

Chapter 5. This chapter presents the design and fabrication of two different wearable antennas, one designed for its use in off-body applications and the other one suitable for in-body communications. An investigation of the power absorption in human tissues, as well as the body effect on antenna performance is presented.

Chapter 6. The evaluation and analysis of the power absorption in the human body due to the different studied sources are presented in this chapter. The EMF exposure caused by the two wearable antennas is studied by means of

simulations, while the power absorption due to WiFi signals was calculated from data acquired in the measurements. Specifically, the measurements in which the highest level of exposure was obtained were selected for these calculations together with new sets of measurements taken for this purpose.

Chapter 7. In this last chapter, the main contributions of the thesis are summarized, detailing the most relevant results. Furthermore, the results dissemination is presented and the identified future lines are provided.

Chapter 1

CHAPTER 2: STATE OF THE ART

This chapter includes the description of the research context of this thesis. A brief introduction and some basic concepts regarding EMF exposure are given. A description of the standards and studies related to exposure assessment are provided. Finally, some information about WLAN and WBAN is given.

1. INTRODUCTION

In the last years, the massive growth of wireless communications has raised concerns about human exposure to RF fields due to possible adverse health effects. In the year 2011, the International Agency for Research on Cancer (IARC) classified RF EMFs as possibly carcinogenic to humans (Group 2B), after the meeting of a Working Group of experts. This decision was based on a slight increase in the risk for glioma - a malignant type of brain cancer - among heavy users of wireless and cordless telephones. In the IARC report of 2014 they specified: "Associations between heavy use of mobile phones and certain brain cancers have been observed, but causal interpretation is controversial; more data are needed, particularly on longer-term use of mobile phones." In addition, based on the information and literature analyzed in that meeting, the above mentioned Working Group decided not to limit the RF EMFs evaluation to the frequency bands used by mobile phones and instead, included also other sources such as, base station antennas, Wireless Local Area Networks, radio and television antennas and smart meters (IARC 2014).

The World Health Organization (WHO) set up the International EMF Project in 1996 with the aim of assessing the scientific evidence of potential health effects of this type of exposure (WHO 2016). The different regions of the WHO are shown in the map of Figure 2.1.

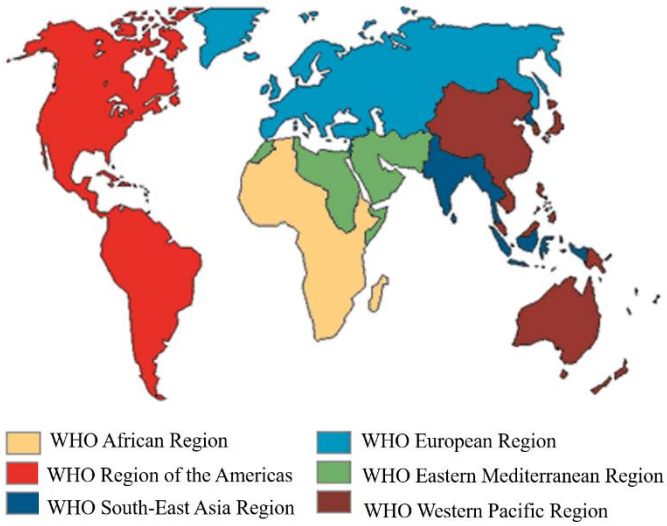

Figure 2.1. Regions of the World Health Organization (WHO 2016).

By clicking on any location of the map, which is on the webpage of the EMF (WHO 2016) project, information on activities about EMF in the area of interest can be found. This project was created in response to public concern regarding health effects of EMFs in the frequency range up to 300 GHz and it was established in order to protect public health. Other objectives of the project are to encourage focused research programs, make possible the development of international standards for EMF exposure, provide information related to the management of protection programs or provide advice about any hazard of exposure to these emissions.

The dosimetry and exposure assessment is one of the research needs listed in the WHO research agenda for RF fields, updated in the year 2010 (WHO 2010). Two of the high-priority types of studies included in this agenda are the assessment of characteristic RF EMF emissions, exposure scenarios and its corresponding exposure levels and the quantification of personal exposure due to different sources operating at these frequencies. In the last years, several studies have been carried out in this regard and with the aim of checking compliance with standards and regulations. Different national and international institutions have provided guidelines in which limits for human exposure to radiofrequency fields were established, differentiating between occupational and general public exposure limitations. Occupational exposure refers to adults who are exposed under known conditions, so they are aware of potential risk and are trained to take safety precautions. On the contrary, general public refers to people of all ages and health status that many times are not aware of their exposure to EMFs and are not expected to take precautions in order to minimize the radiation. For these reasons, exposure limits for general public are more restrictive than those limitations imposed to the occupational population.

Occupation and general public exposure levels due to radio communication systems are increasingly being tested in order to verify their compliance to standards. Although several guidelines and regulations for assessing exposure to EMF have been published, there is a lack of agreement on some terms of the procedure, such as the proper duration of the measurement. Furthermore, there is a free choice of instruments and equipment configuration, which can lead to an increase of the measurement uncertainty. In order to measure accurately exposure levels that can be mutually compared and suitable for testing compliance with safety standards, methodologies must be harmonized.

2. HUMAN EXPOSURE TO EMFS

In this section basic concepts, regulations and methods to assess human exposure to EMFs in the near and far field regions are described.

Regarding EMF standards, several documents that include regulations and guidelines have been developed in order to provide human health protection. First of all, a distinction between the types of standards that ensure EMF protection is drawn.

- Exposure standards are aimed at providing the maximum permitted exposure levels.
- Measurement standards are those that provide guidance on the measurement methods and procedures that should be carried out in order to check compliance with exposure limitations.
- Emission standards give specifications for electrical devices in order to consider aspects such as electromagnetic interference or device efficiency. They have been developed by institutions such as the International Electrotechnical Commission (IEC) or the European Committee for Electrotechnical Standardization (CENELEC).

Although these last types of standards are not explicitly based on health aspects, they must ensure compliance with exposure limits and usually they guarantee that even when more than one device are close to each other, exposure limits will not be exceeded.

In the following subsections, details regarding exposure and measurement standards are provided, since these two types of regulations and guidelines are of interest when assessing human exposure to RF fields.

Then, methods and procedures followed in different studies to assess human exposure to EMFs are described. But first, some basic concepts about human exposure assessment are presented.

2.1. Basic Concepts about human exposure to EMFs

The assessment of human exposure to EMFs can be performed by obtaining values associated with different quantities. A first classification consists of distinguishing between the physical units that can be readily measured out of the body and those that are associated to energy absorbed in body tissues, whose values are harder to obtain. Some explanations regarding the quantities used for assessing exposure to RF fields, as well as some theoretical aspects are given below. More concepts and details can be found in standards and regulations, such as in (IEEE 2013; CENELEC 2008).

Electric (E) and magnetic (H) field strengths are vector quantities obtained at a given point. The first one is expressed in volt per meter (V/m) and represents the force (F) of an infinitely small charge (q) divided by the charge:

$$E = \frac{F}{q} \tag{2.1}$$

H field strength is expressed in ampere per meter (A/m):

$$H = \frac{B}{\mu_0} - M \tag{2.2}$$

Where μ_0 is the permeability of the free space, M the magnetization and B the magnetic flux density, which is the field vector in a point that results in a force on a charge moving at a velocity (v) :

$$F = q(v \times B) \tag{2.3}$$

B is expressed in teslas (T) and in vacuum the magnetic field strength is equal to the magnetic flux density divided by the permeability of the free space.

The power density (S), expressed in watts per square meter (W/m^2), can be calculated from the E field strength and the H field strength:

$$S = E \times H \tag{2.4}$$

Moreover, in the case of plane waves, E and H are related by the impedance of free space Z_0:

$$E = H \times Z_0 \tag{2.5}$$

To be able to use (2.5), far field conditions must be fulfilled, since in the far field region of an antenna the field has mostly a plane-wave character. For calculating the minimum distance where the far field region starts (d_f), if the antenna is physically larger than half a wavelength (λ), being D the largest dimension of the antenna, the following equation can be applied (Rappaport 2010):

$$d_f = \frac{2D^2}{\lambda} \qquad (2.6)$$

On the contrary, for antennas physically shorter than $\lambda/2$, d_f can be considered equal to 3 λ.

For internal dosimetry specific absorption rate (SAR) values are used, whose units are (W/kg). SAR is a measure of the power absorbed per unit of mass and can be averaged over the whole body or over a smaller part of mass. SAR can be related to the electric field at a point by:

$$SAR = \frac{\sigma |E|^2}{\rho} \qquad (2.7)$$

where σ is the conductivity of the tissue (S/m) and ρ is the mass density of the tissue (kg/m^3).

SAR can also be related to an increase in temperature at a point:

$$SAR = \frac{c\Delta T}{\Delta t} \qquad (2.8)$$

where ΔT is the change in temperature (℃), Δt is the duration (s) and c is the specific heat capacity ($J/(kg\ ℃)$).

2.2. Standards regarding EMF exposure limits

These standards provide the maximum permitted levels of exposure and usually include safety factors and guidelines for limiting personal exposure to this type of radiation. They have been developed by the International Commission on Non-Ionizing Radiation Protection (ICNIRP 1998), the Institute of Electrical and Electronic Engineers (IEEE 2005) and many national authorities.

Following the ICNIRP guidelines (ICNIRP 1998), which is a non-governmental organization formally recognized by the WHO, the recommendations are expressed in terms of basic restrictions and reference levels. Basic restrictions are based directly on established health effects and depending upon the frequency of the radiation source, they are expressed in current density (J) and SAR values for frequencies up to 10 GHz. In the specific case of frequencies between 10 MHz and 10 GHz only SAR values are applicable. The reference levels are used for a practical exposure assessment and they are expressed in terms of electric and magnetic field strengths, magnetic flux density and power density, the latter only for frequencies higher than 10 MHz. The WHO states in the EMF Project that the main conclusion from their reviews is that exposure to EMF levels below the ICNIRP limits do not appear to have any known consequence on health. It is important to remark that the fulfillment of reference levels ensure the compliance with basic restrictions.

One of the main problems regarding EMF regulations lies in the disparities between standards around the world, which has caused an increase in the public anxiety about these emissions. For that reason, the WHO provides the chance to develop a framework for harmonization of EMF standards with the objective of establishing limitations on exposure levels identical for all people, as well as control measures that offer the same level of health protection to everyone (WHO 2006). This framework gives advice for developing science-based exposure limits to national regulatory bodies that are developing new standards or reviewing the basis of the existing ones. Figure 2.2 illustrates the different steps of the procedure proposed in the above mentioned framework for developing EMF exposure standards, together with some considerations to be taken at each stage.

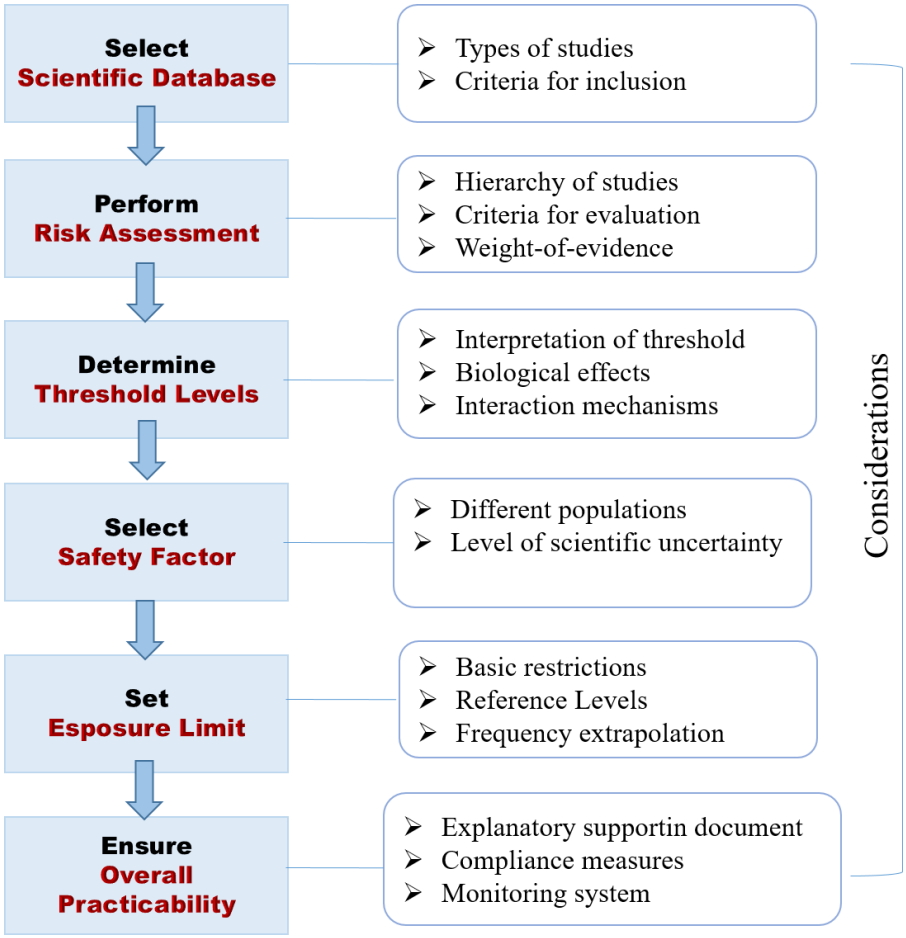

Figure 2.2. Procedure for developing EMF exposure standards.

The first step consists of reviewing and analyzing the scientific literature. Criteria has to be defined to determine if a study is worthy of being included in the scientific database. After performing the risk estimation, the threshold levels have to be determined. The threshold exposure level is the minimum level below which no health adverse effects have been found. However, if the exposure level is above the threshold, biological hazards can be produced. A safety factor should be added to this threshold to take into account possible imprecisions when determining the threshold level, for example the uncertainty derived from lack of knowledge of the biological effects. The final exposure limit is obtained after adding the safety factor to the threshold. The guidelines developed by the ICNIRP (1998) and IEEE (2005) are based on this approach. But there is another way of setting the exposure levels that consists of establishing the threshold as the minimum level below which no biological effect is observed, regardless

whether is an adverse effect or not (WHO 2006). Then the safety level has to be added to this threshold so as to set the reference level. This second method of obtaining the exposure reference level can result in a very conservative standard, which could derive in overly restrictive deployment policies when designing systems or devices emitting EMFs.

The reference levels in terms of electric field specified by the ICNIRP are illustrated in Figure 2.3. These reference levels are expected to be spatially averaged values to consider the entire body of the exposed person and always with the important requirement that the basic restrictions on localized exposure are not exceeded. The maximum permitted electric field levels for the general public and occupational population are provided for frequencies up to 300 GHz (unperturbed RMS values). For example, for frequencies from 2 GHz to 300 GHz the maximum permissible electric field level is 61 V/m for the general public, and 137 V/m in the case of occupational exposure. In addition, the maximum permissible peak values are given for frequencies exceeding 100 kHz.

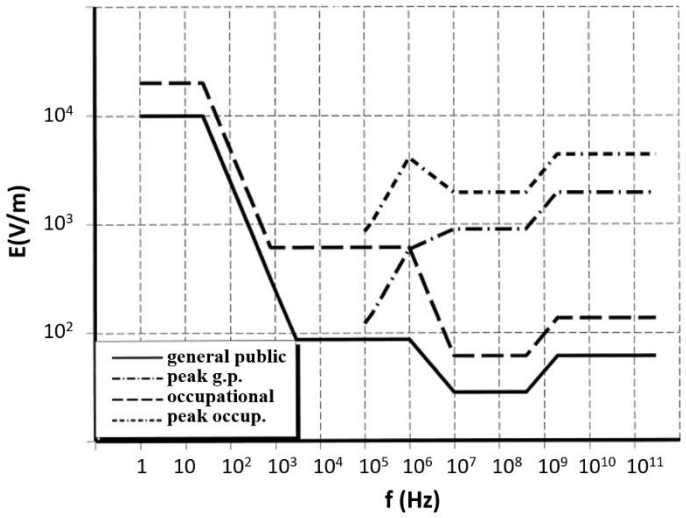

Figure 2.3. Reference levels for exposure to time varying electric fields given in the ICNIRP Guidelines (ICNIRP 1998).

The basic restrictions detailed in these international guidelines and from which the reference levels were determined can be seen in Table 2.1. All SAR values have to be averaged over any period of 6 min and in the case of localized SAR, the averaging mass has to be any 10 g of contiguous tissue. The results that have to be compared with the regulations should be the maximum SAR obtained

from the 10 g averaged values. The whole-body average SAR is obtained by dividing the total power absorbed in the human body by the body weight.

Table 2.1. Basic restrictions of ICNIRP guidelines for time varying electric and magnetic fields for frequencies up to 10 GHz (ICNIRP 1998)

Exposure characteristics	Frequency range	Current density for head and trunk (mA m^{-2}) (rms)	Whole-body average SAR (W kg^{-1})	Localized SAR (head and trunk) (W kg^{-1})	Localized SAR (limbs) (W kg^{-1})
Occupational exposure	up to 1 Hz	40	—	—	—
	1–4 Hz	40/*f*	—	—	—
	4 Hz–1 kHz	10	—	—	—
	1–100 kHz	*f*/100	—	—	—
	100 kHz–10 MHz	*f*/100	0.4	10	20
	10 MHz–10 GHz	—	0.4	10	20
General public exposure	up to 1 Hz	8	—	—	—
	1–4 Hz	8/*f*	—	—	—
	4 Hz–1 kHz	2	—	—	—
	1–100 kHz	*f*/500	—	—	—
	100 kHz–10 MHz	*f*/500	0.08	2	4
	10 MHz–10 GHz	—	0.08	2	4

For frequencies between 100 kHz and 10 GHz, the whole-body average SAR provided in these regulations is 0.08 W/kg for general public and 0.4 W/kg for occupational exposure. These levels increase in the case of localized SAR.

As previously mentioned, apart from the limitations provided by the ICNIRP and the IEEE, several national standards have been created in the last years. Focusing on the Global Health Observatory data repository of the WHO (2017), exposure limits in different countries can be observed for the frequency bands of 900 MHz and 1800 MHz in the case of reference levels and up to 10 GHz for the basic restrictions. These data were updated in the year 2017 and there are still several countries that have not provided these data to the repository, probably because they do not have exposure standards with limits different from those specified in the international guidelines. Amongst the contributing countries it is noteworthy the reduction in some exposure limits compared to ICNIRP or IEEE limitations. For example, examining the general public limitations, in **Greece** the regulation sets reference levels at 70% of those provided by the ICNIRP at 900 MHz and 1800 MHz, and 60% when antenna stations are located closer than 300 m from the property boundaries of schools, kindergartens, hospitals or eldercare facilities. The basic restrictions in that country are also established at 70% of the international guidelines. In **Italy**, the electric field imposed for those frequency bands is equal to 20 V/m. Moreover, in homes, schools, playgrounds and places where people may stay for longer than 4 hours, an 'attention value' of 6 V/m is applied and averaged over any 24-hour period. In other countries, more restrictive limits have been established for mobile phone antenna installations at places of sensitive use, such as in **Switzerland** or in **Turkey**, where 4V/m and 3V/m, respectively are the reference levels only in some specific places. The highest

value is found in **United States**, where 47.6 V/m is the maximum electric fields permitted at 900 MHz. This value of electric field has to be averaged over a period of 30 min, like in the guidelines provided by IEEE and in contrast to the ICNIRP guidelines, in which the average time is 6 min.

The European Commission has also published official documents including the minimum health and safety requirements. In some of them, limitations regarding EMF exposure of workers are provided, such as in the Council Directive 2013/35/EU (EU 2013). Nevertheless, when considering such directive it is important to bear in mind that the limitations are given in terms of exposure limit values and action levels. There are also regulations such as the Council Recommendation 1999/519/EC (EC 1999) that provides basic restrictions and the derived reference levels for exposure of the general public. These directives and recommendations are based on ICNIRP guidelines. The exposure limit values of the Directive and the basic restrictions given in the Recommendation are the basic restrictions given in the ICNIRP guidelines for occupational and general public exposures respectively. Similarly, the action levels and the reference levels of the above mentioned Directive and Recommendation are the same as the reference levels provided by the ICNIRP.

In **Spain**, the exposure limits indicated in European recommendations are adopted, thus, the reference levels and basic restrictions given in the ICNIRP guidelines must be fulfilled. These exposure limits are incorporated in the Royal Decree 1066/2001 (RD 2006).

The decision of a country of developing its own standard is usually based on the premise that in some circumstances the application of the international guidelines may be unclear. This is the case of **Australia**, whose standard is based on the guidelines developed by the ICNIRP committee. The Australian standard specifies that the ICNIRP guidelines were reworked in order to provide an unambiguous technical framework (Arpansa 2002). The differences between the ICNIRP guidelines and the requirements of the Australian standard are provided in the Table 12 of that standard and some of the contributions are, among others, the inclusion of basic restrictions for instantaneous spatial peak SAR in the head and torso or the method for spatial averaging of reference levels.

2.3. Measurement Standards

As explained at the beginning of this section, measurement standards provide guidance on the measurement methods and procedures that should be carried out in order to check compliance with exposure limitations. Among other things, they

give advice about the necessary instruments or the appropriate measurement duration.

Several standards and guidelines giving instructions for assessing human exposure to EMF are in use at present. The most popular ones are those developed by the IEEE (1991) in America, CENELEC (2008) in Europe and those from the International Telecommunications Union ITU (2008, 2011). These standards provide instructions to establish methods for assessing exposure to EMFs up to 300 GHz, but they cannot go into details extensively because of the broad range of frequency and the huge number of different applications. It is also recommended to ensure that exposure assessment is conducted in accordance with the applicable national or regional standards and regulations. The previously described international EMF project, created by the WHO, provides information regarding the standards developed in different countries (WHO 2017). In Spain the procedure for measuring EMFs is given in Orden CTE (CTE 2002).

Regarding the most widely used exposure standards, there is a lack of agreement between some of them on some aspects related to exposure assessment, such as the proper time for measuring EMFs. In this regard, ICNIRP guidelines specify that SAR values are averaged over any 6-min period, as well as EMFs for frequencies between 100 kHz and 10 GHz. For radiofrequency fields exceeding 10 GHz, an averaging period of $68/f^{1.05}$ minutes is proposed, being f the frequency in GHz. Nevertheless, considering the IEEE Standard (2005) different averaging times are proposed. Focusing on Table 9 of such standard an average period of 30 min is proposed for obtaining exposure values for the general public between 100 MHz and 5 GHz. Between 5 GHz and 30 GHz the specified averaging time is $150/f$, and for frequencies lower than 100 MHz also 6 min are specified in some cases.

Based on the above mentioned documents (IEEE, CENELEC, ITU), some aspects to consider when measuring radiofrequency fields are detailed below.

The field region where the measurements are performed is essential, since in the far field region obtaining only the E field or the H field is enough and the other quantities can be calculated using equations (2.4) and (2.5). Nevertheless, in the near field region, E and H fields must be measured separately.

The EMF measurement equipment consists of two parts, the probe or antenna and the measuring instrument. The directivity of the antenna or the probe is an important parameter. When radiation from a specific and well-known

source is measured, a directive antenna can be utilized aiming at the source under study in order to detect the emissions coming from it. However, for compliance measurements, usually an isotropic probe is required, since the radiation source may be not known, more than one source can exist, or the emissions can come from different directions. Therefore, using an isotropic device the signals from different directions can be detected. In fact, if a tri-axial probe is not available, a probe with a single axis sensor should be aligned in the three mutually orthogonal directions to measure separately the three spatial components of the field. Then the total electric field is calculated as follows:

$$E_{Total} = \sqrt{|E_x|^2 + |E_y|^2 + |E_z|^2} \qquad (2.9)$$

where E_x, E_y and $E_z$are the components of the electric field in the three different directions.

An example of a commercial tri-axial probe is shown in Figure 2.4, where the three axes can be observed. On the right illustration, a tri-axial probe connected to the measuring instrument is presented.

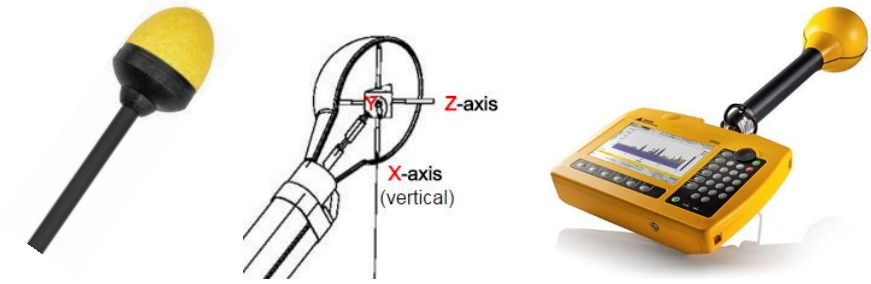

Figure 2.4. Tri-axial probe for EMF measurements (left) and a tri-axial probe together with the measuring instrument (right).

The frequency range of the measuring equipment is another key aspect to take into consideration. Broadband probes indicate the value of the field strength in a wide range of frequencies without distinguishing between frequencies, while selective instrumentations provide field strength levels in different frequency ranges. Moreover, the spectral characteristics of the measured signals can be obtained with the latter instruments. In the case of measuring electric or magnetic field strength by means of different selective instruments suitable for the different frequency ranges, the total field strength value of the location is calculated by:

$$E_{Total} = \sqrt{\sum_i E_i^2} \quad (2.10)$$

$$H_{Total} = \sqrt{\sum_i H_i^2} \quad (2.11)$$

Where E_i and H_i are the electric and magnetic field strength obtained in each frequency range.

To comply with the exposure limits when multiple frequency fields are present, the following equations must be fulfilled:

$$\sum_{i>1\ MHz}^{300\ GHz} \left(\frac{E_i}{E_{L,i}}\right)^2 \leq 1 \quad (2.12)$$

$$\sum_{j>1\ MHz}^{300\ GHz} \left(\frac{H_j}{H_{L,j}}\right)^2 \leq 1 \quad (2.13)$$

where E_i and H_j are the electric and magnetic field strength at frequencies i and j respectively. $E_{L,i}$ is the electric field reference level given in the guidelines and $H_{L,j}$ the magnetic field reference level also provided in the guidelines.

Another parameter that should be provided together with the results is the uncertainty associated to the measurement. The contributions of each component of uncertainty can be obtained by means of appropriate measurements carried out on the equipment, or considering the specifications from the manufacturer. The combined uncertainty is then calculated considering the contributions of each component of uncertainty u_i and its corresponding weighting coefficient (sensitivity coefficient) c_i using:

$$u_c = \sqrt{\sum_{i=1}^{m} c_i^2 u_i^2} \quad (2.14)$$

The expanded uncertainty with a confidence interval of 95% shall not exceed 4 dB, which is calculated as follows:

$$u_e = 1.96 u_c \quad (2.15)$$

Finally, it is important to remember that whenever the measured EMF levels are below the reference levels, the basic restrictions are also met. Nevertheless, when a measured or calculated value exceeds the reference level, it does not imply that the basic restrictions will be exceeded, but in such case the compliance with the relevant basic restriction is necessary, otherwise the reduction in the field levels or additional protective measures are needed.

Some general considerations regarding SAR measurements contained in the described standards are given below.

As previously shown in equation (2.7) SAR can be obtained from internal E field measurements, which are performed using a small probe positioned in a liquid-filled phantom model of the human body or a part of it, such as the head or a hand (See Figure 2.5). The liquids simulate the dielectric properties of the human body tissues and the probe should have an isotropic response. Moreover, it should influence the field as little as possible. The measurements may be taken at many individual points and then these points should be considered to characterize the E field and the SAR distribution. An automatic probe positioning system, such as a robot should be used to move the probe throughout the phantom.

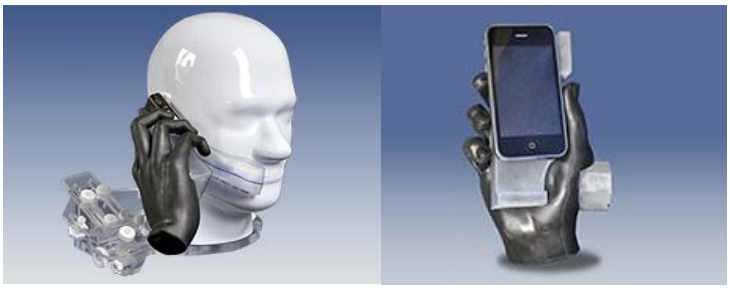

Figure 2.5. Commercial head and hand phantoms from IndexSAR (2018).

With regard to the phantom models, their outer shape and the internal tissues should simulate the anatomical details of a real human body, being as similar as necessary. Phantom models can be homogeneous or heterogeneous. The first ones can be used for conservative exposure assessment. But if higher accuracy is required, a heterogeneous model should be use. Moreover, in the applications in which local SAR values are desired, partial-body phantoms are appropriate. Important factors when evaluating SAR are the dielectric properties of the phantoms (relative permittivity and conductivity), which should be selected considering the measurement frequencies.

The typical measurement uncertainties when performing these types of measurements are associated with the accuracy of the measurement instrument, the influence of the probe on the measured field level, the difference between the actual position of the probe and the planned measurement point and the influence or effect of the environment.

When testing devices such as mobile phones, the measurements are performed at all the operating frequencies and with the device transmitting the maximum power. In addition, the wireless device should be placed at different positions using a mobile phone holder so as not to influence the results. An example of a SAR assessment system is presented in Figure 2.6, where a phantom is deposited on a SAR table and a robot is used to move the probe.

Figure 2.6. System for assessing SAR.

Numerical methods and theoretical approaches can also be used for estimating EMF and SAR levels and, as specified in CENELEC (2008) these methods are not only a complement to verify results, they are also useful tools for analyzing exposure to RF fields, especially when measurements are difficult or impossible to perform. In ICNIRP guidelines they conclude that SAR data obtained in measurements are consistent with the data obtained from numerical modeling.

There are also computational models of human bodies to be used in numerical modeling. The above described characteristics of body phantoms are applicable when using calculation methods. Furthermore, body models of

different age, sex and physical conditions have been developed in order to make them similar to real humans and consider the existing differences between people. An example of different body models is the voxel family available in the CST software (CST 2016) and shown in Figure 2.7. This family includes a baby, a child, a man, three women and a pregnant woman.

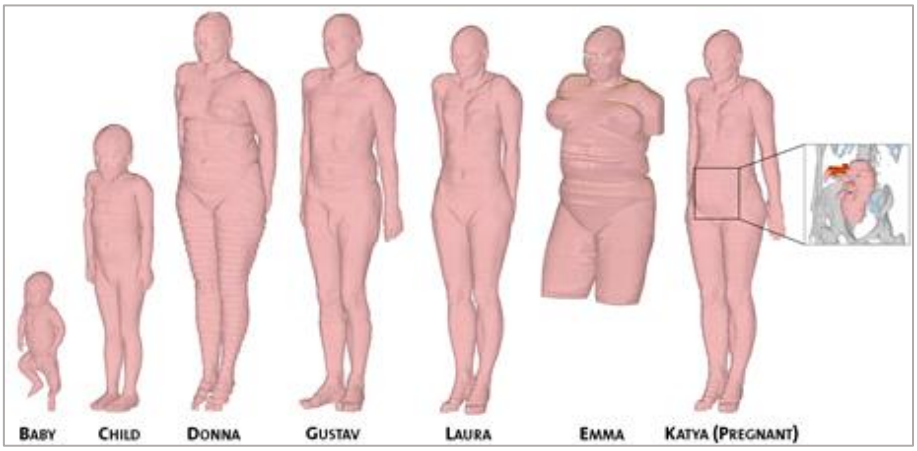

Figure 2.7. Voxel body models available in the software CST (2016).

Several numerical methods are useful for evaluating human exposure to EMFs. To select the proper method, the following factors have to be taken into consideration:

- The field region where the exposure will be evaluated
- The quantity that will be evaluated
- The environment where the exposure will be evaluated

In this thesis the Finite-Difference Time-Domain (FDTD) method has been used. It is applicable for evaluating E and H fields and SAR values in the near field region for different environments. This is one of the most widely accepted numerical method for SAR assessment, since it offers high flexibility in modeling the complex structures of body tissues and organs (Kunz 1993).

2.4. Studies related to EMF exposure assessment

In order to perform measurements of EMF strength, measurement instrumentation has to be selected in accordance with the characteristics of the source of the field, such as the frequency range of interest, and the aim of the measurement. Some of the instruments widely used for this purpose are the broadband isotropic probes connected to a portable measuring equipment. These probes are designed to record samples of the electric and magnetic field in a wide range of frequencies and provide the value of the total field strength in that frequency range. A few examples of these instruments are those from Narda Safety Test Solutions (Narda 2018), Wavecontrol (2018) or ETS Lindren (2018).

These types of probes are often used to assess RF fields and check compliance with limits because of its ease of use. For example, they are part of several of the EMF monitoring networks developed in the last years, such as the Italian national EMF monitoring network, where probes to record emissions from 100 kHz to 3 GHz were installed (Troisi 2008). Also, in the Serbian EMF monitoring network, SEMONT, broadband measurements were performed using a field meter and an electric isotropic probe with a frequency range from 100 kHz to 6 GHz placed at a height of 1.7 m (Djuric 2015). In the latter network, some preliminary samples were acquired to evaluate the spatial variability of the field strength and to determine the point with the maximum field strength level (hot-spot) within the considered location. Then, the instruments were placed in such point to carry out more detailed measurements. Figure 2.8 shows a picture of the different points considered for the evaluation of the spatial variability (P1, P2,...P22) and the measurement equipment placed at the hot-spot.

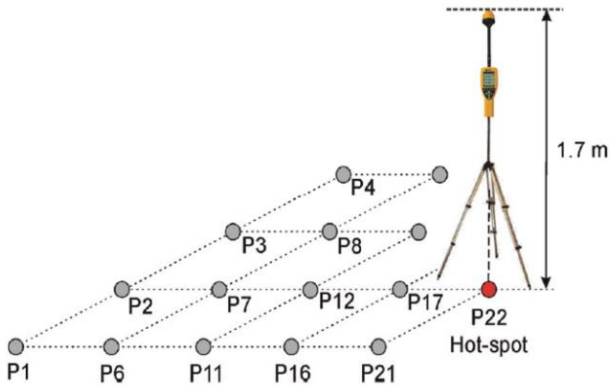

*Figure 2.8. Broadband measuring equipment used in (*Djuric 2015*).*

The reasons of installing these networks in some cities are to inform people about the exposure levels, as well as provide scientific knowledge in order to reduce the social concerns that many times arise because of the lack of information and scientific bases. Moreover, in this way it is possible to demonstrate that RF emissions are usually well below exposure limits, even in the countries with more restrictive levels than the ones provided by ICNIRP guidelines, such as in Italy (Troisi 2008), and in the case of acquiring levels higher than expected, procedures to reduce these levels can be activated.

Apart from the monitoring networks, these broadband probes were used in various measurement campaigns. Sánchez-Montero et al. (2017) used these probes to evaluate human exposure to RF fields between 100 kHz and 3 GHz over a ten-year period in outdoor environments of the city of Alcala de Henares, Spain. The obtained E field levels ranged from 0.02 V/m to 2.05 V/m in the measurement campaigns carried out from the year 2006 to the year 2015. They concluded that a moderate increase in the field strength levels was detected between the years 2006 and 2010 and these emissions did not vary too much from 2010 to 2015. Measurements in the same frequency band were taken in (Seyfi 2013), where exposure to EMFs was assessed during a week in an apartment. The maximum instantaneous E field value was equal to 6.9 V/m.

Recently, some authors have used broadband probes to evaluate the level of exposure between 300 kHz and 18 GHz (Fernández-García 2017). The study was done in an urban area of 2.25 km^2 in Spain, a total of 271 points were selected for taking the measurements, which were performed from September 2016 to December 2016 between 15:00 and 17:00. Samples were recorded during 6 min at each point at a height of 1.5 m and results showed a maximum 6 min averaged field level equal to 3.39 V/m and a maximum sample level of 4.28 V/m. Although the measurement instrumentation could capture emissions up to 18 GHz, probably, and based on the description of the radiofrequency transmitters given in that paper, there are no significant transmissions at frequencies higher than 6 GHz. These measurements were carried out in the street, but previously, authors used the same equipment in an indoor scenario, where they obtained a maximum electric field of 2.53 V/m (Gil, 2016).

In many cases, the broadband instruments are useful for identifying the maximum field strength points so as to perform additional measurements in that location. In (Verloock 2014) measurements of 24-hour duration were carried out in schools and homes with spectrum analyzers. But before performing these long-

term measurements, the maximum radiation point was searched by means of a broadband probe and a broadband field meter.

Other instruments easy to use in order to record signal levels from RF services, but providing more information about the emissions, are the portable selective radiation meters and the personal exposure meters, also known as exposimeters. Both of them are easy to configure and easy to carry since they are handheld, as in the case of the broadband equipment.

The exposure meters have been widely used in these types of studies. They have tri-axial field probes, but they can give different field strength levels for different frequency bands. The frequency ranges are associated to different RF services, allowing in this way the distinction between contributions coming from different types of transmitters. Two examples of the visualization of the results measured with the exposimeter EME Spy 200 of Satimo (EME SPY) are presented in Figure 2.9 and Figure 2.10. In the first one, the instantaneous levels of the measured samples are provided for each frequency band, while in Figure 2.10 the field strength values are averaged over 6 min. In many studies, participants carry an exposimeter with them, for example worn on a belt or in a backpack, during a specific time (1 day, 1 week) in order to estimate radiation levels (Röösli 2008; Frei 2010; Joseph 2010a; Sagar 2018). Participants usually fill in an activity diary so that the measured data can be correlated with the activities written in the diary (Burgi 2008). But these devices are also used for taking samples at a fix point, without having them worn by individuals (Vermeeren 2013).

In the review published in (Bhatt 2016a) 6 different exposimeters were analyzed and compared, giving details of the sampling intervals, detection limits, frequency bands, measurement uncertainty, type of parameter that can be measured (maximum, mean, root mean square…), batteries duration and sizes of the devices. In addition, in the same study various mobile phone-based applications and software-modified phones designed for characterizing exposure in the near field are presented and compared. These applications provide data such as the number and duration of calls, the received power, the amount of transmitted and received data, some of them even give information regarding WiFi transmissions. All these parameters are important and useful to characterize exposure due to the phone use and they can complement the diaries and agendas filled by participants. Some validation studies were carried out to compare the agreement or matching between the actual mobile phone use and the data provided by the participant regarding that use (Goedhart 2015).

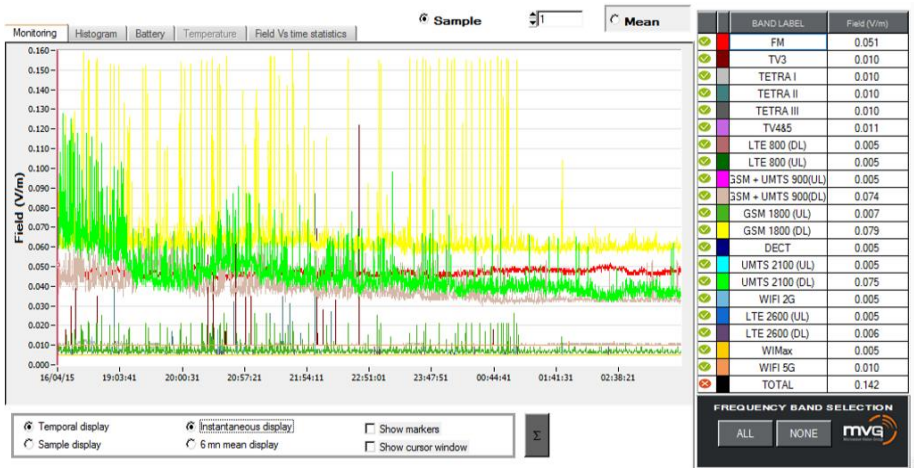

Figure 2.9. Instantaneous sample levels measured with the exposimeter EME SPY 200.

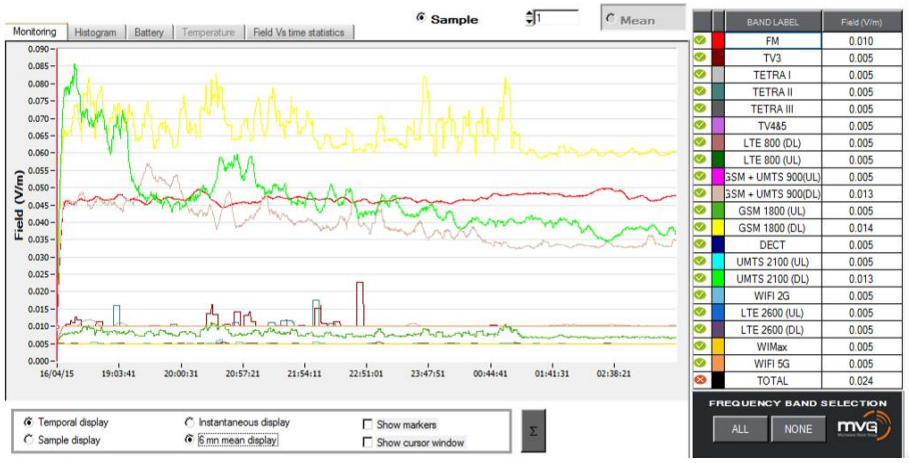

Figure 2.10. 6 min averaged values measured with the exposimeter EME SPY 200.

Some authors have investigated the accuracy of broadband probes (Letertre 2011; Adamson 2010) and personal exposure meters (Bolte 2011) and although they are useful for checking compliance with regulations, correction factors should be applied in order to improve the accuracy of the measurements. In Section 3 of Chapter 3, some examples of the differences in the measured results with these instruments and with a more professional one are presented. The reasons of having higher uncertainties when using these instruments have been associated to the body shielding, the wide range of frequencies measured with the same antenna or the elevation angle of the device (Bolte 2011). These effects have also been analyzed by means of computational tools (Iskra 2010). In

some measurement campaigns, two exposure meters were carried to reduce the uncertainty due to the factors described before.

If more accurate results are required when measuring EMFs, the equipment for taking samples should consist of a spectrum analyzer and an appropriate antenna. For example, in (Cansiz 2016) measurements using these types of equipment were performed in the streets of a city in Turkey during a whole week between 17:00 and 18:20. The maximum E field value was equal to 6.09 V/m and was recorded in the UMTS frequency band. The measurement campaign carried out in (Estenberg 2014) was also in outdoor environments. They proposed a car based measuring system that had the advantage of a fast estimation of exposure to RF fields in a large area. Tomitsch et al. (2015) assessed radiation levels in several bedrooms during nights, repeating the measurements during three different years. The average obtained values were 0.077 V/m in 2006, 0.118 V/m in 2009 and 0.105 V/m in 2012. However, the measurements of this last campaign were recorded with a spectrum analyzer set to 'maximum hold' mode and this can produce an overestimation of the exposure level, as shown in Chapter 3 of this thesis.

Some authors focused on evaluating the exposure due to a specific service rather than measuring in a wide range of frequencies. Several people investigated emissions from mobile communication networks (Gkonis 2017; Lunca 2014; Bhatt 2016b; Miclaus 2013; Baltrenas 2013; Cala 2015; Colombi 2013) or WLANs, which use WiFi technology (Pachon-Garcia 2015; Karipidis 2017; Joseph 2013).

Regarding the basic restrictions, the power absorption in human tissues is often investigated, especially when the RF source is close to the human body. This is the case of user devices, such as mobile phones, laptops or tablets, whose radiation can be evaluated by means of certain standardized laboratory measurements in order to certify the device (Davis 2009). Numerous investigations were conducted to evaluate the energy distribution due to mobile phones (Cardis 2008; Hadjem 2010), concluding that the SAR values depend not only on the use and position of the phone, but also on the different phantom models used in the measurements. More detailed researches were conducted using computational tools or measurements with the aim of investigating the exposure due to personal devices in different situations, such as inside vehicles (Anzaldi 2007; Leung 2012) or considering different postures of a person (Krayni 2017). The variation of the antenna performance due to the power absorption when these devices are close to the body was investigated in (Sibille 2012).

In addition, the probes used for taking samples were analyzed in order to develop new minimally invasive solutions and techniques (Person 2008; Picard 2008), since as detailed above this is one of the requirements provided in the standards when performing SAR measurements.

Numerical methods are widely used in EMF exposure assessment and in dosimetry studies, one of their advantages is that they can be applied to a wide range of analysis providing useful results without having to perform measurements that, many times, are difficult to conduct and much more expensive. For example, numerical calculations were used for assessing the absorption and distribution of EMF levels in different body tissues (Alekseev 2009), to study the influence of the permittivity on SAR calculations (Hurt 2000) and for investigating the near field exposure of mobile phone base stations (Meyer 2003). Espinosa et al. (2014) used different computational tools for analyzing the near field radiation zones of an antenna, making a comparison between the different simulation tools.

Finally, as EMF levels are usually easier to measure than SAR values, some authors proposed methods for converting electric or power density levels to whole-body SAR levels (Joseph 2010b; Piuzzi 2011; Bamba 2014). In this way, data collected with personal exposure meters or spectrum analyzers can be easily converted to quantities that give information of the near field exposure.

Conclusions:

As shown in this section, several instruments and methods have been used to assess human exposure to EMFs. Guidelines and Standards provide general instructions on procedures and equipment, but they cannot go into details extensively because of the broad range of frequency and the huge number of different applications. The measurements performed in the above described studies were useful to check compliance with regulations or to obtain information about exposure distribution. However, the application of different procedures for recording samples makes difficult the comparison between exposure levels acquired in different measurement campaigns. In addition, some instruments give more accurate results than others. For these reasons, there is a need of establishing appropriate measurement procedures for different applications, this includes the service under study or aim of the study. An analysis of the instruments and methods (including those described in this section) used for measuring WiFi exposure levels is presented in Chapter 3.

3. STUDY CASES

3.1. Wireless Local Area Networks

In the last years the deployment of WLANs has experienced a significant growth with the objective of meeting the users demands. These networks have been established in a wide range of scenarios in both public and private areas backed by the huge amount of emerging user devices, such as smart phones or laptops, and the attempt by the authorities and operators to make internet accessible to all users. WiFi is the technology used in these networks, under the standard IEEE 802.11. The original IEEE 802.11 standard for WLAN was published in 1999, reaffirmed in 2003 and some revisions have been published later (IEEE 2016).

These wireless networks have significant advantages and provide great opportunities to users solving the limitations imposed by wired networks. The main benefits of this technology consist of the flexibility and the reduction in the installation time and in the final cost. WLANs offer the possibility of reaching connectivity in areas with difficulties to lay cables and it can eliminate the need of having cables through walls. It provides flexibility to the user since devices can connect to the network from any place within the coverage area of the access point and it is easy to add or remove workstations. Moreover, in some scenarios where the facility is located on different sites, such as on two sides of a road, wireless communications prevent from the need of digging trenches to connect the different sites. Finally, the advantages of eliminating cables in dynamic environments, which require frequent changes, are obvious (Mittal 2014).

3.1.1. WLAN architectures

There are different approaches for deploying WLANs, as well as different ways of establishing communication between the different elements (Sridhar 2006).

Infrastructure and ad hoc modes

WLAN can operate in two different modes, ad hoc or infrastructure mode. In the ad hoc networks two or more devices can establish a wireless connection with each other without the need of an access point (see Figure 2.11(a)). In the infrastructure mode, the user devices communicate between them through an access point. Figure 2.11(b) shows several laptops communicating with two access points; every computer has to use the access point to reach another device

rather than connecting directly with the other computer or device. Furthermore, in the case of establishing a communication between devices located in the coverage area of different access points, also the wired network is used.

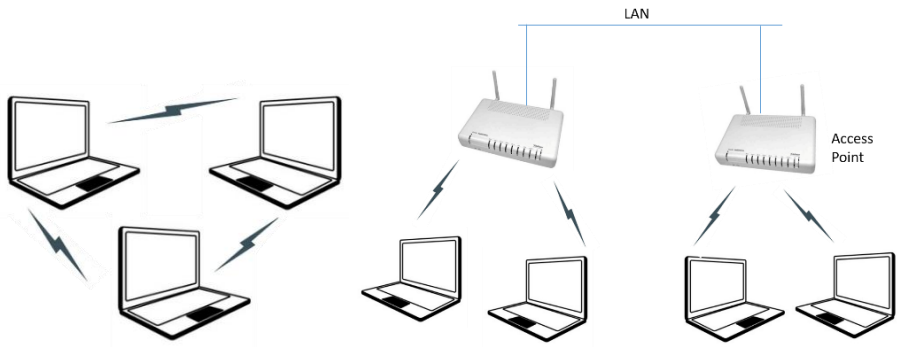

Figure 2.11 (a) ad hoc network, (b) infrastructure mode.

Distributed and centralized approaches

The approaches for deploying WLAN in the enterprise can be categorized into two groups, distributed and centralized networks (Sridhar 2006).

The first WLAN architecture presented is the centralized architecture. It is a hierarchical architecture that involves one or more WLAN controllers, which can be implemented on switches and are responsible for the configuration, control, and management of several wireless termination points (WTPs). All the traffic from the wireless elements is sent to the controller. An example of a centralized architecture is illustrated in Figure 2.12.

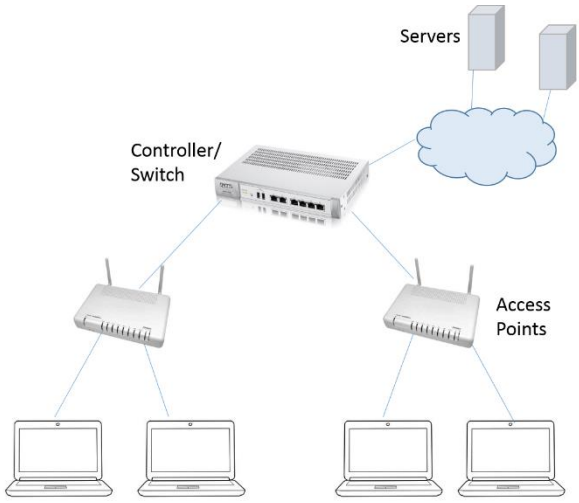

Figure 2.12. Example of centralized WLAN Architecture.

Another approach is the distributed WLAN architecture, which has the wireless traffic load distributed across the access points and does not depend on a centralized element to process all the wireless traffic. In this case various WTPs can form networks with other WTPs through wired or wireless connections. The above described ad hoc mode can be a part of a distributed WLAN.

The main drawback of the centralized approach is that any problem concerning the WLAN controller affects all the traffic of the wireless network, while in the case of the distributed architecture there is no single point of failure.

3.1.2. WiFi channels and frequencies

Most of the devices using WiFi technology operate in the 2.4 GHz or 5 GHz WiFi bands. In Europe the maximum permitted effective isotropic radiated power (EIRP) from access points and user devices are 100 mW at 2.4 GHz and 200 mW at 5 GHz. In the 2.4 GHz WiFi band transmission is set between 2.4 GHz and 2.4835 GHz as allocated by regulatory bodies in China, United States, Europe and Japan, or also in the frequency range from 2.471 GHz to 2.497 GHz in the case of Japan. These frequencies correspond to a part of the bands assigned for industrial, science and medical (ISM) applications, while at 5 GHz devices can operate in the ISM band (5.725-5.850 GHz) or at different frequencies (5.150-5.350 GHz). The channel bandwidth of most of the devices using IEEE 802.11 is equal to 20 MHz, but in some cases 40 MHz of channel bandwidth is possible so as to increase the data rate.

A summarize of different versions of IEEE 802.11 standards taken from the review conducted by Foster and Moudler (Foster, 2013) is presented in Table 2.2. As shown, the modulation techniques for WiFi signals are Direct Sequence Spread Spectrum (DSSS), Frequency Hopping Spread Spectrum (FHSS) and Orthogonal Frequency Division Multiplexing (OFDM).

Table 2.2. Different versions of IEEE 802.11 standard

IEEE 802.11 version	**Frequency band (GHz)**	**Channel bandwidth (MHz)**	**Modulation Technique**
IEEE 802.11 (original)	2.4	20	DSSS/FHSS
IEEE 802.11a	5	20	OFDM
IEEE 802.11b	2.4	20	DSSS
IEEE 802.11g	2.4	20	OFDM/DSSS
IEEE 802.11n	2.4/5	20/40	OFDM

In this thesis the WLANs operating in the 2.4 GHz frequency band have been studied. This frequency band is divided in 14 channels, but in Europe only 13 are allowed by the European Telecommunications Standard Institute (ETSI 2016). Moreover, the separation between adjacent channels is 5 MHz and as described above the channel bandwidth is 20 MHz, having in this way overlapping channels as can be seen from Figure 2.13, where the channel number and its corresponding center frequency are given. Typically, channels 1, 6 and 11 are the most frequently used in a given WLAN. In order to avoid interference from adjacent channels, the proper channel should be selected. Now, most of the access points are able to switch channels dynamically when they detect undesirable signals, being able to choose the channels taking into consideration the least interference.

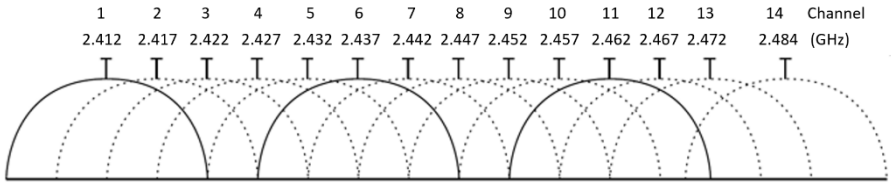

Figure 2.13. WiFi channels in the 2.4 GHz frequency band.

As can be observed from Figure 2.13, channel center frequencies (fc) in the 2.4 GHz band are defined at every integer multiple of 5 MHz. The relationship between center frequency and channel number n_{ch} is given by (IEEE 2016):

$$fc = 2407 + 5 \cdot n_{ch}\ (MHz) \qquad (2.16)$$

When using the OFDM modulation technique, such as in the case of the standards IEEE 802.11g and 802.11n, each 20 MHz channel comprises 64 subcarriers equally spaced 312.5 kHz. The signal is specifically transmitted on subcarriers -26 to -1 and 1 to 26, being the 0 subcarrier the one located at the center frequency. No signal is transmitted in that center frequency. Moreover, in each OFDM symbol four of the subcarriers are dedicated to pilot signals in order to make the coherent detection robust against frequency offsets and phase noise. These pilot signals are located in subcarriers -21, -7, 7 and 21, as shown in Figure 2.14.

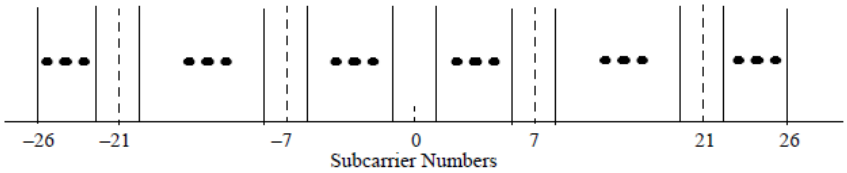

Figure 2.14. Subcarrier frequency allocation (IEEE 2016).

3.1.3. Exposure assessment in WLAN

Emissions specifically due to WiFi signals have caused concerns in the last years, especially because the transmitters are very close to people and WLAN are deployed in indoor environments, such as schools, homes or office buildings where people spend many time.

According to the review carried out by Foster et al. (Foster 2013), different studies state the existence of potential risks and effects caused by the exposure to WiFi radiation. Consequently, EMF levels generated by wireless communication systems operating in different environments should be measured in order to check the compliance with the human exposure limits established by different regulation bodies.

In the last years, considerable effort has made in order to assess exposure in WLANs, measuring the radiation produced by user devices and access points. In addition to the research works mentioned in Section 2.4 of this chapter, some

other measurement campaigns that can be cited are those developed in (Schmid 2007; Peyman 2011; Lunca 2012; Foster 2007; Khalid 2011). However, due to the nature of WiFi emissions, which are transmitted in the form of pulses of short duration, professional equipment is required in order to obtain accurate values of WiFi exposure. Some authors have introduced new techniques in order to obtain more accurate WiFi signal levels. In Chapter 3 of this thesis, a detailed discussion of all these techniques is provided.

3.2. Wireless Body Area Networks

WBANs consist of a number of wireless sensors, strategically placed on the human body, whose main objective is to monitor vital signs (blood pressure, heart rate, activity) or environmental parameters (location, humidity, temperature) (Chris 2005). The aim of WBANs is to improve speed, accuracy and reliability of sensors communication within, on and in the immediate proximity of a human body, which final purpose is to improve the user's quality of life. The use of wireless devices operating on the body solves the problems caused by wires, such as the limitation of the person activity or the decrease in the level of comfort, which can influence the measured results (Martin 2000). In many medical applications such as in electrocardiography or in capsule endoscopy, wireless sensors can replace the electrodes affixed on the body. These electrodes consist of pads with gel that can cause skin irritation, allergic reactions, and inflammation. In addition, as the gel dehydrates over time, the signal quality is reduced (Nemati 2012).

The IEEE 802.15.6 standard (IEEE 2012) was specifically developed for providing an international reference for a short-range (i.e., about human body range), low power and highly reliable wireless communications to be used in the vicinity or inside a human body. This standard is defined for the industrial scientific and medical (ISM) frequency bands together with those bands approved by local regulatory authorities. Moreover, it takes into account the effects that the presence of a person can have on the antenna, the reduction in the SAR into the body and the changes in the characteristics of the antenna due to the human movements.

In a WBAN there are several sensor or actuator nodes placed in the vicinity or inside the body that communicate with a hub. These actuators perform some specific actions according to the data received from the sensors or due to the interaction with the user, for example the administration of the correct dose of insulin to a diabetic patient. The hub is an entity that apart from having the functionality of a node, coordinates the medium access and power management of the nodes in the body area network (BAN). The hub receives and stores the information from the nodes and can also communicate with the exterior, for example with other networks via Internet or other existing wireless technology. Personal devices, such as smartphones or tablets can act as hubs. Figure 2.15 illustrates an example of a WBAN. As shown, the nodes placed on the body are called wearable nodes and they can be located directly on the skin or on the clothes. These nodes, as well as the ones implanted on the body not only gather

information, but also can communicate with the hub and, in some cases, between them. In the example, the hub interchanges information with an access point connected to the internet network, and capable of sending information to a medical network. The different devices of a WBAN establish on-body communications when both devices are on the body, or in-body communications when at least one of the sensors is inside the body. Off-body communications are established when a sensor is placed on the body and communicates with an external source.

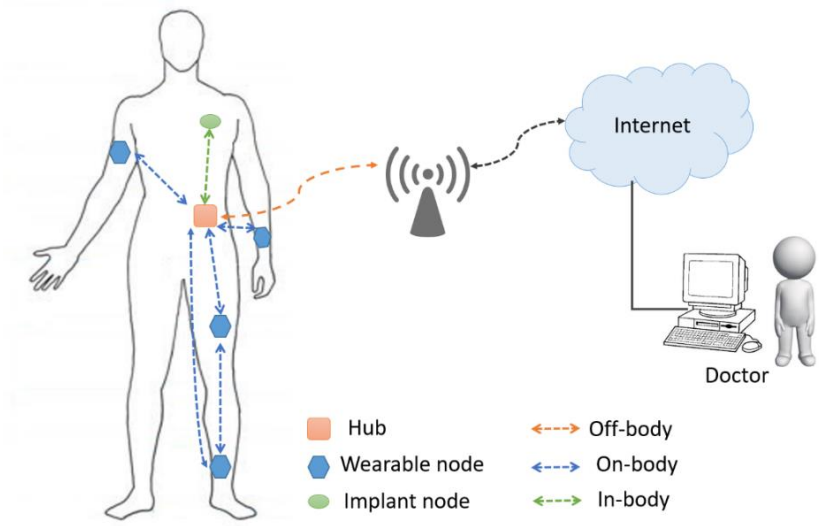

Figure 2.15. Example of a Wireless Body Area Network.

3.2.1. Applications of WBANs

One of the advantages of WBANs is that their use can be extended to a wide range of applications and areas, such as health care, military, sport or entertainment. Several scientific articles can be found in the literature describing and classifying examples of the applications of this type of networks. Also, many reference two big groups, those related to medical purposes and the non-medical applications, as categorized in the IEEE 802.15.6 standard (IEEE 2012). This standard establishes that the different senders (nodes) in these networks are given a priority over the others according to the type of service provided to the body area network, giving the maximum priority to the highest priority medical services. The priorities of the services are detailed below, from the services associated to the lowest priorities to the ones with the highest priority.

- Non-medical services (lowest priority)

- Mixed medical and non-medical
- General health services
- Highest priority medical services (highest priority)

Medical applications

The use of WBANs in medical applications can be very beneficial and useful for the society, since new and effective methods that allow the comfort and improvement in the quality of elderly´s lives are required because of the population aging. As shown in Figure 2.16(a) the aging of the population in Europe is noticeable, in 2001 the largest group of people was between 35 and 39 years old, while in 2016 people between 45 and 49 years old were more numerous. Moreover, this trend is expected to continue as can be seen from Figure 2.16(b), where the expected population pyramid in the year 2080 is represented, together with the distribution of the population in 2016 (Eurostat 2017). Some authors talk about an overload on the health care systems caused by a significant increase in the age of the population, so a shift in current health systems is required in order to meet the society's needs (Patel 2010; Movassaghi 2013). The use of these networks will not only be useful for elderly people, but also for the rest of population, since all the patients can take advantage of WBANs that make possible to continue their normal activities instead of going to a specialized medical service.

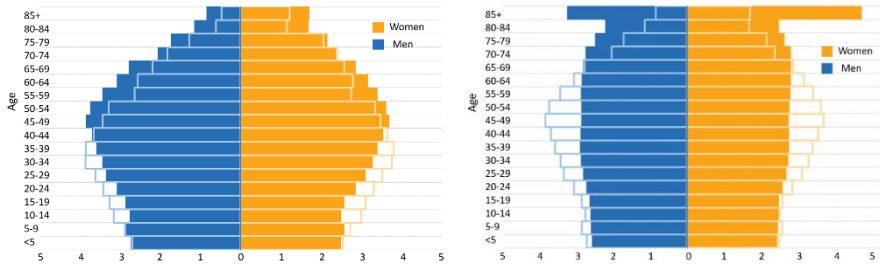

Figure 2.16. Population pyramids in Europe showing the distribution of the population by sex and by five-year age groups (a) solid color: 2016, bordered 2001; (b) solid color 2080, bordered: 2016

According to the different reviews and surveys carried out in the last years regarding these types of networks, the medical applications of WBANs can be categorized depending on the location of the sensors: on-body or wearable applications and in-body applications (Movassaghi 2013; Ullah 2009; Chen 2011). Some examples of this types of applications are given below.

- **Wearable applications:**

  - WBANs used by soldiers, firefighters and policemen

In this case, WBANs are used to report the activities and movements of soldiers in the battlefield to the commander. Also, the policemen and firefighters can take advantage of this technology, for example, by monitoring the levels of toxics in the air in order to send a notification if a life threatening level is detected (Latre 2011).

  - Sport Training

Athletes can control and tuned their training by means of WBANs allowing professionals to effectively measure the athlete training sessions and perform early diagnosis and treatment (Sabti 2015). Moreover, fatigue monitoring during training is important because of different reasons. First, sportspeople may need to be revitalized in order to maximize performance. Second, to aid injury prevention as tendon and muscle functions become impaired with overuse. Third, to diagnose post-injury rehabilitation.

  - Sleep Staging

Sleep disorders affect a significant part of the population, for example a 4% and a 2% of the male and female population respectively suffer from sleep apneas in Europe. Furthermore, the consequences of this disorder can be dramatic and lead to cardiovascular diseases, drowsy driving and sleepiness at work place. For these reasons sleep monitoring is of interest and techniques to implement a system capable of recording parameters while sleeping have been investigated in the last years. WBANs are a solution for sleep staging without the necessity of having cables around the patient, which disturb his/her sleep (De Vicq 2007).

  - Asthma

The detection of allergic agents in the air by monitoring environmental factors by means of a WBAN allows a real-time feedback to a professional or to the patient himself if possible. For example, Chu et al. (Chu 2006) developed a portable Global Positioning System (GPS) device that continuously consults a remote server by sensing users' reports to decide whether current ambient air quality will threaten their health.

  - Wearable health monitoring systems

In general, wearable sensors can be used by patients to sense their vital signs. One example is its use in electrocardiography (ECG) applications to provide appropriate information about the cardiovascular system. The use of wireless sensors has a definite advantage over the conventional ECG system, which usually needs 12 or 15 electrodes affixed to different parts of the body (Nemati 2012). Other examples of medical applications using wearable sensor systems that can substitute the cables are both, the electromyography (EMG) (kundu 2011; Hussain 2016) and the electroencephalographic (EEG) (Singh 2014).

- **In body applications:**

  - Diabetes control

There is a need of monitoring and treating Diabetes to avoid long-term medical issues derived from this disease and thus, glucose sensing techniques have been under active investigation. Minimally invasive, subcutaneously implanted devices can perform continuous glucose monitoring with the aim of giving a rapid response to glucose concentration changes (Zhao 2007).

  - Cardiovascular Diseases

Cardiovascular diseases are the principal cause of death in developed counties. About one-half of those who die do so within 1 hour of the start of symptoms and before reaching the hospital (Abidoye 2011). Using WBANs to continuously sense and transmit the information to a medical server is an improvement in this field of medicine.

  - Cancer Detection

A set of sensors integrated in a WBAN can be employed to distinguish between cancerous cells and healthy ones, identifying in this way tumors without carrying out a biopsy.

  - Endoscope capsule

Ingested implants, such as the radio pill employed in capsule endoscopy, are emerging technologies that contribute to the progress in these medical research area, since the capsule endoscopy permits to observe the complete length of the gastro-intestinal tract (Basar 2012).

  - Artificial retina

Retina prosthesis chips can be implanted in the back of human eye in order to assist people with no vision or with low vision to see (Abidoye 2011).

Non-medical applications

WBANs are also used for non-medical purposes. Some examples of these types of applications are listed below.

- Non-medical emergencies

Sensors located out of the body can detect emergency situations and communicate it to a person using wearable devices. For example, fire or gas leak situations in a home can be reported directly and quickly to the user (Movassaghi 2013).

- Real-time streaming

Real-time video and audio streaming are included in the many non-medical applications. One example of audio streaming is the use of headsets in a museum to listen the explanations given through voice communication (Movassaghi 2013; Kwak 2009).

- Entertainment and gaming

Gamers can use body sensors to get a feedback from the console after performing body movements or to be involved in a virtual reality scenario. This type of applications can involve different devices such as microphones, motion cameras, accelerometers, gyroscopes or head-mounted displays (Chen 2011; Movassaghi 2013). Moreover, the sensors attached on the body can be utilized for communicating to devices such as cell phones or music players for entertainment.

- Emotion detection

Biosensors can detect signals produced by the body due to physical manifestations, enabling in this way the detection of human emotions. For example, the consequences of fear are the increment of heart-beat and respiration rate, which leads to palm swearing. Biosensors implanted in the body or placed on the body or in the clothes can identify these symptoms (Movassaghi 2013).

- Secure Authentication

Biometric characteristics can be used for secure authentication in WBANs. In (Ramli 2013) a system to secure medical information using the patient electrocardiogram feature was proposed. The utility of various biometric characteristics for security purposes was analyzed in (Cherukuri 2003). These authors examined biometrics such as blood glucose, blood pressure, temperature or hemoglobin and analyzed whether they were random enough to be used to build the security system.

– Personal information sharing

Personal information can be stored in body sensors for many daily life applications such as shopping and information exchange (Jaimes 2016; Malik 2013).

3.2.2. WBAN Communication architecture

The communication architecture of a WBAN can be divided in three tiers:

- Tier 1: intra-WBAN communications. This tier refers to communications of about 2 m around the body, which includes the communication between nodes placed inside, on or close to the body and the communication with the hub.

- Tier 2: inter-WBAN communications. Although the node-node and the node-hub communications can be enough in the applications that not require real-time feedback and the hub stores the data for further processing, usually a connection to other networks is required. The aim of this tier is to interconnect WBAN with these other networks. In the example of the previously shown Figure 2.15, the inter-WBAN communication is made between the hub and the access point. This last device can be considered part of the infrastructure or can be strategically placed in a dynamic environment in order to handle emergency situations.

- Tier 3: beyond-WBAN communications. The design of this communication tier is for use in metropolitan areas. The beyond-WBAN refers to the final network and it can be connected to the inter-WBAN network by means of a gateway. The deployment of this last tier is specific for the involved application.

3.2.3. RF Communication technologies: frequency bands, interferences and coexistence with other technologies

Different wireless technologies can be used for establishing communications in a WBAN. Concretely in the case of RF communications, these networks can work at different frequencies that are regulated by the corresponding authorities in this regard.

Frequency bands

One of the reference documents that should be considered by regulatory bodies is the IEEE 802.15.6 standard (IEEE 2012), which distinguishes between narrowband physical layer (PHY) and ultra wideband (UWB) PHY. Table 2.3 and Table 2.4 show the operating frequencies and the corresponding channel bandwidths for narrowband and UWB PHY. As shown, there are seven different frequency bands for RF WBANs operating in narrowband PHY and the channel bandwidths vary from 300 kHz to 1 MHz in these cases. The UWB band is divided into two band groups: low band (3.24-4.75 GHz) and high band (6.6-10.25 GHz).

Table 2.3. Frequency bands in narrowband systems.

Narrowband	
Frequency Band (MHz)	**Channel Bandwidth**
402-405	300 kHz
420-450	320 kHz
863-870	400 kHz
902-928	400 kHz
950-958	400 kHz
2360-2400	1 MHz
2400-2483.5	1 MHz

Table 2.4. Frequency bands in UWB systems.

Ultra wideband	
Frequency Band (Ghz)	**Channel Bandwidth**
3.24-4.75	499.2 MHz
6.6-10.25	499.2 MHz

The work developed in this thesis is focused on the 2.4 GHz band, which is one of the frequency bands for industrial, science and medical (ISM) applications. In the 2.4 GHz band, the IEEE 802.15.6 standard specifies that a transmitter shall be capable of transmitting at least −10 dBm EIRP, but devices should transmit lower power when possible in order to reduce interference to other devices and systems and to protect the safety of the human body. At these frequencies there are 79 channels. The relationship between center frequency f_c and channel number n_c is given by equation (2.17)

$$f_c = 2402 + 1 \times n_c\ (MHz), n_c = 0, \dots, 78 \qquad (2.17)$$

Interferences

The unlicensed ISM bands are defined by the ITU and the frequency range from 2.4 GHz to 2.5 GHz is widely used in WBAN applications, in part because of its worldwide availability (Cavallari 2014). However, as it is an unlicensed part of the spectrum, coexistence issues must be considered when designing the body area network. Cavallari et al. studied these types of coexistence problems in WBANs in their survey carried out in 2014 (Cavallari 2014). Also, other research works investigating this issue can be found in the scientific literature as described below. Some authors analyzed the interference caused by IEEE 802.11 networks in devices using the IEEE 802.15.6 (2012) or the IEEE 802.15.4 (2006) standards (Chen 2009). The latter specifies the physical and medium access control (MAC) layers for short-range wireless communications and its first version was published in 2006. For example, in (De Francisco 2009) and (Chen 2009) experimental measurements to test these technologies were carried out in a hospital room and in an apartment, respectively. Yuan et al. (2007) proposed a coexistence model for these standards and verified it by means of simulations. In (Martelli 2012) authors concluded that an appropriate WBAN channel selection is crucial when WiFi interference is present and the procedure to select this channel should be periodically repeated due to the high variability of the environment where body area networks operate. Interference from house appliances, such as microwaves was also investigated in (Huo 2009) and authors concluded that the impact of this interference source was negligible for distances longer than 2 m.

It has to be emphasized that interference in WBAN is not only due to other transmitting devices such as user equipment or base stations, but also because of other WBANs in the closest environment. An example of this is depicted in

Figure 2.17. The nodes in a WBAN can be centrally coordinated by the hub so interference between the nodes of one network can be solved easily. The problem comes when multiple people wearing WBANs come into range of each other, since people's movements are unpredictable (Boulis 2012). The inter-WBAN interference occurs when there is no coordination between the different networks, and several interference mitigation schemes have been proposed with this regard (Yang 2011; De Silva 2009).

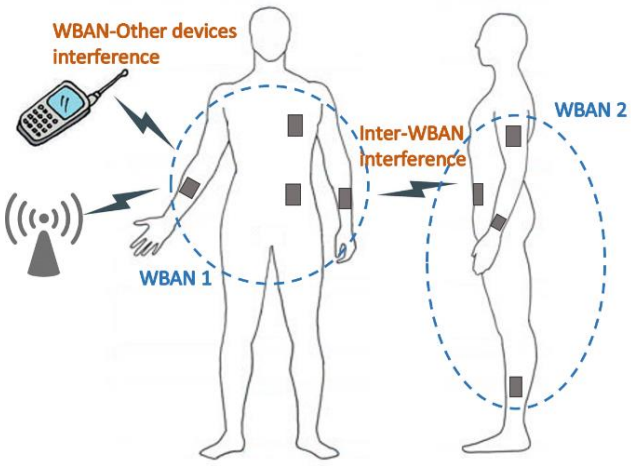

Figure 2.17. Interferences in WBANs

Radio technologies in WBANs

Different radio technologies can be used to implement a WBAN. In addition, communication between WBANs and other wireless networks is crucial, and thus, at least one node in a body network, which can be the hub, should be capable of sending or/and receiving information from WLANs, Bluetooth or cellular networks (Domenicali 2007). Due to the quite large number of available standards, it is necessary to identify the best solution, depending on the application requirements. In the surveys carried out by Movassaghi et al (2013) and Chen et al. (2011) the technologies employed in different projects on WBANs were detailed. Some of these projects using different RF technologies in the 2.4 GHz band are summarized in Table 2.5, showing also the application purpose of each project.

Table 2.5. Technologies employed in different projects on WBANs.

Project	Application	Intra-WBAN Comm.	Inter-WBAN Comm.	Beyond WBAN Comm.
MIMOSA (Jantunen 2004)	Several	Bluetooth, Wibree, RFID	UMTS, GPRS	Internet
CareNet (Cao 2008)	Remote healthcare	N/A*	IEEE 802.15.4	IEEE 802.11
MobiHealth (Wac 2009)	Ambulatory patient Monitoring	Bluetooth	IEEE 802.11, GPRS, UMTS	GPRS/UMTS
WHMS (Milenkovic 2006)	Health monitoring	Zigbee	WLAN	Internet
MAHS (kang 2007)	Healthcare	Bluetooth	Wireless Network	Internet
LifeMinder (Ouchi 2002)	Daily selfcare	Bluetooth	Bluetooth	Internet
Asnet (Sheltami 2006)	Health Monitoring	WiFi	WiFi, Ethernet	Internet, GSM

* The sensors communicate directly with the base stations (two-tier network)

3.2.4. Antenna design

The design of antennas for WBANs is a great challenge due to different factors that can degrade the performance of the sensor network, such as the adaption of the antenna to the shape of the human body or suiting it for wearers' comfort. In the scientific literature can be found several proposals that are less or more suitable depending on the antenna substrates, being more appropriate those solutions designed using stretchable materials (Ma 2008; Salonen 2004; Arriola 2011; Cheng 2009).

One of the main differences when working with these networks is that reliable communication with each node is vital, as opposed to the redundant character of information sensing and exchange in regular wireless sensor networks (WSNs). For this reason, the location of the sensor containing the antenna is particularly important in specific situations, for example in acceleration measurements for biomechanical analyses (Nordsborg 2014; Sabti 2014). In (Sabti 2014) authors analyzed the best node locations on a human body in order to get the maximum connectivity at 2.4 GHz with the receiving node placed on the chest. The experiments were carried out while the participants were running in a sports field to consider body movements in these kinds of activities.

Apart from the above mentioned challenges, the main drawback when designing an antenna to be used in a WBAN is due to the interaction between the antenna and the body tissues. The human body itself can reduce significantly the antenna efficiency, since part of the power radiated from such antenna is absorbed by the tissues. Several techniques have been proposed in order to reduce the interaction between the body and the antenna, some examples are the use of band-gap (EBG) structures (Zhu 2009) or substrate integrated waveguide (SIW) cavities (Kaufmann 2013). However, the sizes of the wearable antennas using these methods are too big to be implemented on small wearable wireless sensors.

The power absorbed in human body is another key aspect of interest, as the transmitters operate in close proximity to the body. The evaluation of the SAR is crucial for the compliance with the safety levels assigned by international standards (ICNIRP 1998; IEEE 2005), and it is often investigated (Anguera 2012; De Santis 2012; Risco 2012; Soh 2015). Designing efficient antennas while maintaining a low SAR is one of the challenges in body area networks. Specifically in the case of 2.4 GHz band, several antenna designs with low SAR have been proposed, e.g. the inverted-F antenna by Sabrin and Rahman (2015), the patch antenna by Rosaline et al. (2015). In (Soh 2015) the exposure of textile antennas was evaluated at different frequencies including the 2.45 GHz, and they concluded that most measured SAR values were well below their respective simulated equivalent.

Regarding the biomedical implants, only non-corrosive and biocompatible material can be employed, such as titanium or platinum. These devices have to work in highly dissipative and dense media (muscle, brain…) and, thus, the surrounding environment of the antenna is different depending in the location. The impedance matching in these antenna designs is essential and hard to achieve, especially when the implant moves inside the body since the surrounding tissue properties vary. In the last years, some antennas that operate inside the human body at 2.45 GHz have been proposed, such as cavity slots antennas to be embedded on the arm (Xia 2009; Usui 2006) or capsule-shaped antennas (Dissanayake 2009).

PART 1: EMF EXPOSURE IN THE FAR FIELD REGION

CHAPTER 3: METHODOLOGY FOR ASSESSING WIFI EXPOSURE

In this chapter a new methodology for assessing WiFi exposure is proposed. Firstly, the drawbacks of actual procedures for measuring WiFi signals are described and several tests carried out to prove the disadvantages and inaccuracies of these methods are presented. Secondly, a procedure for determining the optimal spectrum analyzer configuration that allows obtaining accurate WiFi signal samples is defined. This procedure is based in time and frequency domain measurements. However, the final configuration for assessing human exposure to WiFi signals requires only frequency domain measurements, simplifying in this way the measurement procedure. Finally, the measurement methodology based on the proposed configuration is presented, giving an example of the WiFi exposure assessment.

1. INTRODUCTION

RF fields are usually measured in order to be compared with electromagnetic exposure limits defined by international standardization organizations with the aim of preserving the human health. In the case of WiFi signals, there is special concern about this radiation since WLAN that use this technology are increasingly being deployed in indoor environments, such as homes, schools or offices and the transmitters are very close to people.

However, accurate measurement of WiFi radiation coming from user terminals and access points is a great challenge due to the nature of these emissions, which are non-continuous signals transmitted in the form of pulses of short duration. One of the major problems when measuring these signals is that the measured levels depend directly on the measurement system and its configuration (Verloock 2010). Most of the methodologies defined up to now for determining WiFi exposure levels use or take as reference exposimeters, broadband probes and spectrum analyzers without taking into account that WiFi signals are not continuously transmitted. This leads to an overestimation of the radiation level that cannot be considered negligible when data of the actual exposure are needed. To avoid this, other procedures apply empirical weighting factors that account for the actual duration of burst transmissions (Bechet 2012; Miclaus 2014). However, this implies the implementation of additional measurements for calculating the weighting factors, and thus, increases the complexity of the work. According to this, it was still necessary to define the frequency domain measurement setup that is optimal for obtaining realistic WiFi signal values, without requiring the performance of additional recordings. Thus, the definition of an appropriate methodology to achieve this goal was established as one of the main objectives of this chapter. The set of tasks carried out to identify such configuration, as well as the limitations obtained for other measurement settings have been deeply investigated.

Previous knowledge regarding emissions in the form of pulses

Before assessing WiFi exposure, previous experience regarding signals transmitted in the form of bursts had been acquired, since techniques to characterize impulsive noise were investigated. In fact, impulsive noise can be considered as emissions that are present only for a certain percentage of the time, usually consisting of pulse trains of a limited short duration and sometimes repeating at a certain rate (ITU 2009). As happens in the case of WiFi emissions,

when measuring this type of radio noise, the measured levels also depend on the receiver configuration due to the nature of the emissions.

To illustrate this, several examples of radio impulsive noise and WiFi signal emissions are depicted in Figure 3.1. Time domain measurements were taken using a spectrum analyzer and in both cases rough transitions from low power levels to much higher power levels can be seen. The duration of the pulses depends on the noise source in the case of impulsive noise and on the data traffic in the case of WiFi signals. Figure 3.1(a) and Figure 3.1(b) show impulsive noise emissions at 1720 kHz generated when turning on flickering and fluorescent lights, respectively. Measurements from the signals transmitted by an access point at 2417 MHz when there was no data traffic or it was very low are represented in Figure 3.1(c) and recordings taken at 2457 MHz when data traffic was produced due to a file download are illustrated in Figure 3.1(d). As shown, although the frequencies of the emissions are different, the nature of these signals is quite similar.

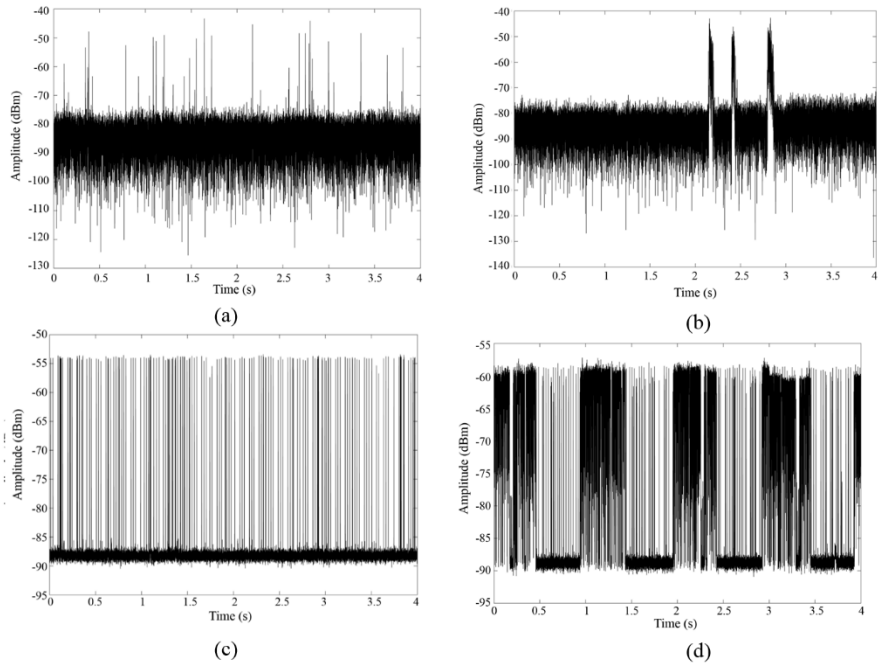

Figure 3.1. Measured emissions (a) of impulsive noise produced by turning on flickering lights, (b) of impulsive noise generated by turning on fluorescent lights; (c) of WiFi signals when there is low data traffic, (d) of WiFi signals when data traffic is generated due to a file download.

A procedure for measuring and characterizing impulsive noise emissions from specific sources was developed. In that first work, the methodology was based only on time-domain measurements since the measurement duration was very short. The objective was to record samples of the noise produced by some devices when performing specific actions, such as switching on a computer, so only few seconds were necessary to obtain the noise samples. This is not the case of WiFi exposure assessment, since longer measurement durations are required and the knowledge of the signal level in the whole WiFi channel or WiFi band is needed.

Regarding the procedure for noise assessment, the integration of the peaks of a pulse train into a burst was investigated and several steps were found to be necessary in order to achieve this integration. First, a distinction between the impulsive noise and the Gaussian noise (WGN) had to be performed (see Figure 3.2). For this purpose, a threshold was set to 13 dB above the root mean square (RMS) value of the Gaussian noise and all the samples above this threshold were treated as impulses. This threshold was selected because 13 dB is the crest factor for WGN, which is the difference between the RMS and the peak value (ITU 2012). Second, the impulse noise samples had to be integrated into bursts. The methodology for including samples in a burst was based on ITU-RSM.1753 (ITU 2012), but some contributions were added.

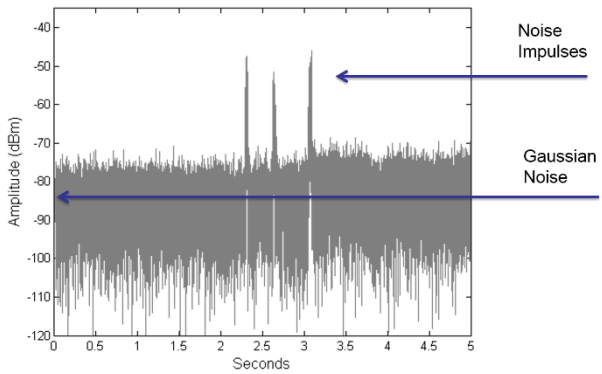

Figure 3.2. Distinction between gaussian and impulsive components.

Once the bursts were defined, four parameters were found to be appropriate for describing the impulsive noise generated by a main source:

- the burst amplitude,
- the burst duration,

- the number of bursts,
- and in the case of more than one burst, the separation between them.

These two last parameters were added to those defined in (ITU 2012). Moreover, as there were changes in the pulses amplitude, the burst amplitude was defined as the linear average of all samples belonging to a burst, regardless of whether they were above or below the threshold.

An example of the combination of pulse trains to bursts is depicted in Figure 3.3. On the left figure, the measured noise samples, the RMS of the Gaussian noise and the calculated threshold are shown. Each burst is comprised of all the noise samples located between the first impulsive sample of a burst and the last one. Combining pulses to bursts ensures that more than 50% of all samples inside each burst are above the threshold. Consequently, some samples below the threshold can be part of a burst if they satisfy some conditions. In the figure on the right the results presentation is provided and as shown, four bursts can be distinguished.

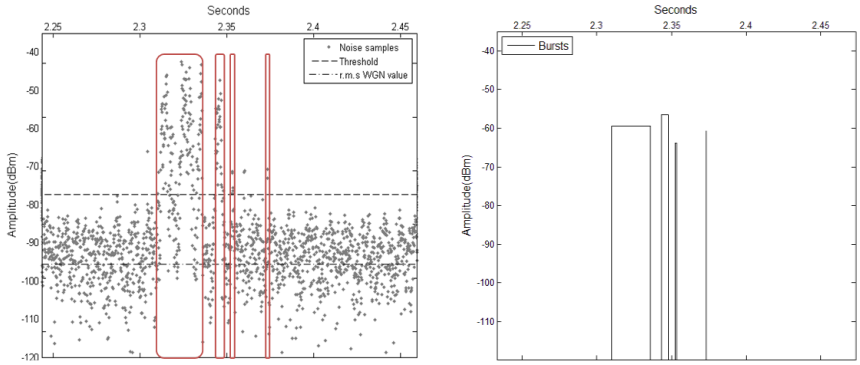

Figure 3.3. Example of combination of pulses to bursts (a) radio noise measurement, (b) presentation of impulsive noise results.

After defining the procedure for measuring and characterizing the impulsive noise, the impulses produced by several events were analyzed, the event being understood as the change in the operation of a device. Specifically, the noise produced by a power supply, a computer CPU, fluorescent lights and flickering fluorescent lights was studied. The studied impulses were associated to plugging in and unplugging the power supply, turning on the computer and turning on the lights, in the case of the flickering ones they flickered for few seconds before turning on completely. The noise was measured at different frequencies free of

local emissions, between 630 kHz and 1910 kHz. The average burst duration obtained for the power supply ranged between 0.25 ms and 1.45 ms, longer bursts were found when unplugging it and in all the cases a unique burst was found. In the case of the computer CPU, the average burst duration took values between 0.39 ms and 0.70 ms and bursts were separated between 0.49 ms and 1.25 ms. When turning on eight fluorescent tubes simultaneously much longer bursts were observed, varying the average duration from 25.29 ms to 48.95 ms, while in the case of turning on seven flickering fluorescent tubes at the same time several bursts appeared, between 27 and 34, with an average duration between 0.48 ms and 0.64 ms and larger burst separation than in the other measurements was observed, between 104.60 ms and 146.31 ms.

The obtained results are comparable to WiFi bursts. For example, when there is no traffic, beacon signals are transmitted by the access point and, as described in the following sections of this chapter, in the measurements taken in controlled conditions, these beacons had a duration of 0.5 ms and were separated 50 ms. When data traffic existed, the bursts were longer and the separation between consecutive bursts decreased. As WiFi exposure assessment has to be done in a wide range of frequencies, taking time domain measurements is not practical, since measurements at many frequencies are required. For this reason, the development of a methodology based on frequency domain measurements for assessing WiFi exposure was established as one of the main objectives of this chapter. The procedure followed to achieve this goal implies time domain measurements in order to fully characterize the WiFi signal levels.

2. EXISTING METHODOLOGIES FOR MEASURING WIFI EXPOSURE LEVELS

Several guidelines and standards have been developed in order to provide general information and techniques for measuring EMFs. However, in the case of WiFi signals they do not provide specific information (ICNIRP 1998; CENELEC 2008). One of the main drawbacks in this regard is that the accurate assessment of this type of radiation poses a challenge because of the quasi-stochastic nature of these emissions resulting from their transmission in the form of bursts. Inexpensive radiofrequency detectors can lead to misleading results (Foster 2015; Bolte 2016). Moreover, the configuration of specialized equipment, such as spectrum analyzers, has significant influence on the obtained values (Verloock 2010). In fact, the influence in the frequency domain of different parameters of a spectrum analyzer when measuring WiFi signals was analyzed in (Betta 2008), considering a power meter equipped with a broadband probe as a reference system. The use of these instruments is suitable for having a rough approximation of exposure that may be useful as long as the levels are well below the exposure limits. Hence, the accuracy of the measurements can be improved if a more appropriate reference system is taken. As stated in (Letertre 2011) and (Adamson 2010), broadband probes do not provide enough accuracy for measuring the radiation caused by OFDM communication systems, and thus, it is necessary to employ other instruments when the objective of the measurements is to obtain realistic values to be used, for example, in medical studies carried out for the characterization of the influence of specific signal levels on the human body, or in the design of network planning methodologies according to criteria based on the actual exposure conditions.

Different methods for measuring human exposure due to WiFi signals with a spectrum analyzer have been defined. Nevertheless, there is still no standardized methodology for this purpose. The most common technique considered up to now is to record maximum power values in the frequency band of interest, so as to analyze the worst-case scenario. However, this also implies an overestimation of the radiation, which could derive in overly restrictive deployment policies because of social concern.

To avoid this, some authors introduced weighting techniques that account for the time variability of these emissions. In (Verloock 2010) an empirical factor called duty cycle T (%) was defined as the ratio of the pulse duration or active duration t_{active} (s) to the total duration t_{tot} (s) of the WLAN signal, in order to consider the time variability of the signal in a specific situation:

$$T = 100 \cdot \frac{t_{active}}{t_{tot}} \ [\%] \qquad (3.1)$$

The duty cycle is estimated from time domain measurements and it has to be calculated for the different active channels, with f_c equal to the channel center frequency (2412 MHz + 5·k MHz, k = 0,…, 12). This results in a measurement time, which is 13 times larger if 13 WiFi channels are present.

Then, the total average electric field E_{tot}^{avg} has to be calculated by multiplying the electric field obtained from frequency domain measurements E_{tot}^{active} with the corresponding duty cycle:

$$E_{tot}^{avg} = E_{tot}^{active} \cdot \sqrt{T} \ [V/m] \qquad (3.2)$$

Also, the spectrum analyzer settings in the frequency domain for measuring maximum signal levels that should be subsequently weighted by that factor were analyzed in that study. These settings as well as the ones employed for calculating the duty cycle are summarized in Table 3.1. As shown, the given parameters are aimed at obtaining WiFi levels in the whole 2.4 GHz WiFi band.

Another approach that takes into account both the amplitude and time variability of the received signals was described in (Trinchero 2008; Bechet 2012; Miclaus 2014). In that case, the weighting factor WF was determined as the ratio of the time-averaged power level $P_{timeAverage}$ to the maximum power level of the signal $P_{timeMax}$:

$$WF = \frac{P_{timeAverage}}{P_{timeMax}} \qquad (3.3)$$

As in the previous case, the maximum electric field obtained from the frequency domain measurements has to be multiplied by the weighting factor in order to obtain the total average electric field value. The spectrum analyzer settings in the time and frequency domain that were selected as appropriate for assessing WiFi exposure using this weighting factor are also summarized in Table 3.1. In this case, the given parameters are aimed at assessing WiFi exposure in one of the channels of the 2.4 GHz frequency band.

Table 3.1. Spectrum analyzer settings proposed in two studies for assessing WiFi exposure considering wighting factors.

	Settings from (Miclaus 2014)		Settings from (Verloock 2010)	
Parameter	**Value in the time domain**	**Value in the frequency domain**	**Value in the time domain**	**Value in the frequency domain**
f_c	Channel f_c	Channel f_c	Channel f_c	2.45 GHz
Span (MHz)	0	20	0	100
RBW (MHz)	1	1	1	1
SWT (ms)	1	20	1	10 if signal is not known t_{active}·n if signal is known*
VBW (MHz)	3	3	10	10
Detector	RMS	RMS	RMS	RMS
Trace	clear/write	Max hold	clear/write	Max hold
Number of sweeps	1700	Until stable status (4 min)	2200	Until stable status or 1 min

* n is the number of display points

All the above mentioned techniques were the solution adopted in different measurement campaigns carried out to assess human exposure to WiFi emissions. For example, the electric field coming from access points and portable devices when doing different activities was analyzed from recordings taken by means of exposimeters (Pachón-García 2015; Gallastegi 2016) or other frequency selective radiation meters (Karipidis 2017). Max-hold WiFi measurements given by a spectrum analyzer were studied for different environments in (Schmid 2007). In (Verloock 2014) different values of the Duty Cycle were considered to correct the empirical measurements. Nevertheless, the methodologies defined in all the previous studies were not optimal. In the case of portable exposure meters, uncertainties due to different factors such as the body influence have been reported in (Bolte 2011). Moreover, the maximum values of WiFi exposure do not reveal a realistic situation and, although these maximum levels can be corrected by using weighting factors, two types of recordings are required in that case: one in the frequency domain to determine those maximum levels, and another in the time domain to fix the proper weighting value for the characteristics of the environment and users' activity under test.

Bearing in mind the problems derived from the previous methodologies, a rigorous procedure to identify the optimal configuration for determining realistic WiFi exposure values was established as the main objective of this work. That

optimal configuration must allow acquiring samples only and exclusively in the frequency domain.

The procedure developed for identifying that configuration has been based on both time and frequency domain measurements. The first type of measurements was necessary to obtain a set of reference samples of the radiation caused by a perfectly known WiFi signal. Once obtained those reference samples, they were compared with the levels registered for the same type of signal considering different values of the spectrum analyzer parameters in order to analyze their influence on the measurements. Finally, the optimal configurations for taken measurements in one WiFi channel and in the whole WiFi band were identified from recordings taken for different cases of WiFi reception.

3. SELECTION OF THE MEASUREMENT INSTRUMENTS

The measurement instruments that are commonly used to acquire values of the exposure to EMFs are broadband probes, exposimeters and spectrum analyzers. As stated in the previous section, the first ones do not provide enough accuracy for measuring the radiation caused by OFDM communication systems, and thus, they were discarded for the acquisition of WiFi radiation samples in the frequency domain.

3.1. Equipment selection

Among exposimeters and spectrum analyzers, it is logical to assume that the second ones are the best option for recording values of the radiation caused by different types of signals, in different environments and under very different conditions, since most of the models include several parameters and options that confer them great measurement versatility. Even so, a set of tests carried out to compare the accuracy of a professional spectrum analyzer connected to a tri-axial antenna with the one provided by a portable exposimeter were initially performed as part of the tasks carried out in this study to identify the optimum solution for obtaining realistic WiFi exposure values.

The specific models utilized to do this were the EMI ESPI3 spectrum analyzer of Rohde & Schwarz (R&SEspi) and the EME Spy 200 exposimeter of Satimo (EME SPY) (Figure 3.4).

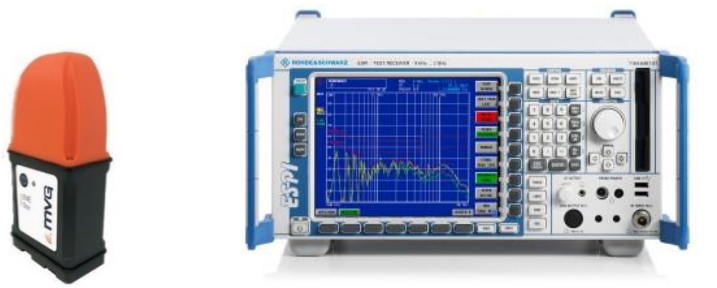

(a) (b)

Figure 3.4. (a) Exposimeter EME Spy 200, (b) Spectrum analyzer EMI ESPI3.

Both of them were selected because they fulfill the specifications defined for the professional equipment to be used for exposure assessment. Nevertheless, the conclusions derived from the results included not only in this section, but also in the following ones are applicable to a great variety of models such as Agilent

E4402B or Agilent E443A from Keysight technologies (Keysight), MS2840A from Anritsu (Anritsu) or FSC from Rohde and Schwarz (R&SFSC) in the case of spectrum analyzers, and ExpoM-RF from Fields at Work (ExpoM) or ESM-140 from Maschek (ESM) in the case of exposimeters, since according to their data sheets all of them present similar measurement characteristics.

Figure 3.5 shows the differences for a set of WiFi field strength samples recorded with both instruments at the same time, separated each other a distance of 40 cm in order to ensure the corresponding far field conditions (Rappaport 2010). Ten measurements of 6-minute duration were taken at two different positions (in total, twenty measurements with each equipment) and the electric field levels were averaged over these 6 minutes, as recommended by the ICNIRP (1998).

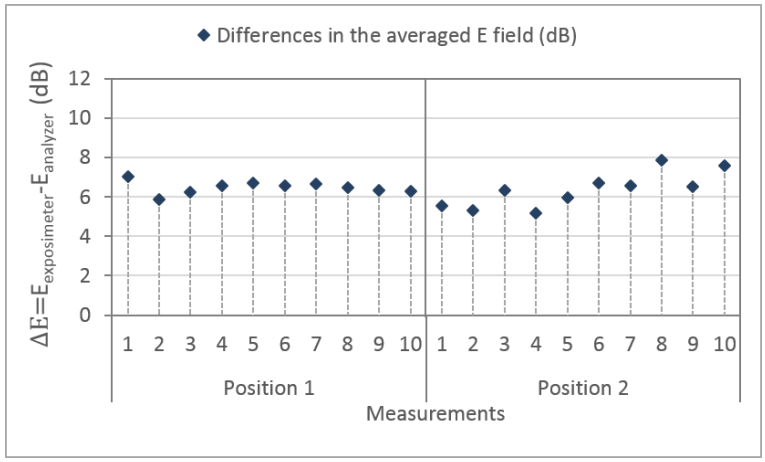

Figure 3.5. Difference between the averaged electric field measured with the exposimeter and with the spectrum analyzer.

As deduced from the curves depicted in that figure, the levels measured with the exposimeter were always higher than the ones recorded with the analyzer. This is in part because the minimum detection threshold of the exposimeter is 5 mV/m, and consequently, that was the value stored by this instrument when lower levels were received. On the contrary, the spectrum analyzer not only captured levels below that threshold, but also recorded samples four times faster than the EME Spy, concluding that it is a better option to obtain empirical values of the radiation caused by amplitude and time varying WiFi signal bursts.

3.2. Equipment configuration

Nevertheless, it has to be considered that the accuracy of the spectrum analyzer is directly related with the configuration used during the measurements, the comparison between the exposimeter and the analyzer previously described was done using the clear/write trace and the RMS detector of the spectrum analyzer. These two parameters were selected in order to take actual values of the signal sample. In contrast to other trace modes, the clear/write trace erases any data previously stored in the trace and continuously displays the signal received at any time. For this reason, in order to reach our objective this trace mode is more suitable than the max-hold trace, which maintains the maximum level for each point in a trace and only updates each point if a new maximum level is detected in successive sweeps. With regard to the detector, it is used to compress the data samples measured in a sweep into the number of displayed pixels. An overview of the results obtained by means of using different types of detectors is provided in Figure 3.6, which is based on the example presented in (R&S 2003). In this figure, 8 samples per pixel are used and as shown, the displayed sample is different for each detector type. The sample detector samples the envelope voltage only once per pixel and displays that result on the screen, so using the sample detector can cause a significant loss of information. The positive peak and negative peak detectors displays the highest and the lowest level detected within the pixel respectively.

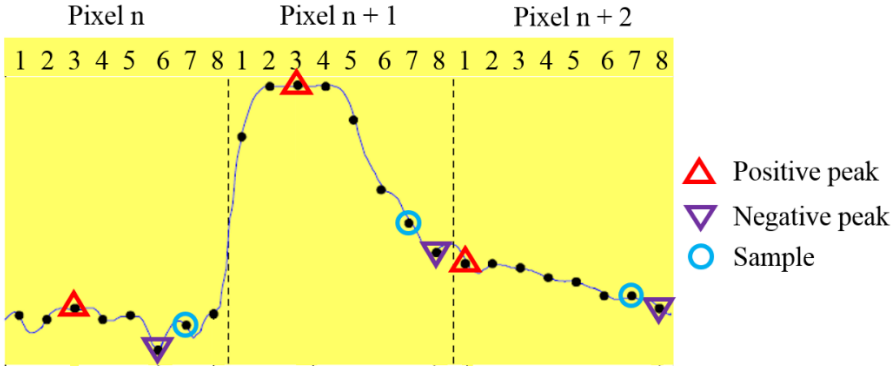

Figure 3.6. Results obtained when using different types of detector.

The RMS detector is not depicted in the example because it does not take one of the detected samples as a result. Instead, it considers all the detected samples within the pixel for calculating the RMS power level.

3.2.1. Preliminary tests

Some preliminary measurements were performed to test the influence of the spectrum analyzer settings on the obtained WiFi levels. One channel measurements of 6 min duration were carried out in controlled conditions when there was no data traffic and thus, only beacon signals were transmitted by the access point. First, a configuration defined for taking actual signal samples (Test 1) was compared with a configuration aimed at obtaining worst-case exposure levels (Test 2). The spectrum analyzer was equally configured in the two tasks, except for the trace mode. The clear/write trace was selected for obtaining the actual WiFi levels and the max-hold trace in the second case. In both cases, the sweep time (SWT) was set to 2.5 ms, the resolution bandwidth (RBW) to 0.3 MHz, the video bandwidth (VBW) to 1 MHz, the sweep points (SWP) to 501 and the RMS detector was used. Table 3.2 shows the average electric field strength measured using these two setups and differences in the mean electric field of up to 28.54 dB were found.

Test 3 consisted on weighting the electric field level obtained from Test 2 (levels obtained using the max-hold trace) in order to consider the temporal variations of the signal. The weighting factor was calculated following equation (3.1) and the final electric field using (3.2). In the studied scenario, the beacon period was equal to 50 ms and the duration of the beacons, this is the t_{active}, was 0.5 ms. Consequently, a weighting factor of 1% was obtained. The difference in the average field level between the one calculated in Test 3 and that obtained when measuring the actual signal levels in the first setup was equal to 8.54 dB, as may be seen from Table 3.2.

As in the work developed by Verloock et al. in (2010), they proposed a formula for calculating the appropriate SWT that should be used to perform the frequency domain measurements when the signal is known, the next step was to repeat Test 2 and Test 3 using the corresponding SWT for a known burst. Having knowledge of the value of the t_{active} and the SWP, the equation proposed in (Verloock 2010) for calculating the optimal SWT is:

$$SWT = t_{active} \cdot SWP \qquad (3.4)$$

In our case, the number of display points of the spectrum analyzer was 501, obtaining a SWT of 250 ms. Test 4 was performed setting this value of SWT and using the max-hold trace. The result of Test 5 was obtained after weighting the field level of Test 4 by the weighting factor previously calculated. The average electric field strength obtained in these two tests are also presented in Table 3.2.

Table 3.2. Average electric field levels obtained in the different tests.

	Method	***SWT***	E_{avg} ***(dBμV/m)***
Test 1	Clear/write trace	2.5 ms	61.97
Test 2	Max-hold	2.5 ms	90.51
Test 3	Max-hold and weighting factor	2.5 ms	70.51
Test 4	Max-hold	250 ms	86.12
Test 5	Max-hold and weighting factor	250 ms	66.12

As shown when using a weighting factor, results approach much better to the actual exposure. However, in this case two measurements are required. The described examples were done when no data traffic was generated, thus in all the other situations the weighting factor would be higher and the final average electric field value would be weighted in a smaller proportion. In addition, when there are different traffic situations, an appropriate weighting factor for each case is necessary, increasing in this way the number of measurements.

But even when using a spectrum analyzer which is not configured for taking max-hold measurements, the setup of the equipment can have a significant influence on the results. Some more measurements of 6 minutes were taken in the same scenario, using the clear/write trace together with the RMS detector and varying only the SWT from one test to another. Changing only the SWT parameter between 2.5 ms and 100 ms led to differences in the median measured power levels of 4.6 dB and differences in the maximum measured power levels of 12.3 dB.

Having concluded that an analyzer configured to use the clear/write trace together with the RMS detector and connected to a tri-axial antenna is a more accurate and versatile measurement solution than an exposimeter, the following step was to identify the optimum configuration for acquiring realistic WiFi exposure values by performing measurements only and exclusively in the frequency domain. To do this, a comparison of a set of reference levels measured in the time domain for a perfectly known WiFi signal with the ones obtained for the same type of signal with different frequency domain configurations was required. Details in this regard, as well the corresponding results and conclusions are given in this chapter.

4. METHODOLOGY FOR DETERMINING THE OPTIMAL CONFIGURATION

4.1. Description of the measurement scenario

The time and frequency domain measurements required to determine the optimal configuration of the spectrum analyzer for measuring accurate WiFi exposure levels in the frequency domain were performed in a laboratory of the University of the Basque Country, Spain, where a Cisco Aironet 1702 Access Point (Cisco 2016) provides access to the Eduroam WiFi network of the university. Tests were carried out at night from 00:00 to 05:00 in order to guarantee that no one was within the coverage area of that access point and that all the computers located in that area were turned off, ensuring this way that the only traffic received was the one produced for the testing. Furthermore, during the post-processing phase, all the recordings were analyzed to check that the received signals matched exactly the WiFi activity desired for the trials. Specifically, for those time and frequency domain measurements carried out to analyze the levels recorded when the access point was working in idle mode, it was confirmed that, as described in the IEEE 802.11 standard (IEEE 2016), only beacons were received periodically, while in the rest of cases, bi-univocal correspondence was observed between the signal traces and the data bursts particularly generated for tests. The access point operated on Channel 1 of the frequency band allocated to services that implement the IEEE 802.11g standard. The center frequency and bandwidth of this channel are 2.412 GHz and 20 MHz respectively. Also, it comprises 64 subcarriers equally spaced 312.5 kHz and modulated by applying the Orthogonal Frequency Division Multiplexing (OFDM) technique, so that the signal is concretely transmitted on subcarriers -26 to -1 and 1 to 26, being the 0 subcarrier the one located at the center frequency previously mentioned, as described in (IEEE 2016).

According to the IEEE Standard C95.3 (IEEE 1991), the measurement of potentially hazardous exposure fields coming from a well-known single-source may be performed with a tunable field-strength meter connected to a directive antenna, which in fact makes full sense, since in that case the exposure levels come from the specific location where that source is placed. Thus, bearing in mind that the objective of the study here described was to define a measurement methodology for determining the optimal settings to record actual WiFi radiation values and that it was necessary to use different WiFi signals coming from a specific access point for achieving that purpose, a Yagi antenna suitable for carrying out measurements in the 2.4 GHz WiFi band and was selected as

appropriate solution to be connected to the spectrum analyzer. Such antenna is shown in Figure 3.7 and it was installed on a mast, aiming at the access point from a distance of 2 m in order to receive as much power as possible from the radiation source under study. Besides, a computer using a wired Ethernet connection to the analyzer was employed to establish the analyzer configuration and save the recorded data. A laptop was used to generate data traffic from the access point.

Figure 3.7. Yagi antenna suitable for the 2.4 GHz frequency band.

During the trials, several data files of three different sizes were downloaded from a server that was part of the same local area network as the access point, so Internet traffic constraints were negligible. Also, two working modes of the access point were considered:

- idle mode, where only beacon packets are transmitted,
- traffic mode, in which apart from the beacons data traffic is generated.

Details of the specific tests performed for each mode are given in the following subsections, where the three measurement phases of the defined methodology can be distinguished.

4.2. Phase 1: Acquisition of reference WiFi exposure values

The purpose of the first trials carried out with the measurement system previously described was to obtain a set of samples of the radiation caused by a perfectly known WiFi signal to be used as reference values for determining the optimal frequency domain configuration of the spectrum analyzer.

To do this, the power levels of the signal generated by the access point when working in idle mode were recorded in the time domain using the configuration indicated in the first column of Table 3.3, which is placed in the second phase of this methodology. Measurements in the frequency domain were discarded during this phase of the methodology since the idle mode signal consisted of a sequence of beacons of 0.5-ms duration transmitted every 50 ms, and according to the

spectrum analysis basics reported in (Keysight 2016), it is impossible to configure an analyzer for sweeping a WiFi channel in that short period of 0.5 ms, without losing the tradeoff between the values of the SWT, Span and RBW required to perform accurate recordings. For this reason, the channel power $P_{channel}$ was calculated from the power levels recorded at the different frequencies P_i in the time domain using equation (3.5), which makes the integration of the P_i values as the spectrum analyzer does when it calculates the channel power from the displayed values at the different frequencies (Keysight 2016). These measurements were taken separately at 65 different frequencies within the WiFi channel, recording data during intervals of one hour at each frequency:

$$P_{channel} = \frac{CHBW}{RBW} \cdot \frac{1}{N} \cdot \sum_{i=1}^{N} P_i \qquad (3.5)$$

where both $P_{channel}$ and P_i are the before mentioned power values in linear units, $CHBW$ is the channel bandwidth (20 MHz), RBW is the resolution bandwidth (0.3 MHz) and N is the number of frequencies within the WiFi channel at which samples were recorded (N=65).

An example of the WiFi signal measured in the time domain at 2.415 GHz when the access point was working in idle mode is depicted in Figure 3.8(a), where two beacons can be distinguished. Figure 3.8(b) shows the values registered at each one of the frequencies measured within the channel whenever the beacons were received, that is, every 50 ms. These values correspond with the maximum power levels recorded during the 1-hour duration measurements, so that the channel power obtained after converting to dBm the result calculated using equation (3.5) was -43.07 dBm in that case.

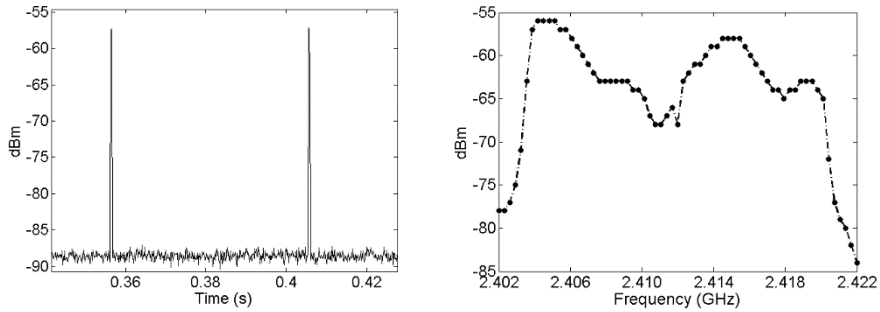

Figure 3.8. Amplitude of the signal coming from the access point in idle mode (a) time domain (b) frequency domain level when the beacon is transmitted, being the channel power in this case equal to -43.07 dBm.

4.3. Phase 2: Study of the influence of the measurement parameters

Although the most accurate way of characterizing the WiFi exposure is to use the power levels obtained by means of the above-mentioned procedure, it is not practical due to the amount of recordings that are required. Moreover, that method is not applicable to perform actual traffic measurements when changing the transmission conditions, since the different time domain measurements cannot be taken at the same time. However, it is the most accurate methodology for obtaining reference power values to assess the accuracy of other techniques. Bearing this in mind, the following objective was to determine the influence of the spectrum analyzer parameters on the measurements, in order to identify the optimal frequency domain configuration for registering the power levels that best fit the reference channel power values calculated by applying the time domain measurement method previously described.

To do this, samples of the signal transmitted by the access point when working in idle mode were taken in the frequency domain at the center frequency of 2.412 GHz, by using the RMS detector and the clear/write trace, while varying the RBW, the VBW and the SWT of the spectrum analyzer. It was observed that 501 points were enough to display that signal. That is, a greater amount of points did not improve the results, and thus, this was the value selected for the SWP parameter of the analyzer. As shown before when describing the detector types, several data points were used for calculating each displayed point value. In this case, as the RMS detector was used, the frequency width $Freq_{Width}$ utilized for obtaining the RMS value of each displayed point is determined as follows, as stated in (Keysight 2016):

$$Freq_{Width} = \frac{Span}{SWP - 1} \tag{3.6}$$

According to this, the RBW had to be larger than 40 kHz, as this was the separation between the displayed points. This fixed also the minimum VBW since, as described in the CENELEC EN 50492 Recommendation, the value of this parameter should be at least 3 times higher than the RBW (CENELEC 2008).

Taking into account the previous thresholds, the measurements carried out during this second phase were finally performed varying the RBW between 0.3 MHz and 1 MHz, the VBW between 1 MHz and 3 MHz and the SWT between 2.5 ms and 40 ms, as indicated in the second column of Table 3.3.

Table 3.3. Spectrum analyzer configurations in the time and frequency domain.

Parameter	Time Domain	Frequency domain
fc (MHz)	2412 ± 0.3125·N N= 0, 1, 2, … 32	2412
Span (MHz)	Zero Span	20
RBW (MHz)	0.3	0.3 - 1
VBW (MHz)	1	1 - 3
SWT (s)	1	2.5×10^{-3} - 40×10^{-3}
SWP	8001 points	501 points
Detector	RMS	RMS
Trace Mode	clear/write	clear/write

Results of these tests are included in Section 5 of this chapter and led to conclude that the SWT is the most influential parameter when measuring WiFi emissions, due to the variability of this type of signals; an effect that was also confirmed in (Verloock 2010).

Nevertheless, although the effect caused by the SWT parameter was clearly observed during the measurements, the error associated with each one of the frequency domain configurations was quantified by applying the following equation, in order to make an objective comparison between them:

$$e\ (\%) = \frac{|P_{channel} - P_{freq}|}{|P_{channel}|} \cdot 100 \qquad (3.7)$$

where e is the error, $P_{channel}$ is the power value obtained for the idle mode signal from the reference samples recorded in the time domain and P_{freq} is the one obtained for the same signal with a specific frequency domain configuration of the spectrum analyzer, both of them expressed in linear units.

4.4. Phase 3: Identification of the spectrum analyzer optimal configuration

Apart from the recordings of the signal transmitted by the access point when working in idle mode, measurements of WiFi signals derived from different data traffic situations were required to identify the optimal configuration of the spectrum analyzer for acquiring actual WiFi exposure values only and exclusively in the frequency domain. To do this, files of three different sizes were

downloaded from a server operating in the same local area network as the access point under test. Data traffic was generated by using a laptop located at a distance of 4 m from the receiver. Frequency domain measurements were taken in different intervals of 6-minute duration, as proposed by the ICNIRP Guidelines (ICNIRP 1998). Specifically, the recording technique was the one following described: each measurement started when the access point was in idle mode, one minute later data traffic was generated and when reaching the 6 minutes, the spectrum analyzer stopped recording samples. Thus, the synchronization of the two software tools designed, on one hand, to download the files from the server, and on the other hand, to configure the analyzer and save the results, was essential for the success of these tests.

Again in this case, different values of the spectrum analyzer parameters in the frequency domain were considered to perform this third set of measurements, with the objective of studying the relationship between the periods of time in which data traffic was generated and the power levels obtained with each configuration. An example of one of the traces recorded in the frequency domain when the access point was working in traffic mode can be seen in Figure 3.9. In this specific case the resolution bandwidth was set to 0.3 MHz.

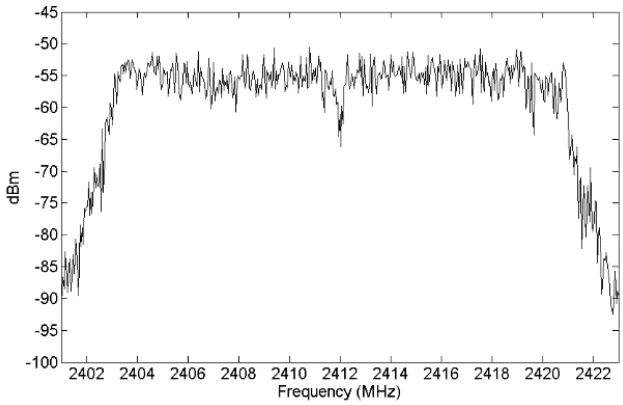

Figure 3.9. Trace of the WiFi signal recorded in the frequency domain when downloading a data file.

In view of such WiFi activity, it was necessary to determine the percentages of signal reception during the 6-minute measurement intervals. Data downloading took between 2 s and 6 s for File 1, between 50 s and 60 s for File 2 and between 228 s and 240 s for File 3. Under such conditions, the access point was transmitting almost continuously, and therefore, taking into account that the duration of each measurement was six minutes, and considering that beacons

were transmitted during the 1% of the time (that is, 0.5 ms each 50 ms) when data traffic was not generated, the time percentage of WiFi reception was 2-3% for the first type of file, 15-18% for the second type and 64-68% for the third one. Table 3.4 summarizes the details of the different file downloads. These values led to conclude that the three file types were suitable to generate WiFi exposure situations different from each other, as well as different from the situation where the access point worked in idle mode.

Table 3.4 Description of the downloads details.

File	Downloading time	Percentages of WiFi activity
File 1	2 – 6 s	2 – 3%
File 2	50 – 60 s	15 – 18%
File 3	228 – 240 s	64 – 68%

5. RESULTS OBTAINED IN CONTROLLED CONDITIONS AND DEFINITION OF SPECTRUM ANALYZER CONFIGURATION

This section includes an analysis of the power levels and error values obtained from the sets of measurements described in the previous section that finally led to determine the optimal setup of the spectrum analyzer for acquiring realistic WiFi exposure values in the frequency domain. To do this, the results were classified according to the types of WiFi signals recorded during the tests.

5.1. Results obtained for the idle mode signal

A suitable function to describe the measured WiFi signal is the cumulative distribution function (CDF), since this function gives information of the probability that the WiFi level takes a value lower or equal to a specific level. In the specific case of idle mode, the WiFi bursts transmitted by the access point had a duration of 0.5 ms and the separation between two consecutive bursts was equal to 50 ms, thus the WiFi signal was present approximately the 1% of the measurement time.

The CDFs calculated from the power values measured in idle mode in the frequency domain were compared with the CDF of the channel power values obtained from the samples recorded for that type of signal in the time domain during the phase 1 of the measurement methodology explained in the previous section. This last one is the so-called "Reference" curve depicted in black color in Figure 3.10(a) and Figure 3.10(b). As mentioned in Section 4.2 of this chapter, the maximum power value of that curve (that is, the highest reference power value) was -43.07 dBm. As seen in those figures, this curve drops to -65.89 dBm for the 99th percentile, and to -69.05 dBm for the 97th percentile, reaching finally a minimum level equal to -71.40 dBm.

CDFs corresponding to the measurements carried out in the frequency domain by using a resolution bandwidth of 0.3 MHz, a video bandwidth of 1 MHz and SWT values of 2.5 ms, 10 ms, 25 ms and 40 ms have been also included in Figure 3.10(a), while a set of curves corresponding to frequency domain measurements performed with the same SWT values, but RBW and VBW values of 1 MHz and 3 MHz respectively, can be observed in Figure 3.10(b). In all these cases, data were stored during time periods of 1 hour. Moreover, different tests of 1 hour and 6-minute duration were performed, concluding that there was no difference in this regard. Thus, as stated in (ICNIRP 1998), an

interval of 6 minutes can be considered long enough to determine the exposure level, if the environment conditions remain constant.

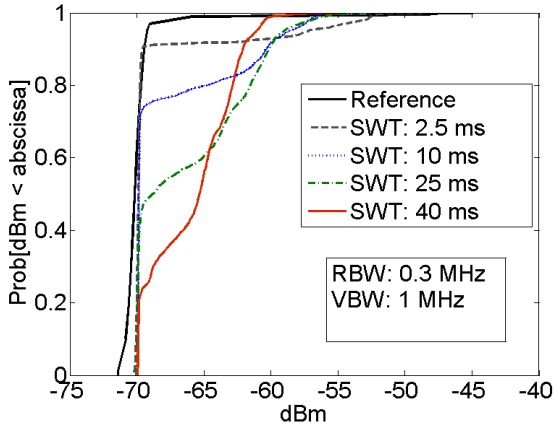

(a)

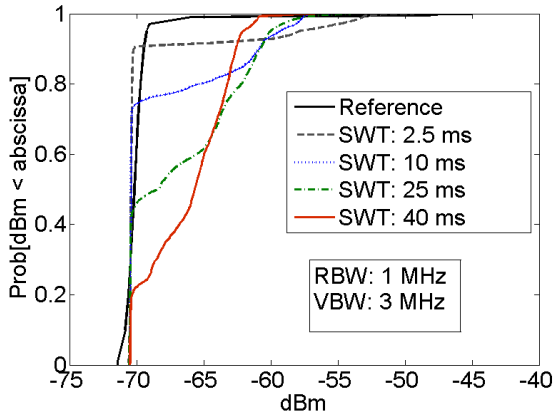

(b)

Figure 3.10. CDFs of the power levels measured, the "Reference curve" is the one obtained from the time domain measurements and the other curves are those obtained in the frequency domain measurements with different configurations (a) RBW=0.3 MHz and VBW=1MHz (b) RBW=1 MHz and VBW=3 MHz.

From the shape of the previous curves, it was determined that data collected when using higher SWT values (25 ms, 40 ms) would account for an idle signal with lower peaks but longer-lasting ones by far. This would imply an overestimation of the exposure levels to WiFi signals, and thus, shorter SWTs should be considered when the purpose is to maximize the accuracy of the measurements. Specifically, the tests performed with a SWT of 2.5 ms fitted better the trend of the reference curve, and thus, the use of this value leads to more rigorous and realistic results. The error of the samples taken in the

frequency domain with this specific sweep time value was calculated by using equation (3.7), considering the 50th percentile of the measurement levels. Values that ranged between 3.40% and 9.06% and an average error equal to 5.73% were obtained when selecting a RBW of 0.3 MHz. However, the use of the same RBW value with a SWT equal to 10 ms led to values of the error between 0.20% and 12.94%, being the average error 7.80% in this case. This error increased for a SWT of 40 ms, reaching a value of 203.94%.

Apart from the previous curves and errors, statistical results of second order were also determined taking into account fifteen measurements performed with each spectrum analyzer configuration. The mean, maximum and minimum values calculated from the 50th percentiles (P50) of the power levels obtained in the frequency domain were compared with the P50 of the reference values measured over time. As observed in Figure 3.11, the P50 value calculated from the measurements carried out in the frequency domain when selecting a resolution bandwidth of 1 MHz, a video bandwidth of 3 MHz and sweep times of 2.5 ms or 10 ms, is lower than the median of the values recorded in the time domain ("Reference"). Thus, the WiFi exposure would be underestimated if those settings are used. For a RBW of 0.3 MHz and a VBW of 1 MHz, the statistical values corresponding to the samples taken in the frequency domain were slightly higher than the ones calculated from the time domain recordings, in 14 out of the 15 measurements carried out with a SWT of 10 ms, and for all the measurements performed with a SWT of 2.5 ms. As mentioned before, the highest error in these two specific cases was 12.94% for a SWT of 10 ms and 9.06% for a SWT of 2.5 ms, concluding that these were the most suitable configurations for assessing the WiFi exposure caused by idle mode signals.

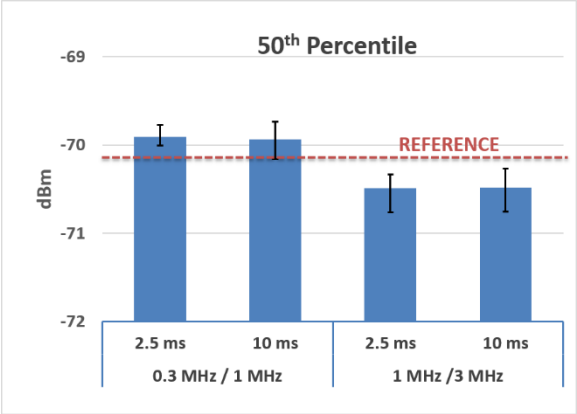

Figure 3.11. P50 values of both, the levels measured using different configurations in the frequency domain and the reference values in the time domain.

5.2. Results obtained for different WiFi data traffic situations

Results obtained from recordings of 6 minute duration performed in the frequency domain while generating data traffic are given below. In this case, the measurements were carried out using the two configurations of the spectrum analyzer that were found to be more suitable for assessing the WiFi exposure caused by idle mode signals, because a setup that is capable of determining real exposure values derived from very low WiFi activity levels is also adequate for measuring WiFi signal bursts that imply higher percentages of reception. Thus, CDFs of the received signal levels when using a resolution bandwidth of 0.3 MHz, a video bandwidth of 1 MHz and sweep times of 2.5 ms and 10 ms are shown in Figure 3.12.

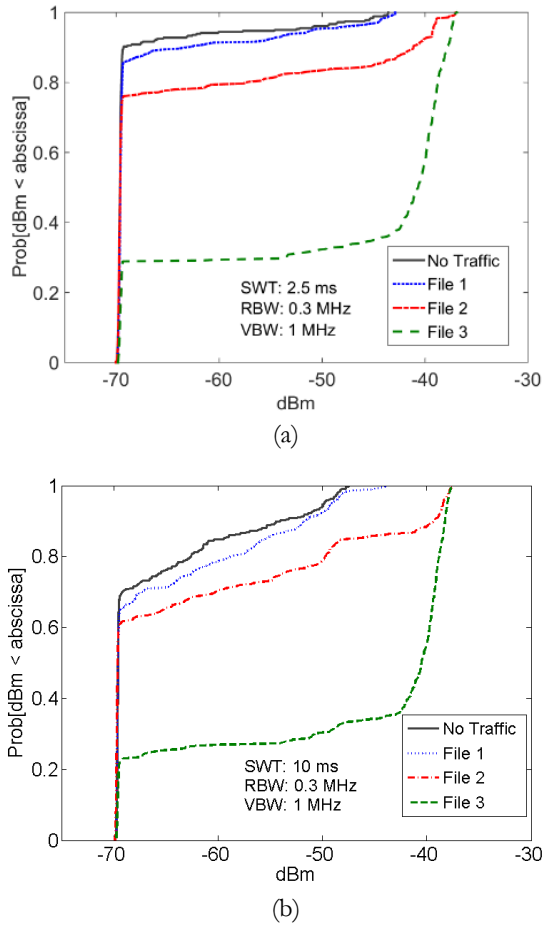

Figure 3.12. CDFs of the power levels measured for different data traffic situations using RBW=0.3 MHz, VBW=1 MHz and (a) SWT=2.5 ms, (b) SWT=10 ms.

According to the percentages of WiFi activity indicated in Section 4.4 and shown again in Table 3.5, the minimum power levels associated with the transmission/reception of WiFi data traffic should be those corresponding to the 97th – 98th percentiles in the case of File 1, the 82th –85th percentiles for File 2 and the 32th – 36th percentiles for File 3. This implies that rough transitions from the lowest to the highest power values of the corresponding CDF curves should happen at those percentiles.

Table 3.5. Downloading time for the different files and percentages of WiFi activity in each case together with the corresponding percentiles.

File	Downloading time	Percentages of WiFi activity	Percentile of rough transitions
File 1	2 – 6 s	2 – 3%	97th – 98th
File 2	50 – 60 s	15 – 18%	82th – 85th
File 3	228 – 240 s	64 – 68%	32th – 36th

Comparing the results of Figure 3.12(a) and Figure 3.12(b), it is concluded again that a SWT of 2.5 ms provides more accurate results than a SWT of 10 ms, since in this last case, the transitions happen at lower percentiles than expected, and consequently, lead to believe that the WiFi exposure is higher than it actually is. To confirm that overestimation, different percentiles corresponding to the transitions due to the existence of WiFi data traffic were identified. The mean power level of those percentiles was finally calculated by using the values of 20 measurements registered for each type of file and measurement configuration. This means a total of 120 frequency domain measurements for obtaining the results of Table 3.6 and Table 3.7. In these tables, the mean power level of the percentiles of interest are given, as well as the mean of the maximum power values. Finally, the range of power levels obtained in the different measurements is provided. The results associated recording performed using a SWT of 2.5 ms are summarized in Table 3.6 and those acquired with a SWT of 10 ms are presented in Table 3.7.

Very similar maximum power levels were determined with both SWT values, and therefore, this parameter has little influence if the measurements are performed to characterize the worst-case traffic mode scenario. However, it turns to be relevant when WiFi signal samples are taken with the aim of doing a realistic analysis of the corresponding exposure. As seen in the previous tables, the time-periods of the power levels derived from the existence of data traffic between the transmitter and receiver match with the durations of the file downloads, when setting the SWT to 2.5 ms. Even more, the P90, P80 and P30 values

corresponding to downloads of the Files 1, 2 and 3 respectively were higher for a SWT of 10 ms than for a SWT of 2.5 ms, concluding also that the lower the WiFi activity is, the worse is the overestimation due to the use of a longer sweep time.

Table 3.6. Power levels measured for different WiFi data traffic situations using a SWT of 2.5 ms

File	Relevant Percentiles	Mean (dBm)	Range of values (dBm)
File 1	P90	-65.6	-69.3 / -59.7
	P97	-44.7	-47.7 / -43.3
	Max	-39.9	-43.4 / -37.2
File 2	P80	-60.3	-69.2 / -51.7
	P85	-44.6	-46.4 / -43.3
	Max	-37.2	-38.8 / -36.7
File 3	P30	-66.8	-69.1 / -53.5
	P40	-47.7	-50.4 / -42.2
	Max	-38.1	-38.4 / -36.9

Table 3.7. Power levels measured for different WiFi data traffic situations using a SWT of 10 ms.

File	Relevant Percentiles	Mean (dBm)	Range of values (dBm)
File 1	P70	-67.4	-69.2 / -61.6
	P90	-50.9	-52.7 / -49.9
	Max	-40.2	-44.4 / -37.9
File 2	P60	-68.7	-69.5 / -65.9
	P80	-50.0	-52.6 / -48.9
	Max	-37.5	-38.1 / -37.2
File 3	P30	-64.4	-66.1 / -63.4
	P40	-47.4	-49.3 / -45.5
	Max	-38.7	-38.8 / -38.5

The influence of the SWT parameter according to the amount of traffic was also assessed by applying the Analysis of Variance (ANOVA) method (Pasquino 2017), since ANOVA is useful for analyzing the relevance of one or more factors. It is a tool that can determine if there is a statistically significant difference among groups. In our study the different groups are the measurements taken by means of each SWT (2.5 ms and 10 ms) and the tests were performed for the different traffic situations, making it possible to determine the influence of the SWT parameter depending on the amount of traffic in a WLAN. Specifically, ANOVA was used in order to obtain the value of the Fisher statistics

(F-value), which is the ratio of the variances of the different groups of samples. When the F-value is below a threshold value, the factor under study does not have relevant effect on the output data. The threshold level is obtained from the Fisher probability distribution and this threshold depends on the chosen risk α, which is selected by the analyst and refers to the probability that the effect of linearity or intermodulation errors is considered relevant (Darco 2012). A parameter α, also known as significance level, of 0.05 (95% confident that your analysis is correct) is commonly used because this value is appropriate for providing reliable results when having one tailed tests.

Table 3.8 summarizes the obtained results. This table provides the F-values and the probabilities (p-value) of obtaining F-values lower than the threshold level, thus the higher the p-value is, the lower is the influence of the SWT. These tests were performed from the power levels received when downloading each type of file using the selected SWTs (2.5 ms and 10 ms). The 6-minute measurements of each type were selected (for both SWT and the three types of files), and a significance level of 0.05 (α parameter) and 359 degrees of freedom (dof parameter) were considered.

Table 3.8. Results obtained from the application of the ANOVA method to different WiFi data traffic situations.

Traffic Situation	WiFi Reception (%)	F-value	p-value
Download of File 1	2-3	2.1863	0.0000
Download of File 2	15-18	1.3904	0.0009
Download of File 3	64-68	1.1643	0.0750

According to the results of Table 3.8, it is concluded again that the overestimations due to the use of longer sweep times will be more critical if the WiFi activity levels are very low, as in the case of File 1. Therefore, once demonstrated that the use of a short SWT increases the accuracy of the results, it can be stated that the optimal spectrum analyzer configuration for obtaining realistic values of the WiFi exposure only and exclusively in the frequency domain is the one indicated in the following table.

Table 3.9. Optimal spectrum analyzer configuration for measuring realistic WiFi exposure values.

Parameter	Value
f_c	Central frequency of the channel
Span	20 MHz
RBW	0.3 MHz
VBW	1 MHz
SWT	2.5 ms
SWP	501 points
Detector	RMS
Trace Mode	clear/write

As described in the IEEE Standard 802.11 (IEEE 2016), all the signals transmitted in the 2.4 GHz WiFi band use the same time and frequency masks, and thus, the settings specified in Table 3.9 can be applied directly to perform WiFi exposure measurements in any of the 20 MHz bandwidth channels defined in that band. By means of the frequency domain measurements, an exposure value per second can be obtained when performing just one measurement and this is the main advantage over the time domain recordings, which require several measurements.

5.3. Configuration for measuring in the whole 2.4 GHz WiFi band

Once the setup for recording accurate and actual WiFi signal levels has been determined for one channel measurements in the 2.4 GHz band, the conclusions drawn from that work can be used to define a configuration for assessing WiFi exposure in the whole band, since usually when evaluating exposure to these signals, the total level in the WiFi band is of interest. Although the signals transmitted by further access points experience a considerable attenuation in their power strength because of the larger distance and the obstacles they find in their way, such as walls or doors, these signals have to be considered as they also contribute to the exposure level. The spectrum of the WiFi signals transmitted in a WLAN working in the 2.4 GHz frequency band when the closest access point is working in idle mode and traffic mode is illustrated in Figure 3.13 and Figure 3.14 respectively. As shown, the closest access point was working on channel one (f_c=2.412 GHz) and several access points were in the surrounding area transmitting signals in different WiFi channels.

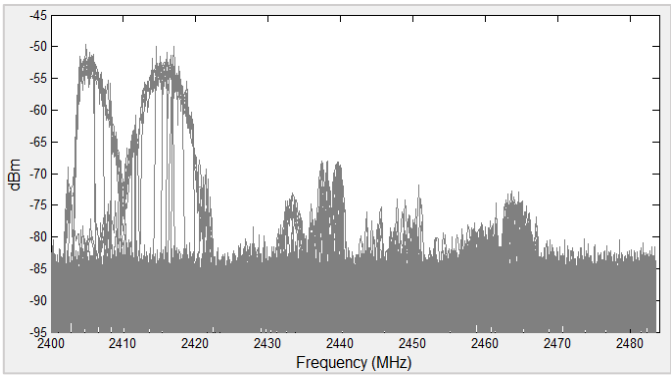

Figure 3.13. Spectrum of WiFi signals in the 2.4 GHz band when the closest access point is working in idle mode.

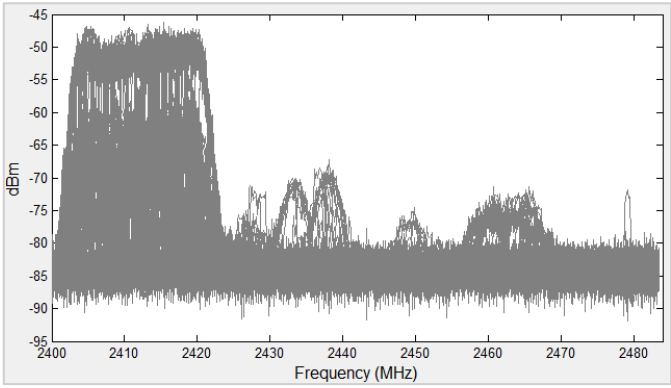

Figure 3.14. Spectrum of WiFi signals in the 2.4 GHz band when the closest access point is working in traffic mode.

As the frequency range is wider than in the case of only one channel measurements, the spectrum analyzer parameters need to be adjusted to take appropriate measurements from 2.4 GHz to 2.4835 GHz. One key parameter is the resolution bandwidth. Narrow RBWs improve the resolution of the signal, however the sweep speed and the trace update rate are reduced with narrower RBW. As shown before, the resolution bandwidth has to be higher than the Span divided by the sweep points, this is 168 kHz, which is the separation between the sweep points. In order to consider an adequate number of detected samples for calculating the RMS value that will be displayed, a RBW of 1 MHz was selected and consequently, the VBW was set to 3 MHz. The center frequency of the WiFi band, which is 2441.75 MHz, was selected as the center frequency and the Span was set to 83.5 MHz. Table Y shows the spectrum analyzer configuration proposed for recording WiFi signal levels in the whole 2.4 GHz frequency band.

Table 3.10. Configuration of the spectrum analyzer for performing measurements in the whole 2.4 GHz WiFi band.

Parameter	*Value*
Centre Frequency	2441.75 MHz
Span	83.5 MHz
Detector	RMS
SWT	2.5 ms
RBW	1 MHz
VBW	3 MHz
SWP	501
Trace Mode	clear/ write

Some tests were performed to validate this setup in the mentioned WiFi band. An example of the CDFs obtained from different measurements of 6 minute duration taken in the WiFi band when the closest access point was working in idle mode and in traffic mode is presented in Figure 3.15. In the case of traffic mode, three different files were downloaded and the download duration in this example was 6 s for File 1, 34 s for File 2 and 190 s for File 3. As shown, in this case the transition from the lowest levels to the maximum peaks is less rough than in the case of one channel measurements. This makes sense since in that previous case, the power level of the whole frequency range of the measurement increased when data traffic was transmitted. In this case, however, only the power strength of one channel (20 MHz of 83.5 MHz) increased when downloading a file.

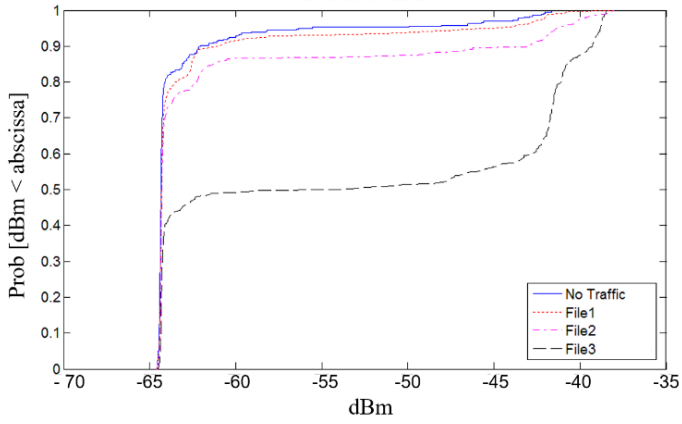

Figure 3.15. CDFs of the measured power levels in the whole 2.4 GHz WiFi band.

The results obtained from various measurements taken when there was no traffic and while downloading the different files are summarize in Figure 3.16. Specifically, 6 measurements of each type (idle mode, File 1, File 2 and File 3) were performed and the median value of the 10th, 50th, 90th percentiles and maximum power levels are depicted. The error bars refer to the minimum and maximum values of the corresponding percentile or max value. The minimum power level recorded in these measurements was equal to -64.82 dBm, around 5 dB higher than when taking samples in one WiFi channel. In addition, the highest reached value was -35.64 dBm, recorded while downloading the largest file.

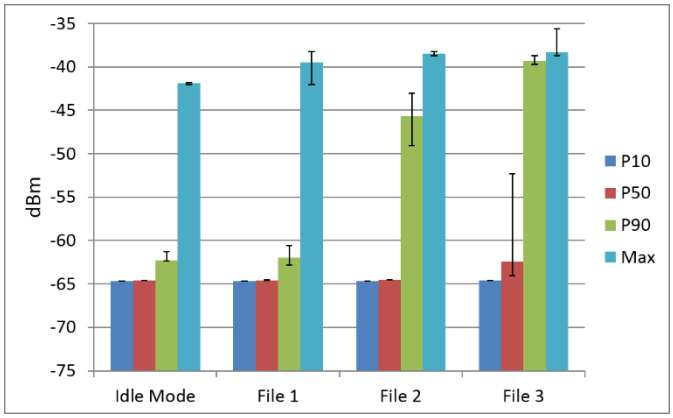

Figure 3.16. Results of the power levels measured in the whole WiFi band.

6. PROCEDURE FOR ASSESSING WIFI EXPOSURE

As stated in the previous sections of this chapter, it is essential to utilize the spectrum analyzer optimal settings for acquiring WiFi radiation samples, when the purpose of the measurements is to know the actual exposure levels caused by this type of signals in a particular environment. Thus, a large proportion of the tasks and results above described were focused on identifying such configuration. Nevertheless, another key question that should be taken into account is the measurement procedure in which that configuration will be adopted. Therefore, a set of guidelines to carry out WiFi exposure recordings is given below, based not only on the use of the spectrum analyzer setup indicated in Table 3.9, but also on the general recommendations of several standards defined in this regard (ICNIRP 1998; IEEE 2005; CENELEC 2008), measurement campaigns performed by other authors and on the experience gained during this thesis.

First, the antenna that will be connected to the spectrum analyzer must be chosen. When the aim of the measurements is to determine the human exposure levels caused by WiFi radiation, an isotropic or a tri-axial antenna system should be used. If this is not possible, three exposure samples can be respectively taken in the x, y and z spatial directions, in order to register separately three mutually orthogonal components of the electric field received at a specific point (CENELEC 2008).

The following step is to select the measurement locations within the area of study, taking into account the potential spatial variability of the WiFi signals, and ensuring that the receiving antenna is not in the near field region of any WiFi source. In case of performing indoor measurements, a good option is to take samples in the middle and the corners of the corresponding rooms, as well as on all those locations where people spend most of their time (Gallastegi 2016; Karipidis 2017). The height of the receiving antenna should be defined in accordance with the height and the position of the individuals who are usually present in such environment (e.g. head location when they are sitting or standing), bearing also in mind that a maximum height of 2 m above the floor is recommended by the Institute of Electrical and Electronics Engineers (IEEE 2005). Besides, the recordings should be done at enough distance from the walls in order to avoid their influence, e.g. a distance equal to 1.4 m, as reported in (Gallastegi 2016).

Apart from the previous recommendations, the use of a software tool developed to control the equipment and save the results is suggested in order to

avoid the influence of the person who performs the measurements. This tool should be programmed to take samples of at least 6-minute duration (ICNIRP 1998), or even of 24-hour duration in the specific case of acquiring data to analyze the time variability of the exposure to WiFi signals. An example of this type of variability is shown in Figure 3.17. In this case, recordings were taken in one channel of the WiFi band, but the procedure followed is applicable to the whole WiFi band. The curves depicted in this figure account for the maximum values and the 50th and 90th percentiles of the WiFi signal levels registered inside a classroom of the University of the Basque Country, Spain, during a whole working day. To do this, an automated measurement system composed of a tri-axial antenna and a spectrum analyzer configured according to the settings indicated in Table 3.9 were used. The central frequency selected to perform the measurements was the one corresponding to the operation channel of the access point located in that classroom (Channel 5 of the 2.4 GHz band). Also, the antenna was placed in the middle of the area under study at a height of 1.2 m above the floor, since people usually sit in that specific location. As expected, the radiation was significantly higher when the university, and therefore the classroom, were open. That is, from 7:00 to 21:00.

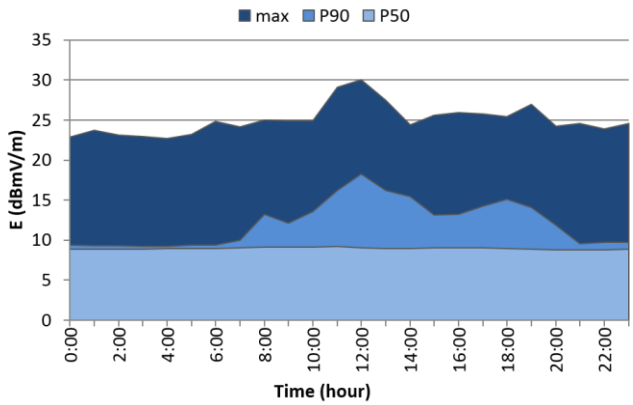

Figure 3.17. Time variability of the WiFi emissions of one channel measured in a classroom of the University of the Basque Country.

7. CONCLUSIONS

Although human exposure to WiFi signals is nowadays a matter of social concern, there is no standardized procedure for measuring this type of emissions. Moreover, many of the scientific studies performed in this regard do not take into account that the WiFi radiation is not received in a continuous way. In fact, the most typical instruments utilized to acquire exposure samples, such as broadband probes, exposimeters or spectrum analyzers are usually configured, or even developed, to measure the maximum field levels. This can lead to significant overestimations that could finally result in a characterization of the exposure not matching the real environment conditions. For this reason, some authors weight the samples by applying empirical factors that account for the quasi-stochastic nature of the WiFi signal. However, in those cases, measurements should be done in both, the time and frequency domain.

Taking into account this, and after concluding that spectrum analyzers using a RMS detector and the clear/write trace mode are the most suitable instruments to measure the actual WiFi exposure levels, a methodology to identify the optimal measurement setup was defined in order to acquire accurate samples of the WiFi radiation only and exclusively in the frequency domain. In fact, the technique adopted to do this can be applied to know the most appropriate setup for registering any type of radiation, since it is based on utilizing a set of reference values from recordings of a well-known signal transmitted by any source radiating the type of emissions under study.

The reference data specifically used in this work were obtained from time domain measurements of the idle mode signal transmitted by a WiFi access point working in the 2.4 GHz band. From their comparison with the power levels recorded for the same type of signal by configuring the spectrum analyzer in the frequency domain to operate at the central frequency of the transmission/reception channel, with a Span of 20 MHz, the RMS detector, the clear/write trace and a SWP value of 501, it was concluded that the optimal SWT, RBW and VBW were 2.5 ms, 0.3 MHz and 1 MHz respectively for assessing the exposure in one WiFi channel of the mentioned frequency band. Other configurations led to higher overestimations, and even in some cases, to underestimations that gave as a result unusable power values to determine if the WiFi radiations sources fulfill the protection thresholds or not. Then, the results and information extracted from these tests were useful to define a spectrum analyzer configuration for assessing WiFi exposure considering all the access

points in the vicinity, since the signals in other WiFi channels also contribute to the exposure and they have to be considered.

The signal levels registered during a second set of frequency domain tests carried out for different traffic situations proved also that the above mentioned configurations can be used to measure accurately the exposure derived from low, medium and high WiFi activity levels. Even more, the time variability of the WiFi radiation that was received during a whole working day in a classroom of the University of the Basque Country, Spain, was determined from recordings performed by applying a measurement methodology in which the configuration proposed for taking one channel WiFi samples was adopted. Therefore, having concluded that the solution proposed in this thesis is optimal for obtaining realistic values of the WiFi exposure at different environments and under different circumstances, further work will be aimed at employing not only the optimal settings here described, but also the methodology defined to determine those optimal settings, in order to identify the best measurement solution to acquire samples of the human exposure levels caused by WiFi signals transmitted in the 5 GHz band, or even by other types of signals, as for example the ones corresponding to 5G mobile communication systems.

CHAPTER 4: ASSESSMENT OF HUMAN EXPOSURE TO WIFI SIGNALS

This chapter presents an evaluation of WiFi exposure levels measured in several locations of the university. WiFi signal samples in the 2.4 GHz frequency band were collected using the methodology defined in the previous chapter. A discussion of the data analysis and the proper statistics for assessing this type of exposure is provided, together with the description of the procedure followed to evaluate the spatial and temporal variability of WiFi signals. Also, a comparison of WiFi levels measured in other scientific papers is made, giving details on the instrumentation and techniques used in each case.

1. INTRODUCTION

In the previous chapter, a methodology for measuring accurate WiFi signal samples was proposed for taking measurements in one channel or in the 2.4 GHz WiFi band. As shown in that chapter, the methodology was based on a frequency domain configuration of the spectrum analyzer, which was tested in controlled conditions. Also, an experiment in a real environment was conducted, taking samples in one of the channels of the WiFi band. The next step is to apply that method in a real environment considering all the channels of the WiFi band. The selected location for carrying out the measurement campaigns is the university, which is the typical scenario where WiFi exposure concerns have increased in the last years, since a WLAN is deployed close to the users and people spend many hours in this place.

During the development of this thesis, a collaboration with some of the participants of the INMA (INfaccia y Medio AMbiente- Environment and Childhood) Project was established. This project is an ongoing prospective population-based birth cohort study concerned with the associations between pre- and post-natal environmental exposures and child growth development (Guxens 2012). One of the factors studied in this project is the children exposure to non-ionizing radiation. For that purpose, measurements of EMFs at frequencies up to 6 GHz were performed in schools, houses and playgrounds. The instruments used for measuring RF fields in these measurement campaigns were broadband probes and personal exposure meters. Our participation in these measurements was focused on contributing on the design of the study and providing technical advice.

When developing the measurement procedure for taking samples of the WiFi signals, some methods used in the measurement campaigns of the INMA Project were applied. For example, within a room, measurements were taken in the middle and in the corners, leaving a distance of 1.4 m from the walls to avoid their influence. This decision was taken because data samples at these points are suitable for assessing exposure variability in a room, not only for WiFi levels assessment but also when studying other RF services.

As shown in Chapter 2, broadband probes and personal exposure meters or exposimeters are widely utilized in exposure assessment. The first one is not suitable for measuring only one RF service, but the exposimeter can give the results for a specific frequency band. In the measurement campaigns carried out in this chapter, apart from the spectrum analyzer, an exposimeter is used.

2. WIFI EXPOSURE ASSESSMENT

The access points of the university network were using the IEEE 802.11n standard, which allows transmissions in the 2.4 GHz or 5 GHz frequency bands. Power measurements were carried out in the 2.4 GHz band where the bandwidth of each WiFi channel is equal to 20 MHz. The maximum data rate supported by this standard for a 20 MHz channel is 288.9 Mbps (IEEE 2009). As described in Chapter 2, in Europe transmission is allowed in 13 different channels in this frequency band and the separation between them is 5 MHz, thus some channels overlap with each others. As specified in the standard (IEEE 2016), adjacent cells using different channels can operate simultaneously without interference if the distance between the center frequencies is at least 25 MHz.

2.1. Measurement scenario and WiFi networks

Measurement campaigns were performed in a faculty of the University of the Basque Country, Spain, which is located in an urban environment surrounded by homes, offices and restaurants. This area is characterized by a high level of activity, next to the university there is a bus station and a soccer stadium. As shown in Figure 4.1, the university includes several buildings, one called B next to the bus station, a narrower one (F), which passes over the highway and connects the parts B and D. Next to the latter there is another corridor called E that connects with the rest of the university: three parts named A, C and G, which form an inner courtyard. Measurements were carried out inside the university, in two labs, three classrooms and three corridors of different floors.

Figure 4.1. Location of the university where the measurements were carried out.

Figure 4.2 shows a map of the 4th floor of the university and the two labs where measurements were performed can be distinguished. Also, the WiFi access points of the university network are represented as green circumferences and its theoretical coverage area is shown using a color scale in which the red indicates greater coverage and the blue tones mean lower WiFi signal.

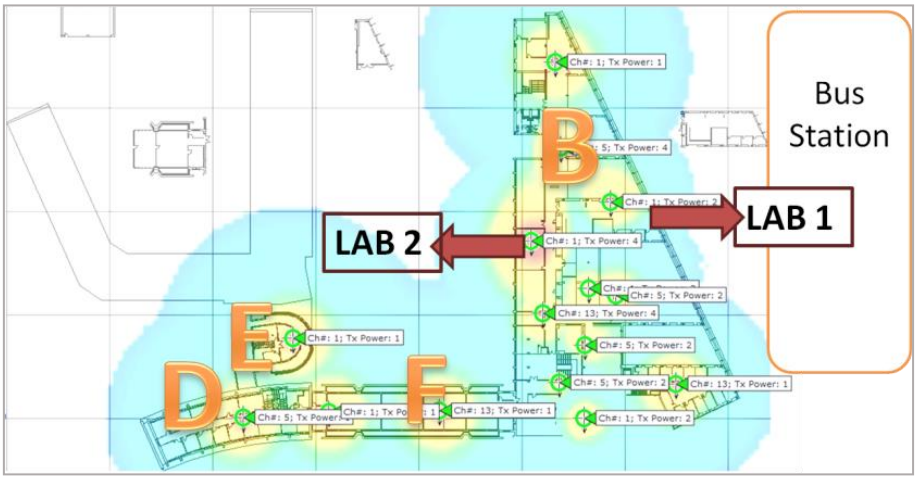

Figure 4.2. Map of the access points of the Eduroam network on the 4th floor.

The number of access points per floor belonging to the university network is summarized in Table 4.1. On the first floor there are not access points on the F part because as it is a bridge to the other building, its height starts on the second floor. The same happens with the top floor, only parts B, D, E and F have four floors.

Table 4.1. Access points of the university network per floor

Floor	***Number of Access Points***	***University Buildings***
1st	22	A, B, C, D, E, G
2nd	24	A, B, C, D, E, F, G
3rd	22	A, B, C, D, E, F, G
4th	15	B, D, E, F

Apart from the access points of the university network (Eduroam network), signals from other access points were found, some of them inside the university, but most of the WiFi emissions coming from other access points were sent from

sources located out of the university buildings. For example, in one of the laboratories of the building B, signals coming from up to 19 different networks in the 2.4 GHz band were found. The existing WiFi networks in the environment were detected by means of a laptop using the command 'netsh' at the command prompt. In that location, signals from 5 different access points belonging to the Eduroam network were identified. One of them was inside the laboratory, which was working on channel 5 and the signal quality was 78% at that moment from the receiving position, and the others were placed in the corridor and in other labs or classrooms, two were working on channel 1 (signal qualities were 28% and 30%) and the other two were working on channels 9 and 13 respectively, both of them with a signal quality of 20%. In this lab, there was another access point belonging to a different network (Network 2), working on channel 6. Regarding the WiFi signals coming from external access points, signals coming from 5 open networks from bus companies were identified and from 12 private networks.

Table 4.2 summarizes this information regarding the signals identified in this lab from access points located inside and outside the university. The type and number of networks, and the 802.11 standard are provided, as well as the number of access points and the channels in which they were working. Finally, the detected signal quality is given and as shown, it has to be highlighted that the power levels from sources located in the lab are significantly higher than the signals received from other sources.

Table 4.2. WiFi Networks detected from one lab of the building B

Network	***Number of networks***	***Mode***	***Nº Access Points***	***Channel***	***Signal Quality***
Eduroam	1	802.11n	5	1(2), 5, 9, 13*	20% - 78%
Network 2	1	802.11n	1	6	65%
Public/ Open	3	802.11n	5	1(2),6,11,12*	18% - 23%
	2	802.11g	2	1,6	23% - 26%
Private	12	802.11n	12	1(7),11,6,10,5,8*	15% - 51%

* 1(2): two access points working on channel 1.
1(7): seven access points working on channel 1.

2.2. Types of measurements

Measurements to assess WiFi exposure were performed with the aim of evaluating the temporal and spatial variability of the signals. For this purpose, two types of tests were carried out:

- long-term measurements, in which samples were recorded continuously during 24 hours at each point to study the variability of the signal throughout the day
- 1-hour measurements at each point, allowing the measurements at multiple points in the same WiFi activity conditions in order to characterize the spatial variability.

Long-term tests were performed in two labs on the 4th floor of building B (as shown before in Figure 4.2). Measurements of 24-hour duration were recorded at 5 different points in each lab: at the center and in the four corners of the room at 1.4 m (diagonally) from the corner, following the procedure used in (Gallastegi 2016; Gallastegi 2017). The receiver instruments were placed at a height of 1.2 m above the floor; since in these labs students and researchers are usually sitting so this corresponds to the average height of their head. Moreover, WiFi signals were evaluated two different days at each point in order to investigate the correlation between different days, so long-term recordings were done during a total of 10 days (240 h) in each lab.

1-hour measurements were carried out at six positions of each corridor and classroom. In the case of the classrooms, the receiver equipment was placed in the four corners, at a distance of 1.4 m from them to avoid walls influence and at two locations close to the center of the room. The height of the receiving antennas was 1.2 m above the floor, as students are usually sitting in these places. In the corridors, evaluation points were in the middle of the two walls of the corridor at a height of 1.7 m, because people are usually walking or standing in these locations. A distance of 3 m between two consecutive measurement points was chosen.

Table 4.3 summarizes the different places where samples were recorded, indicating the building and the floor of each measurement location, the measurement duration (Meas. Time) and the number of positions selected at each location (Nº of Pos.). Finally, the total recording time at each place is given. As in Lab 1 and Lab 2 samples were taken two different days at each point, a total of 10 measurements were performed in each lab. In the corridors and classrooms,

one measurement per position was taken. 1-hour measurements were performed during the weekdays and the three classrooms were empty during the measurements, but beacon signals were received from the closest access points as well as data traffic signals due to people's devices on the corridor or in other classrooms. 24-hour measurements were taken during the 7 days of the week and part of the time people were in the labs while samples were recorded. The university is open on weekdays from 7:30 to 21:30 and on Saturday morning.

Table 4.3. Description of the measurements

Place	*Building /Floor*	*Meas. Time*	*Nº of Pos.*	*Total Time*
Lab 1	B / 4	24 h.	5	240 h.
Lab 2	B / 4	24 h.	5	240 h.
Corridor 1	B / 3	1 h.	6	6 h.
Corridor 2	A / 2	1 h.	6	6 h.
Corridor 3	B / 2	1 h.	6	6 h.
Classroom 1	C / 3	1 h.	6	6 h.
Classroom 2	B / 3	1 h.	6	6 h.
Classroom 3	G / 1	1 h.	6	6 h.

2.3. Equipment

Two different types of instruments were used to measure human exposure to WiFi signals. The differences in the obtained results due to the measurement instrumentation were evaluated. As professional equipment, the same spectrum analyzer than the one used in Chapter 3 was utilized, the EMI ESPI3 of Rohde & Schwarz that works in the frequency range from 9 kHz to 3 GHz (R&SEspi), together with a tri-axial antenna system composed of three Yagi antennas suitable for the 2.4 GHz WiFi band. The antennas were placed in three mutually orthogonal directions and were connected using two combiners and an attenuator, so the power received by the three antennas experienced the same losses (see Figure 4.3). The total losses due to the combiners and to the cables were then added.

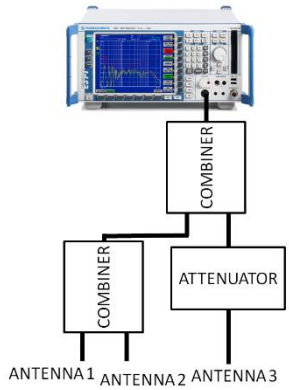

Figure 4.3. Scheme of the combiners and attenuator used for connecting the antennas.

Some concerns may arise regarding the distortion of the radiation pattern of the antennas when setting up the tri-axial system. So, in order to validate it, the electric field strength measured by this system was compared with the electric field strength assessed using a second method. The latter consisted in measuring three times with one of the Yagi antennas placed in the three orthogonal directions each time (E_x, E_y, E_z). Then, the field strength values were combined using:

$$E_{Total} = \sqrt{|E_x|^2 + |E_y|^2 + |E_z|^2} \qquad (4.1)$$

This comparison was made at night to ensure the same situation during the four measurements (the one with the tri-axial system and the three measurements required when using the second method). So, a total of four nights was required to compare these systems. One sample per second was recorded and every hour the median value of the power measured was calculated. Figure 4.4 shows the difference in the median power strength obtained by means of the both methods. The median of the power level measured by means of the tri-axial antenna system was always higher. As seen, the greatest difference was 1.14 dB obtained at 6:00 am. These differences are not only due to the antenna measurement system, but also to different activity in the WLAN, since measurements were performed in different days.

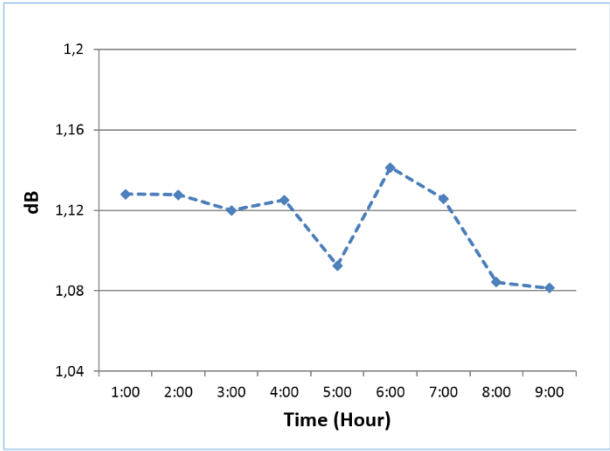

Figure 4.4. Difference in the power levels measured using the two different antenna systems from 1:00 to 9:00 in the morning.

A computer wired connected to the spectrum analyzer was used to configure the analyzer and to save the recorded data. The spectrum analyzer settings were the ones proposed in Table 3.10 of Chapter 3 to take accurate measurements in the whole WiFi band. As explained in that chapter, the center frequency and span were set to 2441.75 MHz and 83.5 MHz, respectively, in order to detect the signals of the different channels in the 2.4 GHz WiFi band. The RMS detector and the clear/write trace were selected to avoid over and underestimations of the WiFi emissions. One sample was recorded each second in a text file for further processing.

The other measurement equipment used in the measurement campaigns was an exposimeter or personal exposure meter, the EME Spy 200 (EME SPY). It was also configured to measure in the 2.4 GHz WiFi band (2400-2483.5 MHz) and a value of the electric field strength was recorded every 4 seconds. This device has a tri-axial electric field probe valid for the frequency range from 80 MHz to 6 GHz and the detection limit in the frequency range of interest is 0.005 V/m. For values lower than this limit, the EME Spy uses the naïve approach, which consists of replacing the measured level by the detection limit (Röösli 2008).

All the measurements were performed using the spectrum analyzer together with the Yagi antenna system and in the case of the 1-hour measurements, also the personal exposure meter was employed. For these last measurements, both instruments were recording samples at the same time, being the minimum distance between them equal to 40 cm in order to ensure that one instrument was not in the near field region of the other receiver. As the receiving Yagi antenna is

physically larger than half a wavelength, the far field region starts at the distance d_f, which is dependent of the largest dimension of the antenna D and the wavelength λ (Rappaport, 2010):

$$d_f = \frac{2D^2}{\lambda} \quad (4.2)$$

This distance was calculated using the lowest λ in the 2.4 GHz WiFi band, which is 12.08 cm, and the largest antenna dimension, which is equal to 15 cm corresponding to the Yagi antenna.

2.4. Data analysis and statistical discussion

The recorded data were saved in a text file for further processing. As above mentioned one sample per second was obtained when measuring with the spectrum analyzer and a sample every 4 seconds when using the personal exposure meter. Regarding the 24-hour measurements, in order to determine exposure variations at different moments of the day, three different periods of time were distinguished:

- Morning, from 6:00 to 14:00.
- Afternoon and evening, from 14:00 to 22:00.
- Night, from 22:00 to 6:00.

In addition, the correlation with the days of the week was statistically investigated.

Every hour several percentiles of the electric field strength were calculated as well as the minimum, maximum and mean values. Data statistics of each position inside a location (lab, classroom or corridor) were evaluated separately. Then, statistic results were calculated taking into account all the data acquired at one lab, classroom or corridor, without distinguishing the receiving position, so the mean WiFi exposure levels at each location were assessed, as well as the standard deviation. For example, the average 50th percentile during the morning period in a lab was obtained by calculating the average value of all the 50th percentiles acquired during the morning. These statistics were calculated in linear units, but for illustrating the results in graphs logarithmic units were chosen.

The 90th percentile was considered an appropriate statistic for representing the WiFi exposure variations because of the nature of these signals, which are transmitted in the form of bursts. The median value or 50th percentile has fewer variations along the day and between the different places. Percentiles higher than

the 99th, which can have higher variations, are not representative of electromagnetic field exposure since they indicate singular occurrences of the signal. However, values such as the median or the maximum reached levels are significant statistics to evaluate exposure levels and to compare with regulations and standards. As explained in (Joseph 2009), median exposure values are more interesting for epidemiological studies, while maximum values are often more important for authorities and legislation.

3. RESULTS AND DISCUSSION

In the following subsections the WiFi exposure values obtained in the different measurements taken with the spectrum analyzer and with the exposimeter are presented and analyzed. These results are separated into two groups, those acquired in the long-term measurements and the ones obtained from the 1-hour measurements.

3.1. Long-term measurements

The results obtained using the spectrum analyzer and the tri-axial antenna system in the two laboratories are presented below. Figure 4.5 and Figure 4.6 show the mean values of the 90th and 99th percentiles (P90, P99) of the electric field measured with the spectrum analyzer in Lab 1 and Lab 2, respectively. The results obtained in the four corners (Pos 1, Pos 2, Pos 3, Pos 4) and in the middle of each room (Pos 5) are represented for the different periods of the day. As shown, the recordings were repeated two days at each position.

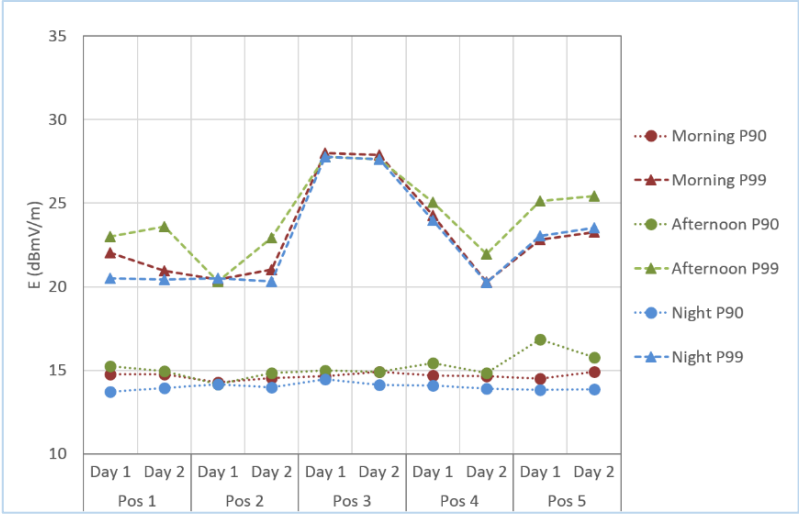

Figure 4.5. 90th and 99th percentiles of the electric field levels measured at the different positions of Lab 1.

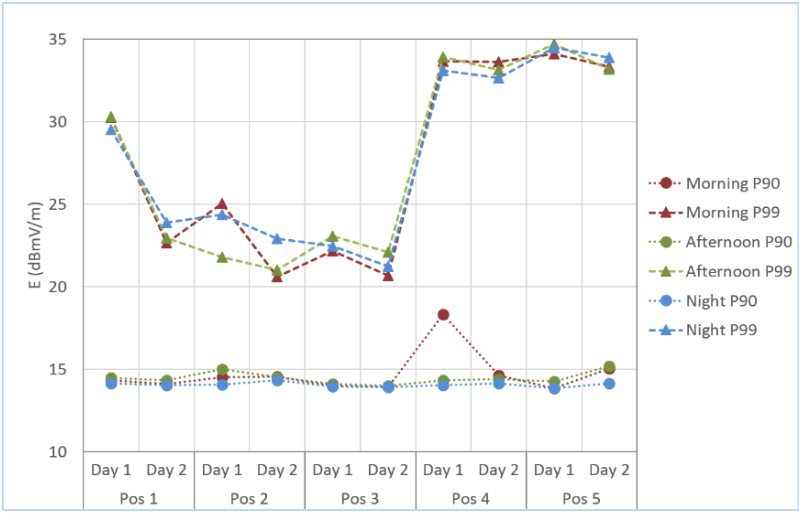

Figure 4.6. 90th and 99th percentiles of the electric field levels measured at the different positions of Lab 2.

Significant differences were observed due to the different positions inside the room. In Lab 1, the maximum difference between the P99 of the different positions was obtained during the morning periods and it was equal to 7.7 dB. For the P90, differences of up to 2.7 dB were found when placing the receiver at different points. In Lab 2, the P99 of the afternoon tests differed by 13.7 dB between positions 2 and 5, while the maximum variations of the P90 due to different positions were found during the morning and reached a value of 4.5 dB. The variability at night was lower than during the day. When considering the P99, the levels of the night tests were higher than the tests carried out during the day in some of the measurements, this is because these percentiles indicate singular occurrences of the signal and they are not representative of WiFi exposure.

Differences between the weekdays and the weekends were also found. An example of this is illustrated in Figure 4.7, where the median (P50), P90, P99 and the maximum levels measured in the position 2 of Lab 1 are represented. The first 24-hour measurement at this point was taken on Sunday and the variability of the WiFi exposure was lower than in the measurement performed the following day. On Monday, the signal increased during the working hours at university.

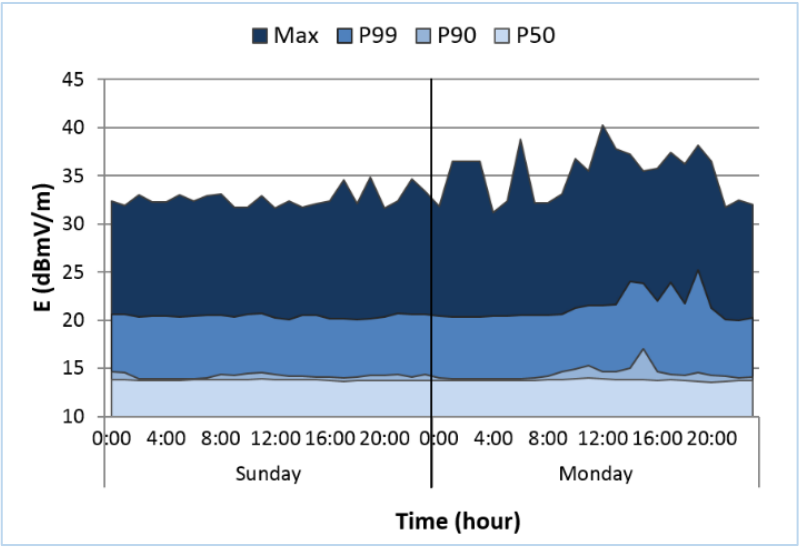

Figure 4.7. Temporal evolution of the electric field strength measured during two consecutive days in the position 2 of Lab 1.

The average WiFi exposure levels for each lab are summarized in Table 4.4. The mean electric field levels obtained in each lab during the different periods of the day are presented together with the standard deviation. The mean values of the different percentiles were calculated considering all the measurements taken during the same period of the day in the different positions of the lab. Finally, the minimum and maximum sample levels measured in the morning, afternoon and night are given. The mean value of the WiFi exposure was higher in Lab 2, being this value 5.25 mV/m in the mornings and afternoons. In both labs the electric field strength measured during the day was higher than the levels obtained at night. Regarding the average P90, in Lab 1 it took values between 5.02 mV/m (at night) and 5.77 mV/m (in the afternoon), while in Lab 2 it ranged between 5.05 mV/m (at night) and 5.51 mV/m (in the morning), the maximum standard deviation associated to these sets of calculations was 0.94. For the average P99, the field strength levels increased considerably, reaching a value of 29.21 mV/m in Lab 2. The maximum level of WiFi exposure in Lab 2 was equal to 407.81 mV/m, while in Lab 1 the maximum measured value was 172.26 mV/m, both of them recorded in the afternoon.

Table 4.4. Average electric field strength values (mV/m) measured with the spectrum analyzer in each lab

	Lab 1			***Lab 2***		
	Morning	***Afternoon***	***Night***	***Morning***	***Afternoon***	***Night***
Min	4.58	4.49	4.57	4.59	4.61	4.62
Mean (SD)	5.17 (0.08)	5.15 (0.09)	5.03 (0.01)	5.25 (0.17)	5.25 (0.17)	5.18 (0.10)
$P50_{Av}$[a] (SD)	4.89 (0.05)	4.79 (0.05)	4.82 (0.05)	4.87 (0.05)	4.84 (0.04)	4.87 (0.05)
$P90_{Av}$[a] (SD)	5.41 (0.11)	5.77 (0.47)	5.02 (0.12)	5.51 (0.94)	5.29 (0.22)	5.05 (0.08)
$P99_{Av}$[a] (SD)	15.05 (5.26)	16.92 (4.41)	14.59 (5.24)	29.14 (16.72)	29.21 (17.09)	29.14 (15.99)
Max_{Av}[a] (SD)	104.78 (36.10)	117.06 (40.20)	91.76 (40.05)	185.95 (129.42)	178.18 (124.94)	177.90 (119.32)
Max	154.82	172.26	149.88	388.77	407.81	380.16

SD: standard deviation.

[a] Mean values of the P50, P90, P99 and maximum levels of the electric field (mV/m) measured in the different positions of the lab.

Finally, Pearson correlation coefficient was performed to determine the correlation between WiFi exposure variability and the days of the week. The mean electric field levels obtained for the different hours of the day were used to investigate the linear relationship between the exposure variability in different days. Table 4.5 and Table 4.6 show the Pearson correlation coefficient in Lab 1 and Lab 2, respectively. The measurement position and the weekday is given in the tables and the first finding is that WiFi exposure variability in Lab 1 showed a more uniform behavior than in Lab 2. This is due to the activity in each lab, since the first lab is use for research purposes and people work there during the same hours on weekdays. However, the second lab is a teaching lab where students go to do laboratory practices and each day the lessons are at different hours. For this reason, in Lab 2 exposure of different days was less correlated, being the Pearson coefficient a negative value in some cases, since at the same hours WiFi levels increased one day and decreased on other day. The best correlation coefficient in this second lab was equal to 0.829, while the largest correlation coefficient in Lab 1 was 0.927, reached between Position 2 on Monday and Position 1 on Thursday. The smallest correlation coefficient in Lab 1 was 0.008 obtained between Position 2 on Sunday and Position 5 on Monday, which makes sense because on Sunday the university is close, so WiFi signal variability is expected to be different than on weekdays.

Table 4.5. Pearson correlation coefficient for the mean electric field at the different hours of a day in lab 1

	Pos 1 Thu	Pos 1 Tue	Pos 2 Sun	Pos 2 Mon	Pos 3 Sun	Pos 3 Sat	Pos 4 Tue	Pos 4 Fri	Pos 5 Mon	Pos 5 Wed
Pos 1 Thu	1	0.855	0.324	**0.927**	0.656	0.717	0.849	0.768	0.571	0.895
Pos 1 Tue	0.855	1	0.454	0.801	0.669	0.577	0.880	0.850	0.540	0.874
Pos 2 Sun	0.324	0.454	1	0.286	0.546	0.273	0.466	0.471	**0.008**	0.301
Pos 2 Mon	**0.927**	0.801	0.286	1	0.643	0.646	0.858	0.769	0.698	0.910
Pos 3 Sun	0.656	0.669	0.546	0.643	1	0.774	0.608	0.771	0.529	0.635
Pos 3 Sat	0.717	0.577	0.273	0.646	0.774	1	0.509	0.508	0.454	0.553
Pos 4 Tue	0.849	0.880	0.466	0.858	0.608	0.509	1	0.811	0.524	0.847
Pos 4 Fri	0.768	0.850	0.471	0.769	0.771	0.508	0.811	1	0.705	0.856
Pos 5 Mon	0.571	0.540	**0.008**	0.698	0.529	0.454	0.524	0.705	1	0.668
Pos 5 Wed	0.895	0.874	0.301	0.910	0.635	0.553	0.847	0.856	0.668	1

Figure 4.8 shows the mean electric field along a day measured the days with the highest Pearson correlation coefficient, on Thursday in Position 1 and on Monday in Position 2.

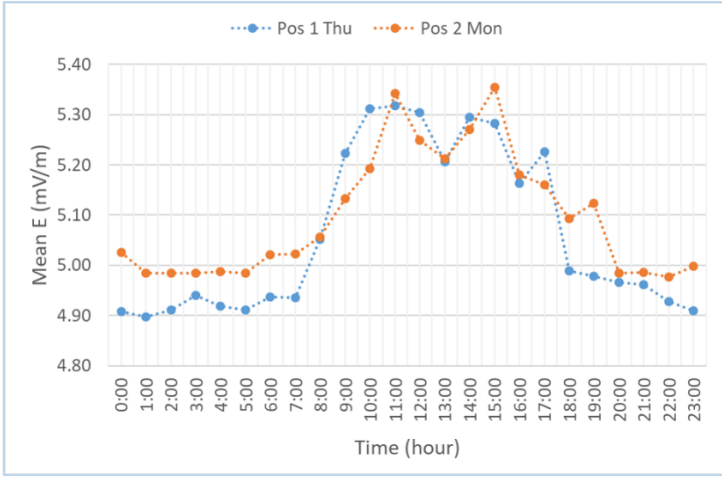

Figure 4.8. Mean electric field levels measured in Position 1on Thursday and in Position 2 on Monday, both in Lab 1.

Table 4.6. Pearson correlation coefficient for the mean electric field at the different hours of a day in lab 2

	Pos 1 Mon	**Pos 1 Tue**	**Pos 2 Thu**	**Pos 2 Fri**	**Pos 3 Sun**	**Pos 3 Sat**	**Pos 4 Tue**	**Pos 4 Wed**	**Pos 5 Sat**	**Pos 5 Fri**
Pos 1 Mon	1	0.590	0.012	0.009*	0.408	0.470*	0.573	0.701	0.436	**0.829**
Pos 1 Tue	0.590	1	0.057	0.281*	0.213	0.262*	0.580	0.315	0.496	0.672
Pos 2 Thu	0.012	0.057	1	0.185	0.278	0.348	0.030*	0.231*	0.040	0.274
Pos 2 Fri	0.009*	0.281*	0.185	1	0.269	0.055	0.087*	0.236	0.367*	0.006*
Pos 3 Sun	0.408	0.213	0.278	0.269	1	0.182*	0.454	0.174	0.212*	0.474
Pos 3 Sat	0.470*	0.262*	0.348	0.055	0.182*	1	0.396*	**0.475***	0.011*	0.314*
Pos 4 Tue	0.573	0.580	0.030*	0.087*	0.454	0.396*	1	0.137	0.119	0.701
Pos 4 Wed	0.701	0.315	0.231*	0.236	0.174	0.475*	0.137	1	0.268	0.448
Pos 5 Sat	0.436	0.496	0.040	0.367*	0.212*	0.011*	0.119	0.268	1	0.390
Pos 5 Fri	**0.829**	0.672	0.274	0.006*	0.474	0.314*	0.701	0.448	0.390	1

* Negative values

3.2. 1-hour measurements

Inside a location (classroom or corridor), considerable variations in the measured field levels were detected due to the different placements of the measuring equipment. Classroom 1 was the classroom with the highest spatial variability of the measured signal, being differences in the maximum measured field with the spectrum analyzer up to 190.82 mV/m when placing the receiver at different positions. The P50, P90, P99 and maximum of the electric field values obtained in the different positions of this location are illustrated in Figure 4.9 in logarithmic units so as to represent better the differences between places and percentiles due to the high variability in the linear units. Moreover, more details of these results are given in Table 4.7 in linear units, where the different percentiles, mean, minimum and maximum field levels at each position are provided. As shown, the maximum measured samples in the different positions took values between 77.85 mV/m and 268.68 mV/m.

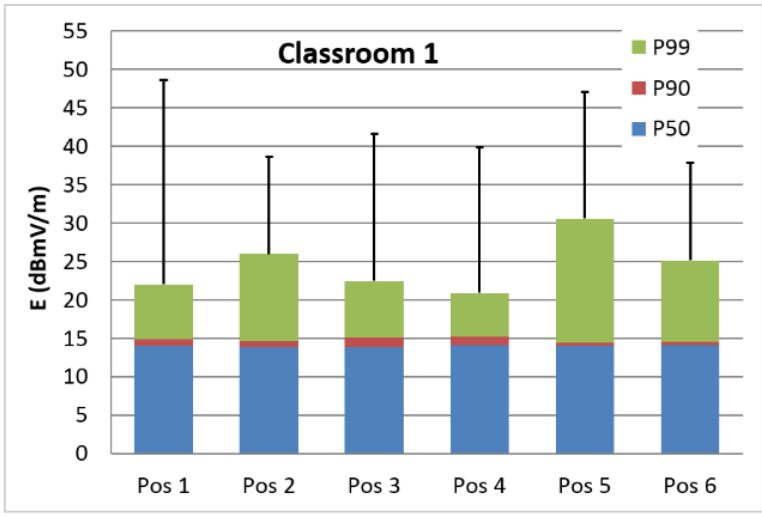

Figure 4.9. Electric field levels E (dBmV/m) recorded with the spectrum analyzer in Classroom 1.

Table 4.7. Electric field levels (mV/m) recorded with the spectrum analyzer in Classroom 1.

	P01	***P10***	***P50***	***P90***	***P99***	***Max***	***Min***	***Mean***
Pos 1	4.90	4.96	5.04	5.54	12.66	268.68	4.84	5.34
Pos 2	4.88	4.92	4.97	5.44	19.90	84.87	4.82	5.31
Pos 3	4.84	4.88	4.94	5.68	13.32	120.83	4.81	5.27
Pos 4	4.96	5.00	5.06	5.73	11.10	98.36	4.91	5.31
Pos 5	4.94	4.98	5.03	5.28	33.81	225.44	4.87	5.53
Pos 6	4.94	4.99	5.04	5.37	18.02	77.85	4.91	5.38

Figure 4.10 shows the P50, P90, P99 and the maximum measured levels in logarithmic units in the different positions of Classroom 2, and Table 4.8 shows also the P01, P10, minimum and mean levels of these recordings in linear units. The mean levels measured in the different positions of Classroom 2 were lower than in the other classrooms, obtaining mean electric field levels lower than 5 mV/m in three positions. The maximum levels measured in this classroom ranged between 11.49 mV/m and 72.78 mV/m for the different positions.

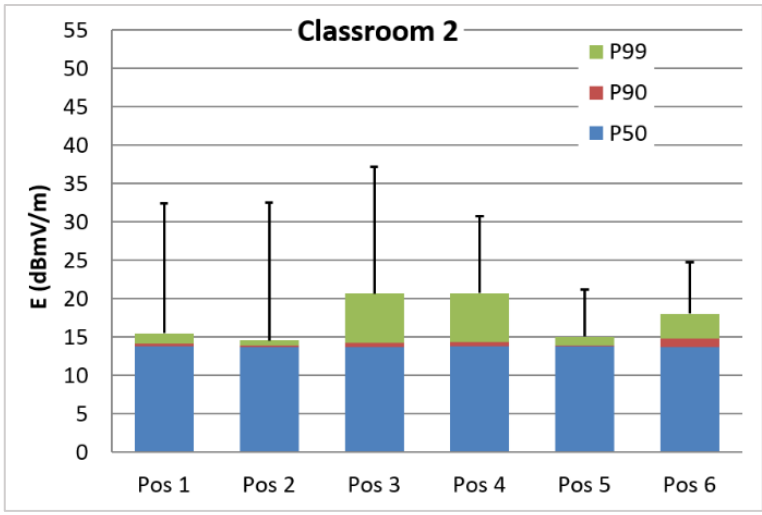

Figure 4.10.Electric field levels E (dBmV/m) recorded with the spectrum analyzer in Classroom 2.

Table 4.8. Electric field levels (mV/m) recorded with the spectrum analyzer in Classroom 2.

	P01	***P10***	***P50***	***P90***	***P99***	***Max***	***Min***	***Mean***
Pos 1	4.77	4.81	4.88	5.09	5.95	42.06	4.73	4.94
Pos 2	4.75	4.79	4.85	4.94	5.35	42.54	4.72	4.87
Pos 3	4.76	4.80	4.86	5.17	10.79	72.78	4.72	5.09
Pos 4	4.77	4.81	4.88	5.22	10.88	34.39	4.72	5.08
Pos 5	4.77	4.81	4.87	4.97	5.64	11.49	4.73	4.91
Pos 6	4.75	4.79	4.85	5.47	7.97	17.21	4.71	5.00

The results obtained from the measurements taken in the different positions of Classroom 3 are given in logarithmic units in Figure 4.11 and in linear units in Table 4.9. As shown, the maximum measured sample was acquired in position 4 and it was equal to 183.98 mV/m. In this classroom, the mean values of the different positions ranged from 5.07 mV/m to 5.42 mV/m and the P50 from 4.87 mV/m to 5.09 mV/m.

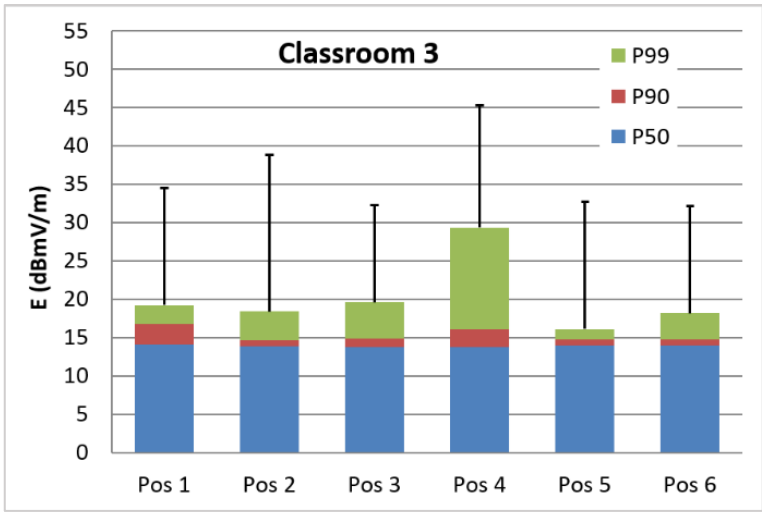

Figure 4.11.Electric field levels E (dBmV/m) recorded with the spectrum analyzer in Classroom 3.

Table 4.9. Electric field levels (mV/m) recorded with the spectrum analyzer in Classroom 3.

	P01	***P10***	***P50***	***P90***	***P99***	***Max***	***Min***	***Mean***
Pos 1	4.88	4.94	5.09	6.88	9.12	53.32	4.83	5.42
Pos 2	4.78	4.83	4.92	5.41	8.32	87.40	4.71	5.10
Pos 3	4.75	4.80	4.87	5.55	9.59	41.16	4.71	5.07
Pos 4	4.77	4.81	4.88	6.34	29.28	183.98	4.71	5.30
Pos 5	4.81	4.86	5.00	5.44	6.38	42.99	4.74	5.10
Pos 6	4.82	4.88	5.00	5.49	8.11	40.72	4.76	5.15

Regarding the corridors, the highest variability due to the different positions was found in Corridor 1, where the maximum signal level varied up to 99.29 mV/m, the P99 up to 6.69 mV/m and the P90 up to 2.46 mV/m when using the spectrum analyzer. Different statistics of the WiFi signal recorded in the different positions of this corridor can be seen in Figure 4.12 (in logarithmic units), and more detailed results in linear units are given in Table 4.10. As shown the maximum sample level was recorded in position 2 and it was equal to 113.15 mV/m. Position 5 was the placement where the minimum mean electric field level was obtained in this corridor.

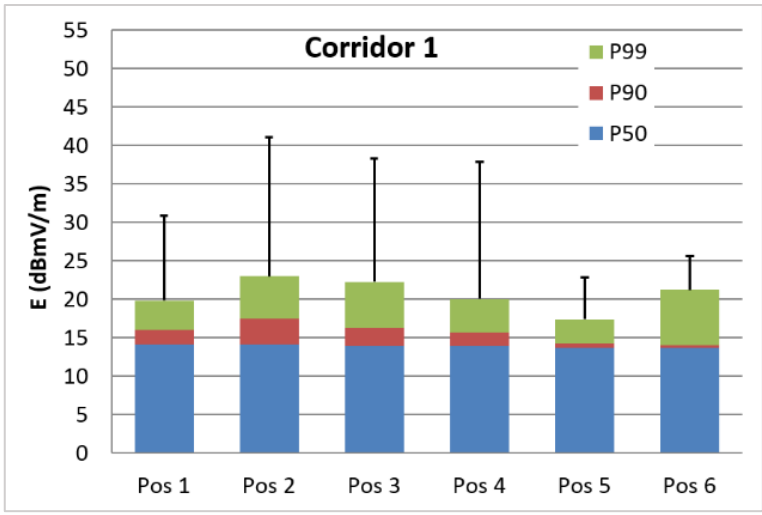

Figure 4.12. Electric field levels E(dBmV/m) recorded with the spectrum analyzer in Corridor 1.

Table 4.10. Electric field levels (mV/m) recorded with the spectrum analyzer in Corridor 1.

	P01	***P10***	***P50***	***P90***	***P99***	***Max***	***Min***	***Mean***
Pos 1	4.85	4.92	5.10	6.31	9.78	34.82	4.80	5.36
Pos 2	4.86	4.91	5.07	7.46	14.12	113.15	4.82	5.67
Pos 3	4.80	4.85	4.99	6.50	12.97	82.05	4.74	5.36
Pos 4	4.79	4.84	4.95	6.12	10.06	78.28	4.74	5.27
Pos 5	4.76	4.80	4.86	5.14	7.42	13.86	4.71	4.98
Pos 6	4.76	4.80	4.87	5.00	11.50	19.26	4.71	5.00

The electric field levels corresponding to Corridor 2 are presented in Figure 4.13 and in Table 4.11. The exposure levels in this corridor varied less than in the previous one, the electric field took maximum levels between 17.51 mV/m and 46.98 mV/m, this highest level was acquired in Position 6. Focusing on the other 5 positions, the maximum measured sample was very similar between different receiving points, taking values between 17.51 mV/m and 21.94 mV/m. In this corridor the mean exposure level ranged between 4.92 mV/m and 5.18 mV/m.

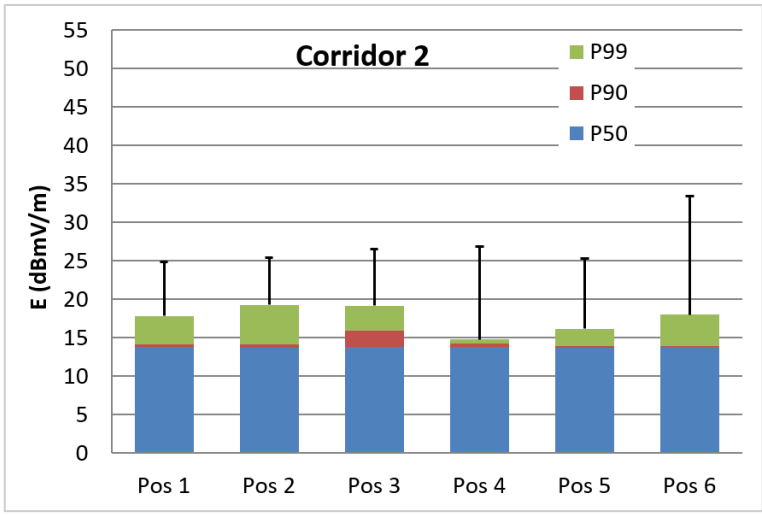

Figure 4.13. Electric field levels E (dBmV/m) recorded with the spectrum analyzer in Corridor 2.

Table 4.11. Electric field levels (mV/m) recorded with the spectrum analyzer in Corridor 2.

	P01	***P10***	***P50***	***P90***	***P99***	***Max***	***Min***	***Mean***
Pos 1	4.79	4.83	4.88	5.06	7.80	17.51	4.74	4.99
Pos 2	4.75	4.79	4.84	5.06	9.17	18.76	4.68	4.96
Pos 3	4.77	4.81	4.87	6.24	9.08	21.27	4.72	5.18
Pos 4	4.79	4.83	4.90	5.17	5.47	21.94	4.74	4.95
Pos 5	4.76	4.80	4.85	4.99	6.45	18.48	4.70	4.92
Pos 6	4.80	4.84	4.89	4.95	7.96	46.98	4.73	4.96

Finally, the results of the measurements performed in Corridor 3 are illustrated in Figure 4.14. Electric field levels E(dBmV/m) recorded with the spectrum analyzer in Corridor 3.Figure 4.14 in logarithmic units, showing the P50, P90, P99 and maximum electric field level in the different positions of this place. Moreover, Table 4.12 provides detailed results in linear units. As shown, the maximum electric field levels ranged between 24.47 mV/m and 69.29 mV/m, reaching this highest level in position 6.

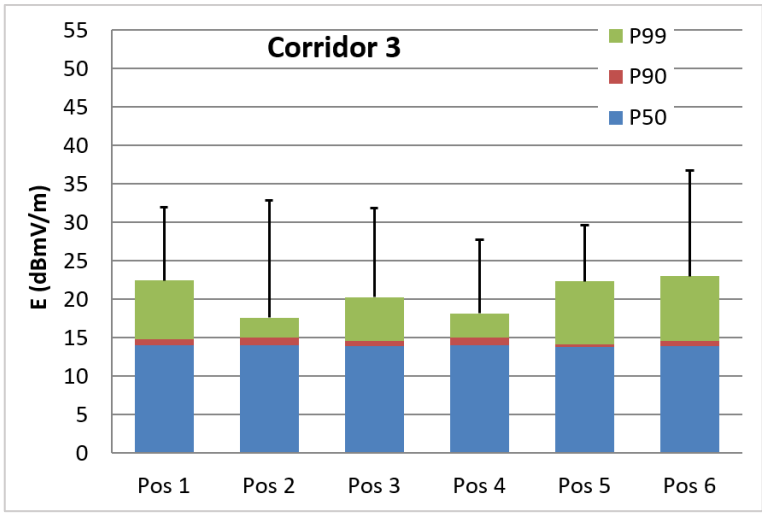

Figure 4.14. Electric field levels E(dBmV/m) recorded with the spectrum analyzer in Corridor 3.

Table 4.12. Electric field levels (mV/m) recorded with the spectrum analyzer in Corridor 3.

	P01	***P10***	***P50***	***P90***	***P99***	***Max***	***Min***	***Mean***
Pos 1	4.91	4.96	5.05	5.47	13.21	39.51	4.85	5.38
Pos 2	4.90	4.95	5.03	5.62	7.61	43.74	4.85	5.18
Pos 3	4.87	4.92	4.99	5.39	10.31	38.98	4.82	5.20
Pos 4	4.84	4.89	5.00	5.61	8.07	24.47	4.80	5.16
Pos 5	4.81	4.85	4.90	5.09	13.06	30.26	4.75	5.13
Pos 6	4.85	4.89	4.95	5.36	14.11	69.29	4.81	5.21

Finally, the exposure assessment in each corridor (Cor) and classroom (Cla) when using the spectrum analyzer and the personal exposure meter are summarized in Table 4.13 and Table 4.14, respectively. Different percentiles and the mean electric field value were calculated taking into account the six positions inside a classroom or corridor. The maximum and the minimum WiFi sample level acquired in each location are also provided in the tables. Differences in the obtained results can be seen due to the different instrumentation used. Focusing on the data recorded by means of the spectrum analyzer, the minimum field strength value obtained in the six locations was below the detection limit of the exposure meter (5 mV/m). An overestimation could be produced by the EME Spy when there was low WiFi signal, since it cannot detect field levels lower than

that limit. Furthermore, the personal exposure meter was recording a sample each 4 seconds while the spectrum analyzer recorded a sample per second, so more information about the signal could be obtained in this second case. This is important due to the signal transmission characteristics. WiFi signal is transmitted in the form of pulses of short duration, so a high signal variability in a short period of time is produced. Furthermore, both instruments were not exactly in the same position, they were separated a distance of 40 cm to fulfil the far field region requirement.

Table 4.13. Spectrum analyzer results (mV/m)

	Cor 1	***Cor 2***	***Cor 3***	***Cla 1***	***Cla 2***	***Cla 3***
Min	4.71	4.68	4.75	4.81	4.71	4.71
Mean (SD)	5.27 (0.23)	4.99 (0.09)	5.21 (0.08)	5.36 (0.09)	4.98 (0.08)	5.19 (0.13)
P50$_{Av}$[a] (SD)	4.97 (0.09)	4.87 (0.02)	4.99 (0.05)	5.02 (0.04)	4.86 (0.01)	4.96 (0.08)
P90$_{Av}$[a] (SD)	6.09 (0.84)	5.25 (0.45)	5.42 (0.18)	5.51 (0.16)	5.14 (0.18)	5.85 (0.56)
P99$_{Av}$[a] (SD)	10.98 (2.20)	7.66 (1.33)	11.06 (2.56)	18.14 (7.65)	7.76 (2.33)	11.80 (7.88)
Max$_{Av}$[a] (SD)	56.90 (36.54)	24.15 (10.32)	41.04 (14.16)	146.01 (73.76)	36.75 (19.94)	74.93 (51.39)
Max	113.15	46.98	69.29	268.68	72.78	183.98

SD: standard deviation.
[a] Mean values of the P50, P90, P99 and maximum levels of the electric field (mV/m) measured in the different positions of each place.

Table 4.14. Exposimeter results (mV/m)

	Cor 1	***Cor 2***	***Cor 3***	***Cla 1***	***Cla 2***	***Cla 3***
Min	5.00	17.00	5.00	13.00	8.00	5.00
Mean (SD)	15.62 (7.44)	50.16 (12.96)	16.24 (10.35)	70.90 (28.57)	19.35 (3.80)	12.39 (1.62)
P50$_{Av}$[a] (SD)	15.33 (7.70)	47.83 (15.43)	15.17 (11.13)	67.33 (28.98)	18.17 (3.80)	11.67 (1.70)
P90$_{Av}$[a] (SD)	22.32 (9.67)	64.83 (11.45)	24.52 (13.07)	84.87 (31.83)	25.33 (3.77)	19.00 (3.45)
P99$_{Av}$[a] (SD)	37.32 (13.96)	72.84 (9.97)	47.01 (22.95)	115.03 (50.64)	38.00 (2.58)	37.00 (9.97)
Max$_{Av}$[a] (SD)	89.33 (64.79)	83.00 (3.83)	84.83 (44.61)	186.54 (31.66)	46.17 (4.52)	53.83 (26.70)
Max	223.00	87.00	165.00	242.00	54.00	113.00

SD: standard deviation.
[a] Mean values of the P50, P90, P99 and maximum levels of the electric field (mV/m) measured in the different positions of each place.

The maximum measured level by means of the spectrum analyzer was equal to 268.68 mV/m, while when using the EME Spy it was 242 mV/m, both of them obtained in Classroom 1. Despite the differences in the results, both instruments are useful and suitable for assessing WiFi exposure variability at

2.4 GHz, as well as for comparing with exposure limits. Although the spectrum analyzer can provide more accurate results, personal exposure meters are useful to obtain information about the exposure distribution.

4. COMPARISON WITH WIFI LEVELS OBTAINED IN DIFFERENT MEASUREMENT CAMPAIGNS

Several measurement campaigns carried out by different authors were selected in order to compare the WiFi exposure levels obtained in different investigations. The instrumentation and the measurement scenarios in the different studies are described below. All the values were converted to electric field units (V/m) to allow the comparison with the exposure levels obtained in this work, as shown in Table 4.15.

Some studies in which data were recorded by means of personal exposure meters were selected. The EME Spy 120 was used in (Röösli 2008) and in (Joseph 2010a). In the first work, two different methods were used to calculate the statistics of the electric field when the measured level was below the detection limit of the instrument:

- the naïve approach, which was the one used in our work, and as explained before consists of replacing the measured level by the detection limit
- and the robust regression on order statistics (ROS) method, which consists of calculating statistics by fitting an assumed distribution to the observed data when they are below the detection limit. In this way, data values below the detection limit could be obtained.

Participants carried out an exposimeter during one week and the weekly statistics from 109 participants are given in Table 4.15. In (Joseph 2010a) the electric field levels in various locations of five countries were assessed and the average field levels measured in offices are given in Table 4.15, since this is a similar environment to the one considered in our work.

In (Sagar 2018) two different exposure meters were employed, the ExpoM-RF and the EME Spy 201, with a detection limit of 0.005 V/m at 2.4 GHz in order to measure electric fields in 5 different countries. The selected values for the comparison, the ones presented in Table 4.15, were the average exposure levels obtained in university areas.

In (Karipidis 2017) measurements in several schools were performed using a selective radiation meter and a tri-axial probe at 1.5 m above the ground. They performed some stationary measurements and also took samples while walking through the classrooms. For this comparison, the stationary measurements taken under the access point (average field value 0.114 V/m) and at the furthest student

desk to the access point (average field level 0.060 V/m) were selected. The average values of the field strengths were recorded, but no information about the detector employed is given.

A spectrum analyzer and a tri-axial probe were used in (Joseph 2010c) to receive signal levels in 27 outdoor locations and 3 indoor places and the WiFi exposure ranged between 0.006 and 0.1 V/m. Results were obtained measuring the maximum field strength and weighting it by means of a weighting factor (Verloock 2010).

In (Tomitsch 2015), measurement campaigns were carried out in several bedrooms during nights, repeating the measurements during three different years. The instrumentation employed consisted of a spectrum analyzer configured for obtaining maximum power levels (max-hold) and two biconical antennas. The median values of the electric fields were 0.00 V/m in 2006, 0.006 V/m in 2009 and 0.013 V/m in 2012, while the average values were 0.077 V/m in 2006, 0.118 V/m in 2009 and 0.105 V/m in 2012. Significant differences were observed between the median and mean values, explained because of the high standard deviation in the mean results.

Table 4.15. Electric field levels (V/m) obtained in different measurement campaigns

Ref	***Mean***	***Median***	***Range***	***Description***
(Sagar 2018)	0.01-0.03	-	-	Eme Spy 201 ExpoM-RF
(Joseph 2010a)	0.019-0.082	-	-	Eme Spy 120/ 121
(Joseph 2010c)	0.020	-	0.006-0.1	Weighting factor
(Röösli 2008) ROS	0.05	0.02	NA-0.23	Eme Spy 120
(Röösli 2008) Naïve	0.06	0.05	0.05-0.22	Eme spy 120
(Karipidis 2017)	0.060-0.114	-	-	Radiation Meter
(Tomitsch 2015)	0.077-0.118	0.000-0.013	-	Max-hold
Our work	0.005	0.005*	0.004-0.408	Analyzer 24 h
Our work	0.005	0.005*	0.005*-0.269	Analyzer 1 h
Our work	0.031	0.029	0.005-0.242	Eme Spy 200 1 h

* The calculated values were between 0.0045 and 0.0049 V/m, but when rounding to the nearest third decimal a value of 0.005 V/m is set.

As shown in Table 4.15, the results obtained with the EME Spy 120/121 are higher than those acquired in our work or with the EME Spy 200. One reason is that the detection limit of the EME Spy 120/121 is 0.05 V/m, while the EME

Spy 200 and 201 can detect field levels higher than 0.005 V/m, so the probability of overestimation in the first instrument is higher. When using spectrum analyzers, differences due to the equipment configurations can occur. We used the clear/write trace and the RMS detector to avoid overestimations of the signals, but for example in (Tomitsch 2015) max-hold measurements were taken. This is usually done when verifying compliance with the regulations in order to check the worst case scenario in terms of exposure levels. However, an increase in the average results is produced.

Finally, a comparison with the exposure limits given in the standards was done. The maximum sample level was obtained with the spectrum analyzer in Lab 2 and it was equal to 0.408 V/m. The exposure limit established in (ICNIRP 1998) for the general public in the 2.4 GHz frequency band is equal to 61 V/m, so the maximum measured sample is far below the reference limits.

5. CONCLUSIONS

An evaluation of the WiFi signal levels in the 2.4 GHz frequency band inside the university has been presented in this chapter. The first objective of this work was to perform measurements in real environments using the methodology and the configuration of the spectrum analyzer proposed in Chapter 3. As detailed in that chapter, the usefulness of this configuration lies in the acquisition of accurate and realistic WiFi signal samples, performing only frequency domain measurements, since in order to increase the accuracy provided by personal exposure meters and max-hold measurements with spectrum analyzers, some authors introduced weighting factors, but in these cases additional measurements are needed to calculate the weighting factors.

A measurement campaign based on recordings of 24-hour and 1-hour durations was carried out using a spectrum analyzer appropriately configured together with a tri-axial antenna system, in order to assess the temporal and spatial variability of WiFi exposure levels. A personal exposure meter was also employed for the 1-hour measurements and the differences in the results obtained with both instruments were explained.

Finally, exposure levels due to WiFi signals measured in other studies were compared, detailing the equipment and environments of these measurement campaigns, concluding that despite the differences in the results due to the use of different equipment or configurations, all the values presented were far below the exposure limits. The methods shown in the different measurement campaigns are useful to obtain the field distribution and to check compliance with exposure limits. However, if more accurate and robust results are required, professional equipment appropriately configured should be use.

Regarding the statistical analysis, it was observed that as signal levels can vary significantly, many times the mean values do not provide enough information because of the high standard deviation of the results. Although the mean, median and maximum values are suitable for epidemiological studies and for checking compliance with exposure limits, when more information about the signal is desired, percentiles are more appropriate statistics, since they give information on exposure levels for the different percentages of the measurement time.

PART 2: EMF EXPOSURE IN THE NEAR FIELD REGION

CHAPTER 5: WEARABLE ANTENNA DESIGNS

This chapter presents two wearable antenna models operating in the 2.4 GHz frequency band, both of them developed in this thesis not only with the purpose of improving previous works and provide solutions to current needs, but also in order to analyze the human exposure to the radiation coming from WBANs. The first antenna was designed for off-body communications and it was designed to minimize the interaction between the body and the antenna. An investigation of the body effect on antenna performance, as well as the power absorption in human tissues is presented. The second antenna was based on the off-body antenna model, but it was developed for inward radiation purposes in order to satisfy the demands of this types of devices.

1. INTRODUCTION

Wearable and implantable sensors are increasingly demanded because of its applications in many fields, such as healthcare, wellbeing, sports or entertainment. Several antenna designs have been proposed in the last years for use in WBANs. At first, the communication between sensors placed on the body was mainly done through wired connections, but now there is a growing trend towards wireless communications due to the advantages of removing cables. In addition, the 2.4 GHz frequency band, which is one of the spectrum bands allowed for wireless transmissions in these types of networks, is usually selected in WBANs, in part because of its worldwide availability (Cavallari 2014). Although several antenna models had been proposed for its use on and inside the human body, further improvements could be made concerning antenna performance and low power absorption. In addition, more research regarding the power absorbed in the body due to these devices was needed. Two antennas were designed during this thesis and the context that led to the development of each of the models is described below.

1.1. Research context of the antenna for off-body communications.

Author of this thesis had the opportunity of doing a research stay at Griffith University, Brisbane, Australia. There, small wireless sensor nodes had been developed to monitor human movement in sports during both training and match play (James 2013). The final design was packed in a box (see Figure 5.1) and had contact pins for electrical connections and an inset for buttons, where a keypad was put. This device can include a meander-line monopole antenna for communicating with other devices at 2.45 GHz. In (Varnoosfaderani 2015a) authors investigated the performance of the sensor with the meander-line monopole when it was placed on the human body and a huge decrease in the radiation efficiency of the antenna was reported, so any improvement in the antenna efficiency when wearing the sensor is desirable.

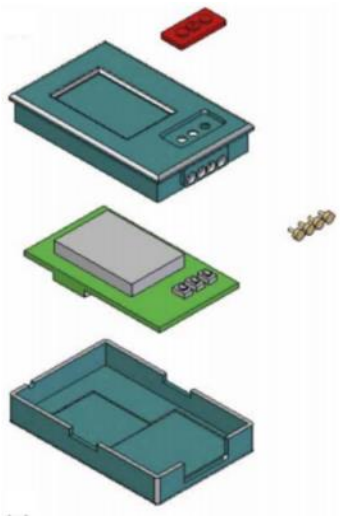

Figure 5.1. Assembly of the sensor node developed in (James 2013).

It is noteworthy that the sensors can also be used during sporting activities without real-time requirements. In such case, the sensor needs to be programmed to store the measurements. During the research stay at Griffith University, the author of this thesis had the opportunity of taking part in a research activity in which these types of devices were employed to investigate deteriorations in knee and ankle dynamics during running. Changes in these parts of the body due to fatigue were analyzed by utilizing a wearable musculo-skeletal monitoring system. This system includes a number of sensor modules as the one shown in Figure 5.2(a), which have a triaxial accelerometer (MMA7260QT) with a sensitivity of 2 g and a battery (3.6 V, 240 mA) that supports several hours of data logging. The sensors can be worn within pockets of Velcro straps or sports garments, as can be observed in the example of Figure 5.2(b), where a sensor module previously placed inside a box is shown. During the experiments, the sensors were attached to the lateral sides of the right knee and right ankle of the participants and were programmed to store accelerometer measurements during running. Once the activity was finished, data were transferred to an external computer using a CP2102 UART interface.

(a) (b)

Figure 5.2. (a) Sensor module, (b) Velcro strap with a pocket to insert the sensor.

This monitoring system allowed to investigate the changes in lower limbs accelerations and some conclusions were withdrawn, such as that the onset of fatigue appeared to be more distinct for runners having greater body mass. Moreover, it was possible to infer a runner's travelled distance and energy expended with an average error of 15%. However, for applications in which real-time is required, off-body communication is needed between the sensor and other device located out of the body. In such case, an appropriate antenna for establishing this communication is essential, but radiating as little power as possible inside the human body. Consequently, the design of this antenna tuned into one of the objectives of this chapter.

1.2. Research context of the antenna for in-body communications

The second antenna model presented in this chapter has the objective of contributing to improving in-body communications in WBANs.

The invention of wireless capsule endoscopy brought about the greatest revolution in the technology used to diagnose gastro-intestinal (GI) problems. One of the main issues that must be overcome in order to have wider clinical applications of wireless capsule endoscopy is the localization of the capsule without the need to employ cables (Basar 2013).

The "radio pill" extends the range of optical fiber endoscope technology to observe the complete length of the GI tract (Colson 1979; Basar 2012). The cylindrical pills (diameter 10 mm) equipped with a battery, camera and radio transmitter, are swallowed by the patient, and the images are recorded as the pill passes through the GI tract. Imperfections in the inside of the tract such as bleeding from tears, polyps and swelling can be identified and, if precisely located, can be repaired (Quirini 2007). The video signal from the pill is recorded using an array of surface electrodes similar to those used in electrocardiogram

recording. The electrodes are attached to the skin using conductive gel and connected by an array of wires to a central, wearable recording unit. This allows the patient freedom of movement during the 24-78 hours required for the pill to pass through the complete GI tract. Normal movements aid the movement of the pill.

Algorithms to track the pill using radiofrequency signals have been proposed using the signal intensity received at four locations (Adepoju 2015), however, little research has been done regarding the receiving antenna. The detection of subsurface transmitters and the irradiation of conductive materials using a surface antenna have applications in many different fields including ground probing radar (Clouch 1976), non-destructive testing of concrete (Kijewski-Correa 2006), motion sensors for swimmers (Lecoutere 2016), earth movement radio beacons during blasting (Appleby 2015) and ocean buoy transmitters (Loni 2017). The surface electric field profile from a subsurface transmitter is quite complex as the surface propagating wave (lateral wave) and the direct wave can result in a significant interference pattern (Wu 1982; Emelyanenko 2017) which can make the location of the transmitter using a sparse array of sensors very difficult. In addition, the input impedance of an antenna placed on the body can be significantly modified due to the dielectric loading experienced by the antenna (Scanlon 2003) which can have a significant effect on the power received values, particularly during movement. Another alternative is the use of gelled electrodes as the ones employed in ECG and EEG measurements taped to the skin. These are uncomfortable to wear, are influenced by movement and muscle activity, require a wired network and can be prone to significant external interference.

The second antenna presented in this chapter consist of a new electric field sensor which requires no conductive gel and forms part of a wireless sensor network worn on the torso. The elimination of wires and gel reduces external noises and greatly increases the comfort of the user.

2. ANTENNA MODEL FOR OFF-BODY COMMUNICATIONS

Wearable sensors are used in athlete monitoring and human monitoring in normal living. The wireless transmission off the body is usually a line-of-sight radio link. A communications transceiver conveys relevant information off the body to a coach, a television channel and /or a data logging facility to score, analyze and suggest improvements in human activities (Armstrong 2007; Lee 2009; Pantelopoulos 2010; Yang 2014). The wearable sensors and communications transmitters must be physically small, low powered and conformal to the human body for wearer comfort. The small size of the antenna and the close proximity to the human body greatly reduce the radiation range. For example, Varnoosfaderani et al. (2015a) reported a decrease in the off-body range at 2.45 GHz from 20 m in free space to 3 m for a +10 dBm transmitter located in an arm band positioned on the upper arm to a far field receiver with sensitivity of -95 dBm. The location of the sensors on the body is an important fact. Clearly, the movement of each limb and above/below each joint is different, and so the off-body communications might use a central node with other sensors distributed around the body and connected wirelessly to the central node. This is exemplified in Figure 5.3 with a central node located on the torso.

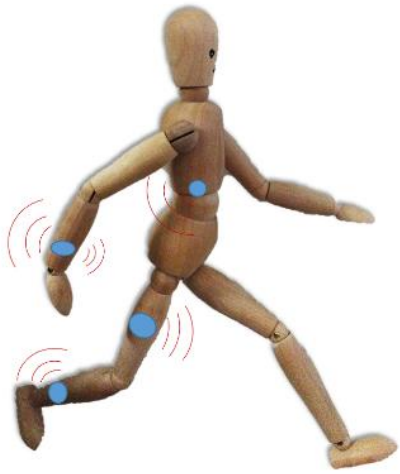

Figure 5.3. Wearable sensors in different locations of the body and a central node on the torso to be connected to an off-body receiver.

Antennas placed on or close to lossy materials show a decrease in the efficiency and a shift in the resonant frequency, even though the directivity is increased. These three effects are undesirable as the human body moves. For

example, in the work developed by Khan at al. (2012), the performance of five different wearable antennas at 2.45 GHz was investigated when these transmitters were located on several positions of the body. Results showed frequency shifts from the free space value up to 33%, and the efficiency was reduced between 20% and 96% for the different types of antennas when they were at 1 mm away from the body.

Any improvement in the antenna efficiency will increase the transmission distance and/or the battery life of wireless sensors. On many conductive surfaces, the antenna can be isolated from the conducting materials using a ground plane. For wearable technology, this is not practical for reasons of human comfort and the separation distance required between the active element and the ground plane. A flexible patch antenna is one strategy, however, the antenna center frequency and efficiency change with movement (Galehdar 2007; Lecoutere 2016). A more efficient antenna design uses a rectangular resonant cavity with a slot (Takei 1999; Varnoosfaderani 2015b).

Based on the model developed by Varnoosfaderani et al. (2015b), a new cavity slot antenna operating at 2.45 GHz that improves the performance of the previous one is presented, together with the relationship between the total radio frequency absorption and the antenna efficiency when the antenna is mounted on different parts of the body. The main advantage of this redesigned antenna is the improvement of the efficiency, which lies between 62% and 75% when it is placed on the body. In (Varnoosfaderani 2015), the efficiency was 55% when the antenna was on the arm. The S11 parameter is also improved compared to the previous design. Moreover, the slot dimensions of the new antenna (47 mm × 9 mm) are significantly smaller than the previous one (54 mm × 30 mm), and the material of the box in which the slot is printed is biodegradable (PLA). Specific absorption rate values were evaluated at 2.45 GHz in different simulation scenarios. The effect of positioning the antenna assembly on different locations on the body was investigated using participants with different body mass index (BMI). Practical information about experimental results and simulation accuracy compared with measurements is provided.

2.1. Theory and Modeling

A wire dipole antenna above a perfectly conducting ground plane of infinite extent can be modeled as an image antenna (Balanis 2008), and the radiation pattern can be calculated assuming two identical antennas in free space. As the distance above the ground plane decreases, the dipole impedance decreases until

a zero separation distance, approaching the dipole antenna impedance to zero. If the ground plane is not perfectly conducting, it is possible to use complex image theory (Smith 1981). Given the complexity of the human anatomy and the many body parts with different conductivity and permittivity, numerical modeling was implemented to investigate the performance of the antenna on the human body using commercially available FDTD software (CST 2016). Antenna efficiency, various absorption coefficients and the radiation patterns of the antenna on human anatomy were determined.

The radiation efficiency η in the vicinity of a series resonance of a generic antenna is defined by the following equation:

$$\eta = \frac{R_r}{R_r + R_L} \tag{5.1}$$

where R_r is the radiation resistance of the antenna and R_L is the resistive loss in the antenna.

The total absorbed power in biological tissue P_a is given by:

$$P_a = \int_V \sigma E^2 dV \tag{5.2}$$

where σ is the conductivity of the tissue, E is the root mean square of the internal electric field generated within the tissue and contained in a volume element dV.

Radiation efficiency and the power absorbed in the body are related by:

$$\eta = \frac{P_r}{P_{in}} = \frac{P_r}{P_r + P_d + P_a} \tag{5.3}$$

where P_r is the radiated power, P_{in} is the input power and P_d is the power dissipated in the antenna.

The SAR is a measure of the power absorbed per unit of mass and it can be averaged over the whole body, or over a smaller part of the mass. In this study, SAR was averaged over 10 g of contiguous tissue and the maximum SAR reported for the exposure at 2.45 GHz, as specified in (ICNIRP 1998; IEEE 2005; McIntosh 2010), is given by:

$$SAR = \frac{\sigma |E|^2}{\rho} \tag{5.4}$$

where ρ is the mass density of the biological tissue.

A voxel body model (Gustav) included in the CST software was used in the simulations. The model represents a 38 years old male with height of 176 cm and weight of 69 kg. The dielectric properties of human tissues, which affect the performance of wearable antennas and influence the power absorbed by the body, have been evaluated at different frequencies in the past years (Gabriel 1996; Gabriel 1999). However, the conductivity and permittivity values differ for every individual due to different factors such as anatomical aspects and the age (Peyman 2001; Vallejo 2013). At 2.45 GHz the conductivity and relative permittivity of the different body tissues vary from 0.095 to 3.458 S/m and from 5.147 to 68.361, respectively (IFAC). The biological material properties of the body model incorporated in the simulations were recalculated using the 4-Cole-Cole formulation in the frequency band of interest, which can be found in (IFAC).

2.2. Antenna design and implementation

A box made of biodegradable Polylactic Acid (PLA) material was fabricated using 3D printing technology (ε_r = 4, tanδ = 0.02, where ε_r is the relative permittivity and tanδ is the dielectric loss tangent). The internal walls of the box were coated with conducting silver paste (σ = 4.3×106 S/m), except for the resonant slot, which was not coated. The antenna was designed following the procedure described in (Varnoosfaderani 2015b), where the effects of the slot dimensions were reported. The internal box dimensions were 56 mm × 33 mm × 11 mm, and the wall thickness was 1.5 mm. A rectangular monopole made of brass (thickness 0.1 mm and σ = 1.59×107 S/m), was used to excite the slot. A PLA support (5 mm × 5 mm × 6.7 mm) was used to position the monopole at a fixed height. An SMA connector was soldered to the monopole and attached to the box. The 3D model of the antenna is shown Figure 5.4(a) and the final design in Figure 5.4(b). Top and side views are shown in Figure 5.4(c) and Figure 5.4(d), respectively. Table 5.1 specifies the values of the parameters of the antenna given in the figures, this is, the dimensions of each part of the antenna.

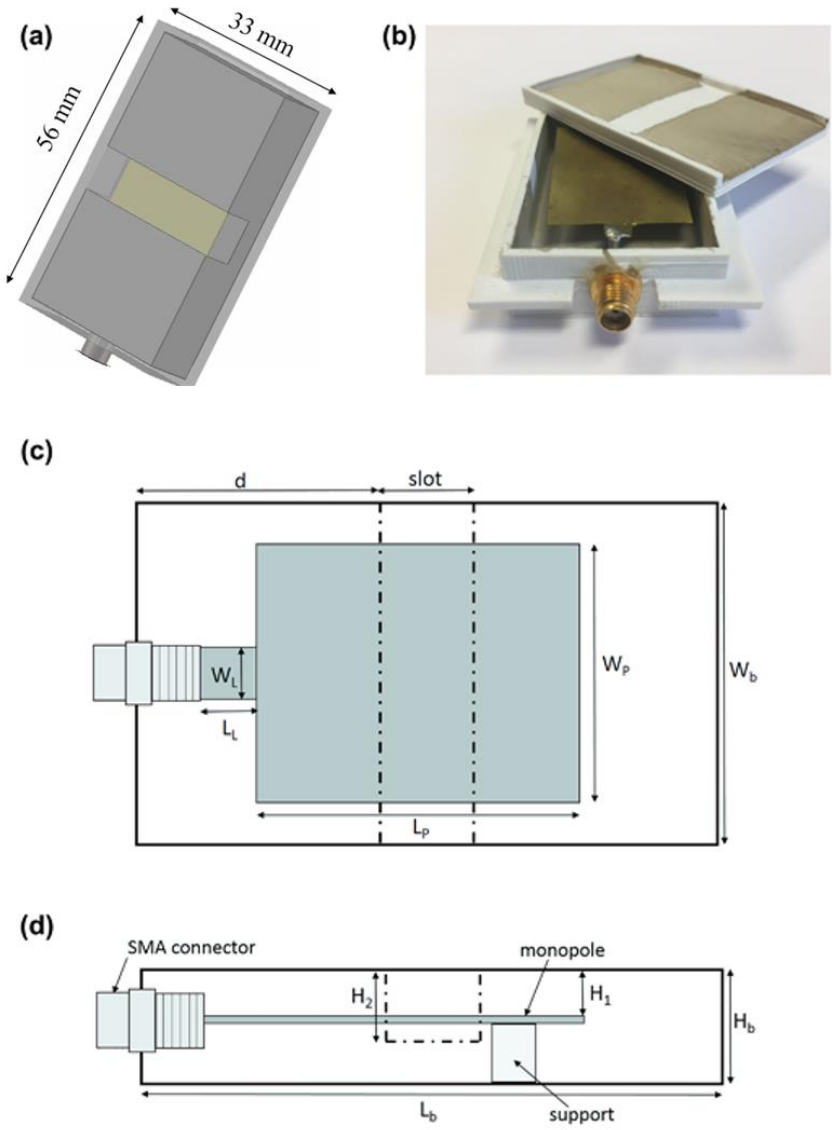

Figure 5.4. (a) 3D Model of the off-body slot antenna, (b) Final antenna design, (c) Top view, and (d) Side view.

The length of the slot was $\lambda/2$ (λ is the wavelength of radiation on the surface of the medium) and the monopole $\lambda_0/4$ (λ_0 is the free space wavelength) were determined by:

$$\lambda = \frac{c}{f\sqrt{\varepsilon_{eff}}} \qquad \varepsilon_{eff} \cong \frac{\varepsilon_r + 1}{2} \tag{5.5}$$

where f is the frequency, c is the speed of light, ε_{eff} is the effective permittivity and ε_r is the relative permittivity. The length of the $\lambda/2$ slot on the surface of the PLA material was initially calculated as 38.5 mm, and after optimization, the length was 47 mm long and 9 mm wide. As the length of the slot was bigger than the width of the box, it was folded onto the side walls perpendicular to the major axis (see Figure 5.4).

The CST software with the previously described human body model (CST 2016) was used to optimize the slot and to simulate antenna performance in free space and when placed on the human body. The optimization of the antenna was performed in order to improve the radiation efficiency in the frequency range of interest. Table 5.1 shows the parameters of the antenna and the box after the optimization.

Table 5.1. Optimized dimensions of the slot antenna for off-body communications

Parameter	W_b	L_b	W_p	L_p	W_L	L_L	**d**	H_1	H_2	H_b
Value (mm)	33	56	27	34	5	5.5	23	4	7	11

The bottom of the box was placed on different parts of the arm, torso and thigh with no air gap between the body and the antenna in order to analyze the effect of the body on the antenna performance and the power absorption in the human tissues. Figure 5.5 shows an example of the box placed on the arm above the elbow of the human model.

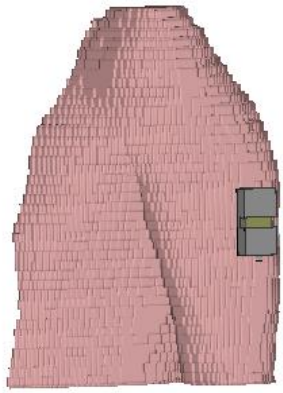

Figure 5.5. Antenna placed on the arm above the elbow of the human model.

2.3. Parameters analyzed

An analysis of the antenna-body effects can be done from power absorption, return loss and antenna efficiency. All these parameters were obtained in simulations, analyzing the total power absorbed together with the SAR values, the antenna efficiency and the return loss. This last parameter was also obtained through experimental measurements, evaluating the frequency shift experienced when the antenna was placed on different locations.

As the dielectric properties of body tissues can vary from person to person, it is important to evaluate the antenna properties not only on different parts of the body but also on different participants. People with different BMI (17 and 29 kg/m2) and different age (22-59 years old) participated in the experiment. The locations on the body where the antenna was placed during simulations and measurements are indicated in Figure 5.6. These locations include several positions on the outer arm (the wrist, above the elbow and on the upper arm), and also locations on the middle of the torso close to the navel (Torso 1), on the left side of the torso (Torso 2) and on the thigh.

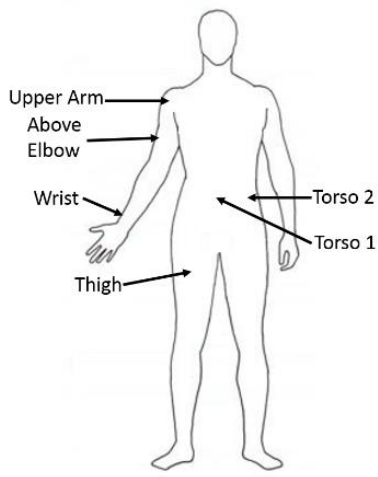

Figure 5.6. Positions of the body where the antenna was placed in simulations and measurements.

2.4. Results of the off-body antenna model

Radiation absorption

Figure 5.7 shows the relationship between the antenna radiation efficiency and the power absorbed in body tissues. The antenna was placed on ten locations

of the body to achieve different values of efficiency. As shown, the calculated power deposited in human tissues was found to be linearly related to the antenna efficiency (Pearson's correlation coefficient r = 0.99). The input power was 100 mW at 2.45 GHz. The radiation efficiency was 97% in free space, and decreased when the antenna was on body with values between 62% (on the upper arm) and 75% (on the side of the torso). On the other parts of the arm, the efficiency was between 67% and 72%, on the thigh it was 64% and on the middle of the torso 68%. The maximum power absorbed in the body was 33.9 mW corresponding to the lowest performance of the antenna.

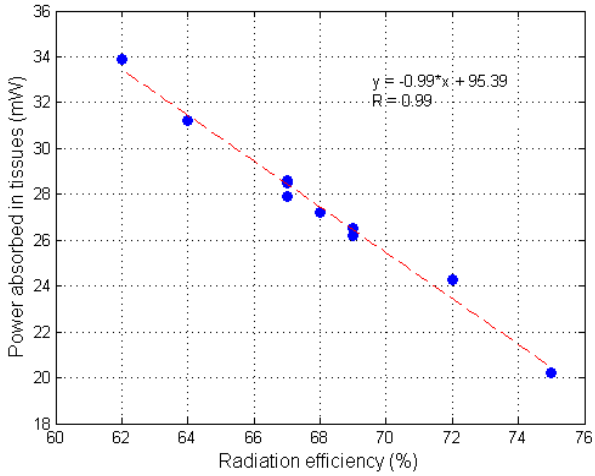

Figure 5.7. Power absorbed in tissues as function of antenna radiation efficiency.

The SAR at 2.45 GHz was averaged over 10 g of mass and the results can be seen in Figure 5.8. As illustrated, on some locations simulations were performed more than once, but moving the antenna some cm. The maximum value was 0.316 W/kg when the antenna was located on the upper arm. The two simulations carried out on this part of the body differ from each other more than in the other parts. This can be explained because the antennas were more separated from each other than on the other locations. The maximum SAR values for the other parts of the body were 0.165 W/kg on the wrist, 0.148 W/kg above the elbow, 0.196 W/kg on the thigh, and 0.185 and 0.147 W/kg on the middle and side areas of the torso.

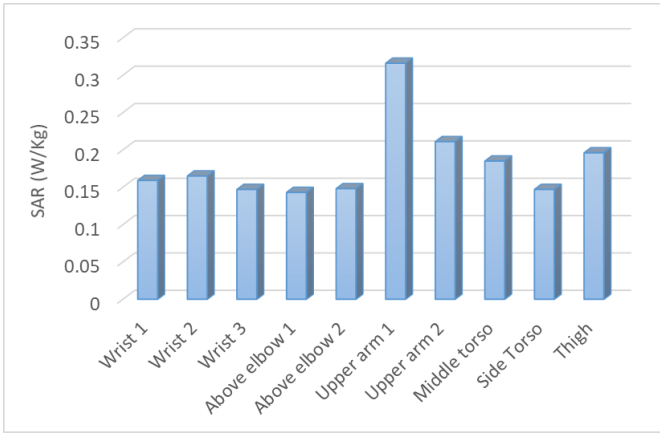

Figure 5.8. SAR values obtained for the different parts on Gustav body model.

All values are well below the basic restrictions provided by international standards; at 2.45 GHz the basic restrictions for general public are 2 W/kg for the head and trunk and 4 W/kg for the limbs when SAR is averaged over 10 g of tissue, as indicated by IEEE Standards and ICNIRP Guidelines (ICNIRP 1998; IEEE 2005). Figure 5.9 shows an example of SAR distribution in 3D and in three orthogonal cuts. The cuts are made through the maximum 10 g SAR point. As shown, the highest amount of power is absorbed in the first layers of the body.

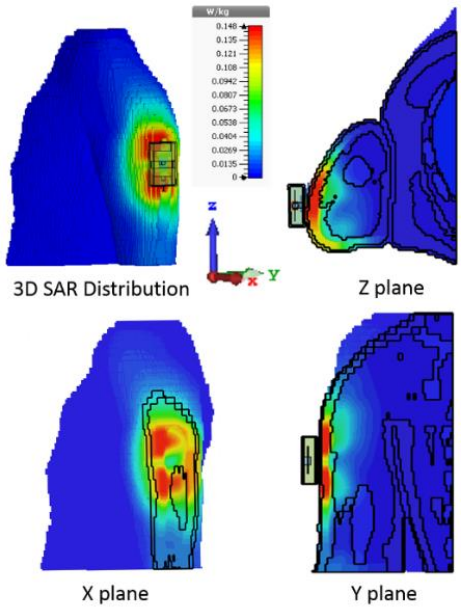

Figure 5.9. SAR distribution averaged over 10 g when the antenna was placed on the arm above the elbow.

To evaluate the behavior of the antenna on the different parts of the body, a figure of merit F proposed in (Anguera 2012) was used. This parameter defines the ratio of the antenna efficiency over the SAR for a given frequency. The antenna efficiency considers the radiation efficiency and the mismatch losses. The best performance (highest figure of merit) was found for locations on the left side of the torso, as evident in Figure 5.10. This means that in this location the power radiated out from the body over the SAR is maximized. The smallest F value occurred when the antenna was placed on the upper arm and on the thigh, since these positions resulted in the highest SAR values. When the antenna was placed on these two parts, the results showed the highest power absorbed by the body and therefore, the lowest radiation efficiencies.

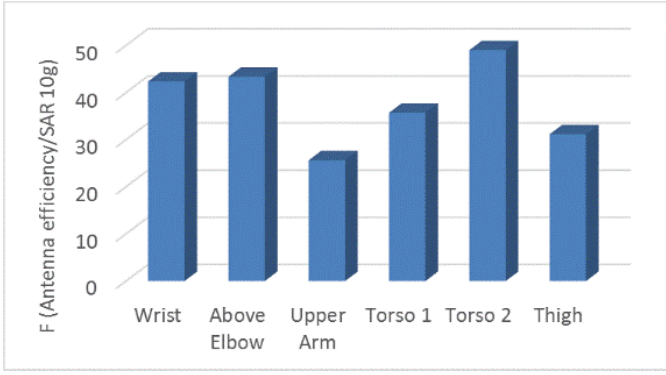

Figure 5.10. Figure of merit F (Antenna efficiency over 10 g averaged SAR) at 2.45 GHz calculated at different locations of the body.

Frequency shift

Experimental measurements were performed on six participants to study the frequency shift when the antenna was in free space and placed on different parts of the body. The six participants had BMI between 17 and 29 kg/m^2 and ages between 22 and 59 years old. The antenna was placed on various parts of the body (Figure 5.6) corresponding to the simulations. The antenna was attached to the participants using plastic film. A portable Vector Network Analyzer (N9923A Field Fox Handheld RF VNA @6Hz) with 50 Ω impedance was used to measure the frequency shift in each situation. The -10 dB bandwidth of the antenna in free space was 12.5% in simulations (2.27 – 2.57 GHz) and measurements, and it did not change when the antenna was on the body. The resonant frequency changed between 2.26 GHz and 2.32 GHz in simulations on body and between 2.36 GHz and 2.45 GHz in measurements. An example of the simulated and measured return loss when the antenna was in free space and on the human body is shown

in Figure 5.11. In this case, the antenna was above the elbow and the participant had a BMI of 23.57 kg/m². The measured resonant frequency in free space was less than the frequency calculated in the simulated result. This is thought to be due to small differences between the fabricated antennas and the simulation design. This includes variations in material properties, like those due to the ink thickness and the curing process of the conductive silver ink. Moreover, a procedure based on measurements and simulations was followed to establish the relative permittivity of the PLA box, which resulted in $\varepsilon_r = 4$ for simulations. Several monopoles of different lengths were used to feed the PLA box with a slot, and comparisons between measurements and simulations with different permittivities were performed. Small differences in box dimensions can occur, as the 3D printer had a tolerance close to 0.5 mm. When placing the antenna on the body some deviations were observed due to different body properties (anatomical, different dielectric properties).

The frequency shift was found to be higher in simulations compared to that observed in the experimental measurements. The maximum difference occurred when the on body antenna was close to the elbow (6.61%) and on the thigh (5.86%). The minimum frequency shift in simulation results was obtained in the middle of the torso (4.21%), followed by upper arm (4.75%) and the side of the torso (4.95%). In measurements, the resonant frequency varied up to 2.51%.

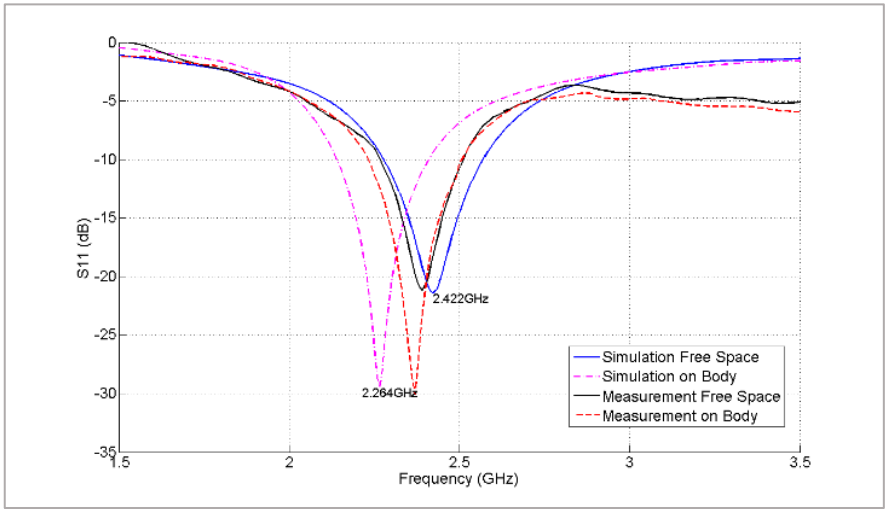

Figure 5.11. Measured and simulated S11 parameter relative to 50 Ω of antenna in free space and placed above elbow.

Table 5.2 shows the mean and the standard deviation of the resonant frequency when the antenna was placed on the different parts of the body for all

participants. Although six people participated in the experiment, a total of ten measurements on each part of the body were carried out. Four people participated on two different days. In this way, uncertainties due to different positions of the antenna and skin condition could be taken into account. Simulation results are included in the column 'modeled' and the probability of being statistically identical to measurements is given by the probability mass function in the column 'probability'. The simulation results with a better match with measurements correspond to situations in which the antenna was placed on the upper arm and on the side of the torso. The BMI of the participants was found to be not an influential factor on the measurement results.

Table 5.2. Mean and Standard Deviation of Measurements, Simulation Results and Their Probability

	Frequency (GHz)			
Position	**Mean**	**STD**	**Modelled**	**Probability**
Free Space	**2.390**		**2.422**	
Wrist	2.386	2.46×10^{-2}	2.282	2.11×10^{-3}
Above Elbow	2.413	2.45×10^{-2}	2.262	9.43×10^{-8}
Upper Arm	2.411	3.38×10^{-2}	2.307	1.04×10^{-1}
Torso 1	2.438	6.67×10^{-3}	2.320	1.01×10^{-66}
Torso 2	2.384	2.60×10^{-2}	2.302	1.02×10^{-1}
Thigh	2.425	1.85×10^{-2}	2.280	1.04×10^{-12}

Radiation patterns of the antenna in free space and on-body at 2.45 GHz are shown in Figure 5.12. The back radiation of the antenna is reduced when worn on the body. No correlation was found between the front-to-back isolation of the antenna and the power absorbed in the body.

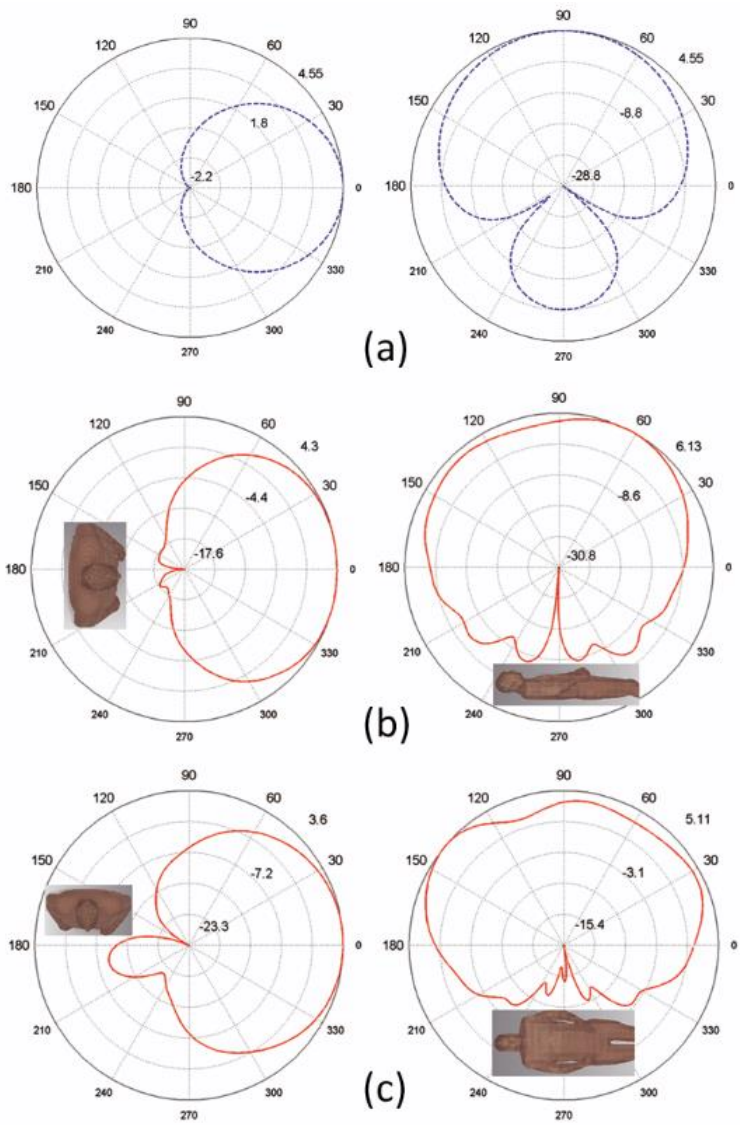

Figure 5.12. Simulated radiation patterns at 2.45 GHz in both horizontal (x-y) and vertical (x-z) planes (a) in free space, (b) when antenna is on the middle of the torso, and (c) above the elbow.

2.5. Conclusions of the Off-body antenna design

One of the main problems of wearable antennas is the interaction between the body and the antenna. As part of the power is absorbed in the human tissues, the radiation efficiency of the antenna is reduced. In addition the body causes a shift in the resonant frequency. A slot antenna in a conductive box was used to minimize the interaction between the human body and the antenna. In this way

not only the absorption loss is reduced, but also the human effect on the antenna performance.

The antenna design was optimized to work at 2.45 GHz, achieving a radiation efficiency of 97% in free space and between 62% and 75% when it is placed on the body. In simulations, the resonant frequency reached its maximum shift when the antenna was above the elbow (6.61%). Experimental measurements showed a maximum frequency shift of 2.51%. Moreover, when using this antenna design results did not depend on the body-mass index for each individual. One limitation of this wearable antenna is that it has to be fixed and in contact with the skin to prevent changes in performance. The probe inside the box needs to be precisely positioned for maximum performance.

The SAR was studied by means of simulations and results proved that this antenna is appropriate for on/off body communications since the maximum 10 g averaged SAR value was 0.316 W/kg for 100 mW input power. This is well below the international limits and this value would be reduced if the distance from the body was increased (Sabrin 2015). These SAR values are also satisfactory in comparison to results at the same frequency reported by other authors (De Santis 2012; Soh 2015).

SAR values are useful to verify compliance with health standards and they are representative of localized absorption. But this does not allow the evaluation of the power absorbed by the different parts of the body, since SAR results give information about the maximum absorption averaged over 10 g. The power absorbed in tissues was found to be the best parameter for measuring the total absorption in parts of the body (Risco 2012). These authors demonstrated that two similar values of SAR can be related to very different values of head absorption. In our study results showed that when the slot antenna was above the elbow, absorption was less correlated with SAR than at other locations.

Considering all the parameters studied in this work (radiation efficiency, frequency shift, power absorbed and SAR), it can be concluded that this antenna performs efficiently at most locations of the body and by different people.

3. ANTENNA MODEL FOR IN-BODY COMMUNICATIONS

Considering the advantages of the off-body slot antenna previously presented, we decided to make an antenna for inward radiation purposes based on that previous design in order to satisfy the demands of this types of devices. Due to the necessity of an antenna for tracking the gastro-intestinal radio pill, this new design was fabricated to be placed on the body skin being appropriate for communicating to a capsule inside the body.

Different systems for capsule endoscopy have been developed to operate at different frequency bands, which usually are 433 MHz, 868 MHz, 915 MHz or 2.4 GHz (Kim 2012). The size of the capsule and receiver is a key aspect in this type of applications. The higher the operating frequency, the smaller the size of the pill and the receiver can be. However, attenuation at 2.4 GHz is higher than at lower frequencies. The algorithms developed for radio localization of endoscopic capsules require several receivers around the body (Ye 2011). In (Vitas 2014) an algorithm for radio localization of a capsule using several receivers worn in a vest around the body was presented (See Figure 5.13). These authors state that any application of localization requires at least three receivers and that their localization algorithms can benefit from collecting RF signal power from as many as possible receiving antennas. Thus, they remark that the high attenuation factor obtained at 2.45 GHz will be low if several receivers are placed on the body, making this frequency appropriate for the capsule endoscopy.

Figure 5.13. Vest with receiver antenna array proposed in (Vitas 2014).

As little research has been done regarding the receiving antenna, this part of the chapter is focused on redesigning the off-body antenna model for making a receiver appropriate for tracking the radio pill.

This antenna followed the design of the previous one, but in this case, the slot was pressed against the body skin since it was intended for in-body communications. In order to have this second design working in the 2.4 GHz frequency band, the box and slot dimensions as well as the feed were optimized to match the body impedance.

3.1. Theory and Modeling

One approach describing the function of an antenna is to match the impedance of the transmitter circuit to the surrounding media, in most cases this medium is air with an impedance of 377 Ω and the feed transmission line has a characteristic impedance of 50 Ω. In the case of matching an antenna to the human soft tissue, the characteristics of the antenna must be modified to match the complex impedance (conductivity and permittivity).

As shown in the case of the off-body design, a rectangular slot antenna in air is resonant when the length l is approximately one half free space wavelength λ_0:

$$l = \frac{\lambda_0}{2}\sqrt{\frac{2}{1+\varepsilon_r}} \qquad (5.6)$$

Moreover, the width of the slot influences the bandwidth of the antenna. When the slot is fabricated on a thin, insulating substrate, the length must be reduced slightly to maintain the same resonant frequency due to the relative permittivity ε_r of the substrate. The equation (5.5) showed the relation between the wavelength and the permittivity of the medium. But in the case of an inward directed antenna, the signal travels though several mediums (the different tissues of the human body). When there is more than one medium, the equivalent relative permittivity ε_{eq} is given by (Nakamura 2005):

$$\varepsilon_{eq} = \left(\sum_{n=1}^{N}\frac{d_n}{\varepsilon_n}\right)^{-1} \cdot \left(\sum_{n=1}^{N} d_n\right) \qquad (5.7)$$

where d_n is the thickness of each medium (in case of human body is the thickness of each tissue), ε_n the permittivity of the n^{th} tissue and N is the number of tissues. Changing the antenna used for off-body communications to an inward radiating antenna requires a reduction in the slot length, which depends on the electromagnetic characteristics on the skin and subsurface tissues. The basic

tissue layers of the human torso from the outside to the inside are: skin, subcutaneous fat, muscle, visceral fat and intestine (Arab 2013). Table 5.3 shows the dielectric properties at 2.45 GHz of these layers, as well as their thickness in a female subject with low visceral fat (Nakamura 2005; Arab 2013; Gabriel 1999). All these tissues can be described as lossy dielectric materials as $0.14 < \frac{\sigma}{2\pi f \varepsilon_r \varepsilon_0} < 0.28$ where σ is the conductivity, f is the frequency and ε_0 is the permittivity of free space. Selecting the thickness of each tissue as the average of the range of values shown in Table 5.3 and using equations (5.6) and (5.7), the slot length was estimated to be l = 31 mm. The box thickness (1.5 mm) in which the slot is printed was also considered.

Table 5.3. Tissue properties at 2.45 GHz

Tissue name	Conductivity σ (S/m)	Relative permittivity ε	Thickness (mm)
Dry Skin	1.464	38.007	1.1-1.6
Subcutaneous Fat	0.104	5.280	17-34
Visceral Fat	0.104	5.280	15-36
Muscle	1.738	52.729	8-16
Small intestine wall	3.173	54.425	1-3

Following these calculations, a new slot was designed and optimised using the previously employed simulation software (CST Microwave Studio), together with the anatomical voxel model also used in the previous work.

3.2. Antenna Design

The antenna box was 3D printed in PLA material and lined with conductive silver paste apart from the slot on the lid (see Figure 5.14). The relative permittivity (εr) and the dielectric loss tangent (tanδ) of the box are εr = 4 and tanδ = 0.02. The conductivity of the silver paste is σ = 4.3×106 S/m. A rectangular monopole made of brass (thickness 0.1 mm and σ = 1.59×107 S/m) was used to excite the slot. The antenna was placed on different locations of the torso in a way that the slot was covered completely by the skin. The inward antenna placed on the torso works at 2.45 GHz with return loss lower than - 10 dB for a slot length higher than 22 mm. After optimizing the impedance matching, the slot dimensions were 28 mm long and 7 mm wide. Table 5.4 defines the most significant dimensions of the new antenna.

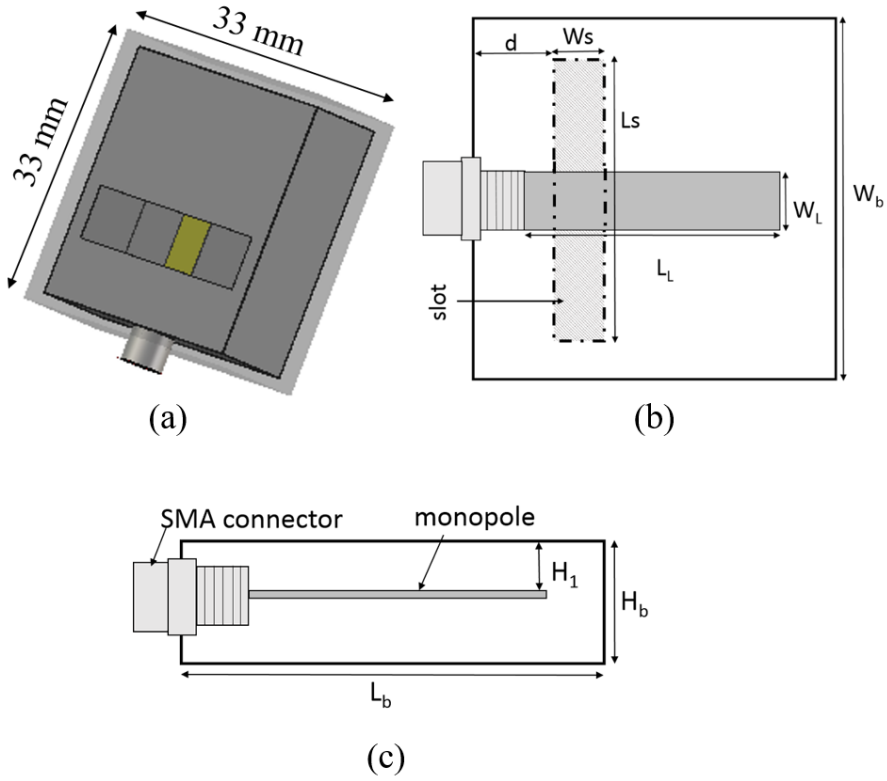

Figure 5.14.(a) 3D Model of the in-body slot antenna, (b) Top view, and (c) Side view.

Table 5.4. Dimensions of the slot antenna for in-body communications

Parameter	W_b	L_b	W_s	L_s	W_L	L_L	d	H_1	H_b
Value (mm)	33	33	7	28	5	21.5	8	6	11

3.3. Simulations and measurements

Simulations and measurements were performed when the antenna was placed on different locations of the torso. In simulations, the torso of the voxel body model included in the CST software was used to test the antenna. As previously defined, this model is a 38 years old male with weight of 69 kg and height of 176 cm. The biological dielectric properties were recalculated for the frequency range from 1.5 GHz to 3.5 GHz using the 4-Cole-Cole formulation, which describes the frequency dependence of the dielectric properties.

Experimental measurements were performed in order to evaluate the return loss of the antenna. Six participants with Body-Mass Index (BMI) between 17 and 27 kg/m² took part in the experiment. For each individual, the antenna was tested on several locations around the torso with no gap between the face of the box with the slot and the body skin. Three of these locations correspond to the front part of the torso: the center, the front left and the front right; the antenna was also placed on the left and right sides and on the back below the rib cage. Some of the positions in which the antenna was tested in simulations and measurements are depicted in Figure 5.15.

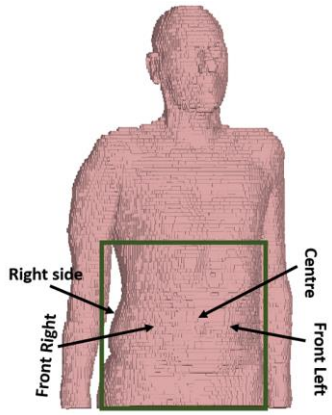

Figure 5.15. Human body model with some of the locations where the antenna was placed.

3.4. Results of the in-body antenna design

Figure 5.16 shows the return loss as a function of frequency when the antenna was centered on the front part of the torso (Figure 5.16(a)) and when it was placed on the right front (Figure 5.16(b)). These locations are shown in the body model of Figure 5.15. Differences between simulations and measurements can be due to differences in dielectric properties of body tissues of the body model and the participants, as well as different anatomical aspects.

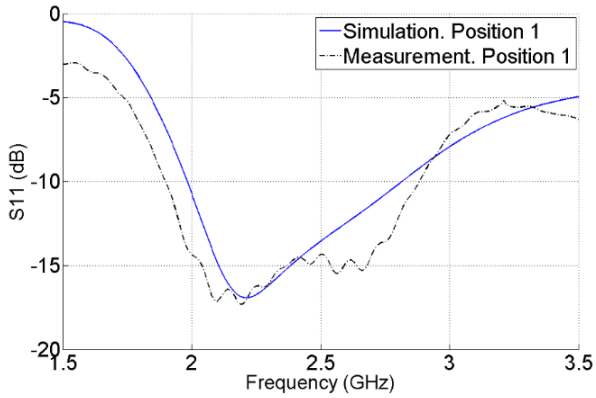

(a)

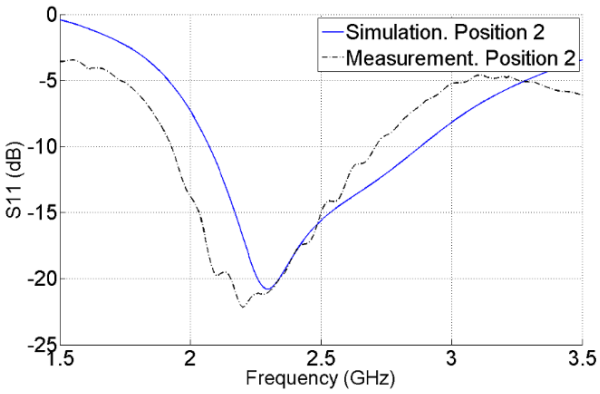

(b)

Figure 5.16. Measured and simulated S11 of the antenna on two locations of the torso (a) on the center front, (b) on the right front.

Table 5.5 and Table 5.6 summarize the center frequency of the antenna when it was placed on the six different parts of the torso, together with the -10 dB bandwidth achieved in each case. In the measurement results, the range of values obtained for all participants is reported. For example, when the antenna was placed on the back of the six participants, the center frequency ranged between 2.27 GHz and 2.72 GHz. The -10 dB bandwidth of the antenna ranged between 0.51 GHz (21%) and 1.15 GHz (46%) in all the measurements and between 0.75 GHz (30%) and 0.97 GHz (40%) in all simulations. These results all adequately cover 2.45 GHz.

Table 5.5. S11 simulation results when the antenna is on different parts of the torso

	Simulations		
Part of Torso	fc (GHz)	-10 dB BW (GHz)	-10 dB BW (%)
Front left	2.6	0.82	31.5
Front right	2.48	0.81	32.7
Centre	2.41	0.86	35.6
Left side	2.59	0.92	35.5
Right Side	2.65	0.97	36.5
Back	2.48	0.75	30.3

Table 5.6. S11 measurement results when the antenna is on different parts of the torso

	Measurements		
Part of Torso	fc (GHz)	-10 dB BW (GHz)	-10 dB BW (%)
Front left	2.32 - 2.58	0.54 - 0.83	22.4 - 33.8
Front right	2.32 - 2.58	0.63 - 1.12	24.4 - 46.0
Centre	2.37 - 2.58	0.51 - 1.15	21.0 - 46.4
Left side	2.42 - 2.51	0.71 - 1.01	29.3 - 41.3
Right Side	2.39 - 2.51	0.71 - 1.04	28.3 - 42.9
Back	2.27 - 2.72	0.61 - 0.87	24.8 - 32.2

Different antenna properties were obtained through simulations. The Voltage Standing Wave Ratio (VSWR) varied between 1.13 and 1.54 at 2.45 GHz, on the different parts of the torso. The antenna design showed front-to-back isolation higher than 15 dB at the specified frequency.

At 2.45 GHz, the real part of the impedance (R) took values between 33 Ω and 64 Ω, and the reactance (X) between -2.37 Ω and 1.29 Ω, as shown in Table 5.7.

Table 5.7.Resistance and reactance at 2.45 GHz when the antenna is on different parts of the torso.

Part of the Torso	**R (Ω)**	**X (Ω)**
Front left	63.75	-2.37
Front right	37.22	0.27
Centre	33.74	-0.04
Left side	33.76	-1.37
Right Side	56.33	1.21
Back	38.98	1.29

Figure 5.17(a) shows the SAR distribution for an input signal of 10 mW at 2.45 GHz, and it shows the direction of the radiation into the body. The SAR was averaged over 10 g of mass and the horizontal cut was made through the maximum 10 g SAR point. It is evident that a transmitter on the surface propagates a significant amount of radiation close to the surface. When the transmitter is located beneath the surface, the radiation pattern on the surface is significantly different.

Finally, to characterize the communication link between the transmitter and the slot antenna, a half-wavelength dipole was placed in the intestine and the S21 was evaluated at 2.45GHz by means of simulations. The transmitter was repositioned along the horizontal axis (Figure 5.17 (b)), being always in the intestine. When moved along the vertical axis, similar results were obtained, e. g. S21 was -43.49dB when the distance was 61 mm.

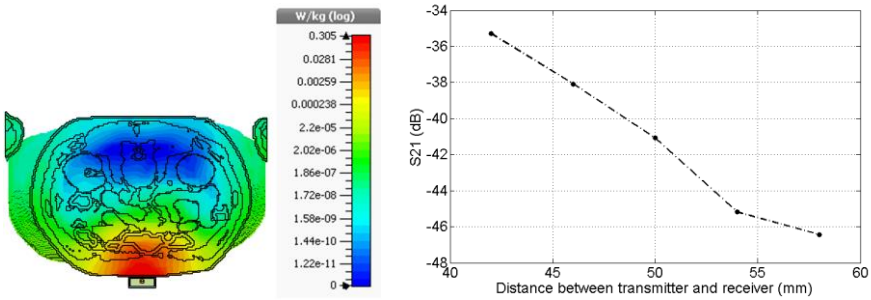

Figure 5.17. (a) SAR distribution in W/kg (body top view) when the radiating antenna is placed on the front part of the torso, (b) Variation of S21 (dB) with respect to the distance between the two antennas.

3.5. Conclusions

A slot antenna in a conductive box was optimized to match the body impedance when placed on the torso at 2.45 GHz. Previously the authors used this type of antenna for off-body communications in which the conductive box reduced the interaction with the body. The antenna was modified for inward radiation (i.e. the slot was covered by the body skin) and retuned. The slot size was reduced due to the dielectric properties of body tissues. This antenna is suitable for receiving the signal coming from inside the body. This design removes the need for wires and the gel used in the past in specific medical applications.

Experimental measurements were performed to verify the antenna properties. The return loss was obtained when the antenna was placed on several parts of the torso of 6 participants. Simulations and measurements showed the variability in the center frequency and the bandwidth for the different placements of the antenna, as well as for the different participants. The antenna was always functional within the band at 2.45 GHz (S11 < -10 dB). The body-mass index of the participants was found not to influence the measurement results. The S21 was evaluated to characterize the communication link. Further work is aimed at reducing the size of the box and improving the stability of the feed probe. The box must include the receiver electronics and so a very small size is not possible. In these modelling investigations a half-wavelength dipole was used as a transmitter, but using a smaller radio pill would improve the performance of the communication because it is optimized for sending signals from the body.

CHAPTER 6: ANALYSIS OF THE EMF EXPOSURE IN THE NEAR FIELD REGION

This chapter presents the analysis and evaluation of the power absorption in the near field region due to different radiation sources, all of them working in the 2.4 GHz frequency band. Firstly, computational tools were used to analyze the power absorption in human bodies due to the two wearable antennas presented in the previous chapter. Secondly, SAR levels caused by WiFi signals measured in the far field region were calculated applying three different methodologies defined to this end in order to compare the corresponding results.

1. INTRODUCTION

As shown in Chapter 5, wearable antennas and implantable devices are increasing in demand because of its utility and application in various fields, such as medicine, sports or entertainment. One of the main challenges when designing a wearable antenna is to keep the efficiency of the antenna when it is placed on the body while maintaining low power absorption in the human tissues. In Chapter 5, two antenna models working in the 2.4 GHz band have been proposed and as previously shown, these models are suitable for reducing the interaction between the antenna and the body, making them appropriate for being part of WBANs. In the work presented in that chapter, both antennas were fabricated and tested on different bodies for people with different BMI. This ensured that the antennas were working properly in a real environment.

In this chapter a detailed analysis of the power absorption due to these antennas is presented. In addition to the extension of exposure evaluation to more locations in the body, in this study two body models are included, a male and a female, with higher resolution. Moreover, the exposure evaluation is performed at three different frequencies (2 GHz, 2.45 GHz and 3 GHz), because as shown in Chapter 5, the interaction of the antenna with the human body causes a shift in the resonant frequency, so the assessment at close frequencies is of interest. The analysis of the difference in power absorption between the off-body antenna design and its equivalent for in-body radiation is performed, together with the evaluation of the power absorbed in different tissues due to these types of antennas.

Moreover, in Chapter 4 an evaluation of human exposure to WiFi signals in the 2.4 GHz band has been presented. In that case, measurements were carried out in the far field region and electric field levels were obtained. Measurements in the far field region are usually much less complex to perform. In addition, in some situations only far field measurements are possible. For this reason, some authors have developed methods for converting far field measurement data to SAR_{WB} values. The second work of this chapter consists of converting WiFi data acquired in the far field region to SAR data using methods proposed by different authors.

Finally the SAR_{WB} values obtained due to the wearable antennas and WiFi signals are compared.

2. METHODS FOR EVALUATING EXPOSURE OF WEARABLE ANTENNAS

The body models used in this study are the AustinMan and AustinWoman high fidelity anatomical voxel models, both of them are open source models constructed from the Visible Human Project (VHP) datasets (Massey 2016). The resolution of the voxels is 2×2×2 mm^3. The same computational tool than the one used for designing the antennas was employed for calculating the power absorption in body tissues (CST 2016), using the FDTD method.

Each antenna was placed at 8 different positions of the human body, shown in Figure 6.1. In the case of the antenna designed for off-body communications, the bottom of the box was in contact with the skin. A simulation per antenna and body location was performed, repeating the process for the two body models. The dielectric properties of body tissues were recalculated using the 4-Cole-Cole formulation in the frequency band of interest (IFAC). Two different computational analyses were performed: the SAR and the total power absorbed in the human body. The SAR was averaged over 10 g of contiguous tissue and the maximum value was reported in each case.

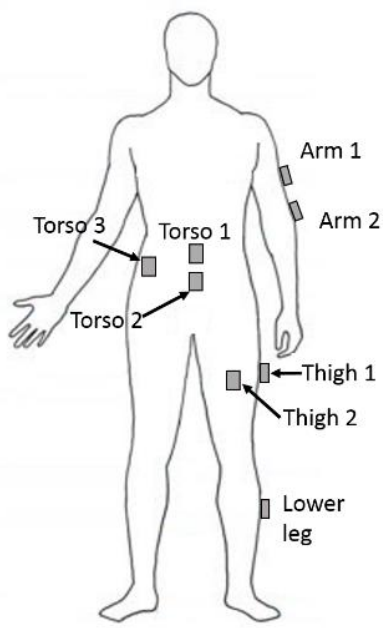

Figure 6.1. Positions of the body models where the antennas were placed.

3. RESULTS OF PERSONAL EXPOSURE TO THE RADIATION COMING FROM WEARABLE ANTENNAS

In this section, the simulation results are provided in terms of SAR and total power absorbed. Moreover, the percentages of power absorbed by the different tissues are investigated. All the results have been obtained with the two different antennas (at different times), for each body model and body location.

3.1. SAR average over 10 g of mass

The SAR values obtained when placing the antennas on the different parts of the body models are presented in Figure 6.2 for the off-body antenna, and in Figure 6.3 for the in-body antenna. The maximum SAR values obtained at 2 GHz, 2.45 GHz and 3 GHz are given for each body model, man (M) or woman (W), and for each body location. The input power was 10 mW. As shown in both figures, when using the antenna designed for off-body communications, the maximum SAR value was equal to 0.0369 W/kg, this was obtained when placing the antenna on one side of the torso of the woman model. But, as explained later in Section 3.3, this was due to the proximity of the arm to the antenna. The minimum SAR level due to this antenna at 2.45 GHz was 0.0113 W/kg, obtained when it was placed on the woman's leg (Thigh 2).

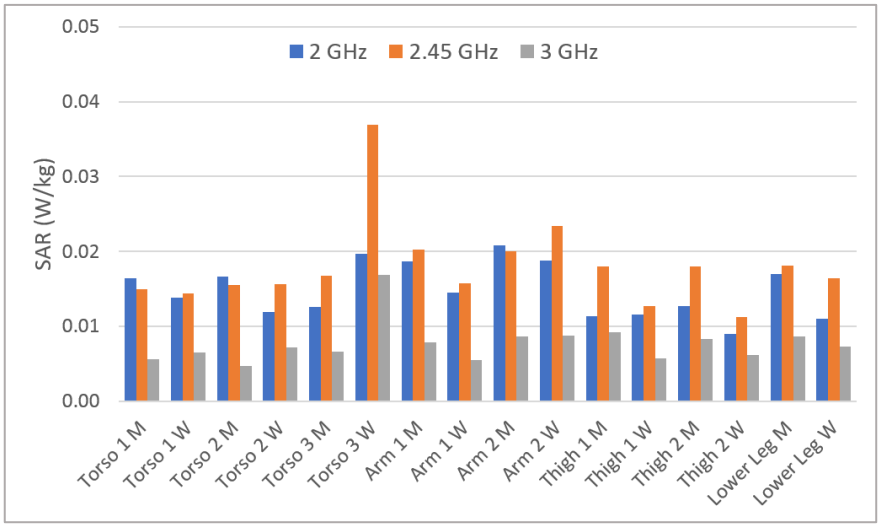

Figure 6.2. SAR values obtained for the woman (W) and man (M) voxel models at 2 GHz, 2.45 GHz and 3 GHz for the off-body antenna.

When using the antenna intended for in-body communications the SAR levels increased significantly, taking values between 0.2278 and 0.4479 W/kg at 2.45 GHz, getting this highest value also on the side of the torso of the woman body. The SAR value at 3 GHz was sometimes higher than at 2.45 GHz. In fact, the maximum SAR value at 3 GHz was 0.4686 W/kg, acquired when placing the antenna on the woman's leg. This is due to the frequency shift produced because of the different biological properties.

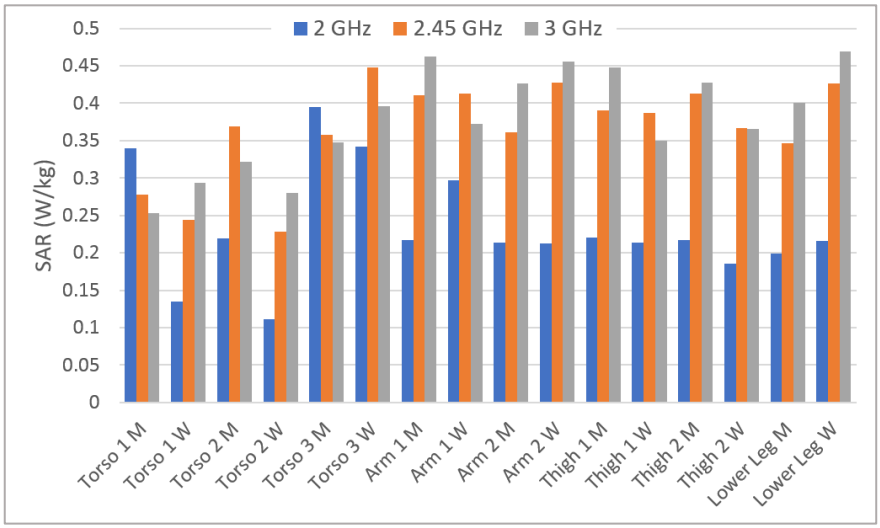

Figure 6.3. SAR values obtained for the woman (W) and man (M) voxel models at 2 GHz, 2.45 GHz and 3 GHz for the in-body antenna.

In order to illustrate graphically the differences on the SAR distributions due to the two antenna models, an example is given below. Figure 6.4 shows the antenna designed for off-body applications placed on the lower leg of the woman body, together with the 3D SAR distribution caused by this antenna at 2.45 GHz. Also, on the illustration of the right, the SAR distribution inside the body is shown in a cut plane perpendicular to the antenna, made through the maximum 10 g SAR point. Figure 6.5 shows the SAR distribution for the in-body antenna model when it is placed on the same location of the woman body model. As in the previous case, the SAR distribution in 3D and in a cut perpendicular to the antenna is given. The cut was also made through the maximum 10 g SAR point. As shown, the antenna designed for in-body communications causes maximum SAR levels much higher, being the maximum SAR equal to 0.426 W/kg. In both cases, the highest values of SAR are found in the first layers of the body models.

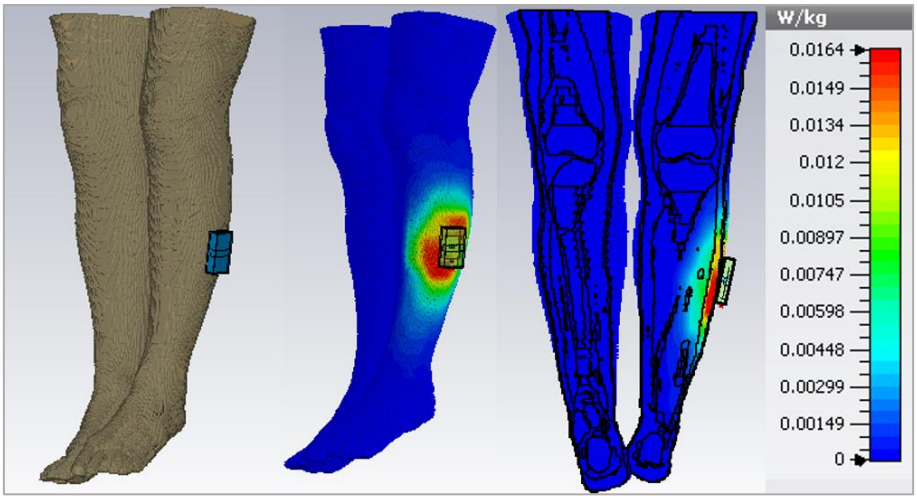

Figure 6.4. Off-body antenna model placed on the lower leg of the woman and SAR distribution due to this antenna at 2.45 GHz.

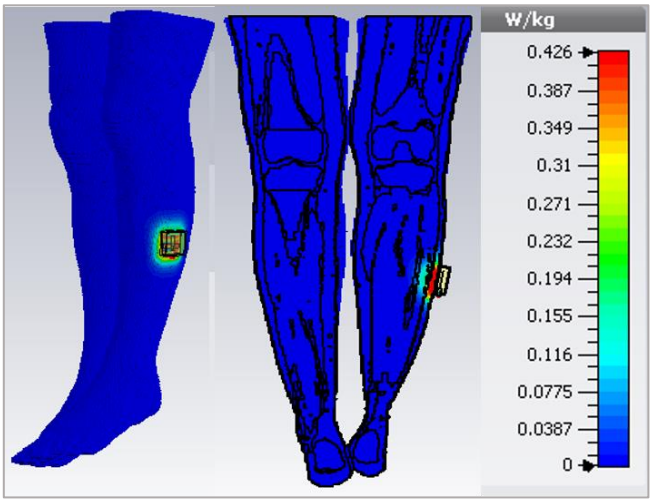

Figure 6.5. SAR distribution at 2.45 GHz due to the in-body antenna placed on the woman's leg.

With regard to the exposure limits at these frequencies, the basic restrictions for the general public when the SAR is averaged over 10 g of mass are 4 W/kg for the limbs and 2 W/kg for the head and trunk, as indicated in (ICNIRP 1998; IEEE 2005). Considering that the maximum SAR value was acquired on the trunk and it was equal to 0.4479 W/kg for an input power of 10 mW, the maximum permitted input power for the in-body antenna should be lower than 44.65 mW so as not to exceed the 2 W/kg indicated in the guidelines. However,

for the off-body antenna, this input power can be much higher and even with 500 mW the limits are fulfilled (the input power should be lower than 542 mW).

3.2. Power absorbed in the human bodies

The power absorbed in the body was also reported for an input power of 10 mW. Regarding the antenna design made for off-body applications, as can be observed from Figure 6.6, the highest power absorbed at 2.45 GHz was found on the side of the torso of the woman and man voxel models, being equal to 5.21 mW and 3.85 mW, respectively. As shown, the power strength absorbed at 2.45 GHz was higher than at the other two frequencies, this is because despite the frequency shift, the center frequency was closer to that frequency than to 2 or 3 GHz. When placing the antenna at different locations on the leg, the maximum power absorbed at the same frequency was 3.84 mW on the Thigh 2 position of the man model. Regarding the arm positions, the highest value was 3.41 mW on the Arm 2 location of the woman model.

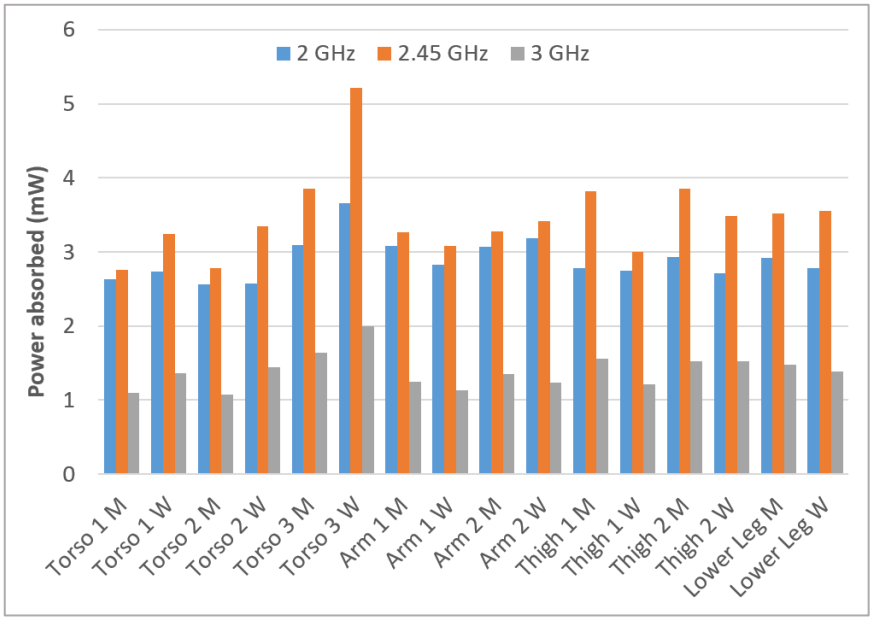

Figure 6.6. Total power absorbed in the woman (W) and in the man (M) voxel models at 2 GHz, 2.45 GHz and 3 GHz for the off-body antenna model.

Figure 6.7 illustrates the results of the power absorbed by the bodies due to the radiation of the in-body antenna model. As shown, the maximum power absorbed by the body at 2.45 GHz was found when placing the antenna on the Thigh 1 position of the woman body model, reaching a value of 9.78 mW. The

highest levels obtained on the torso and arm locations were 9.62 mW (Torso 2 M) and 9.50 mW (Arm 2 W), respectively. The total power absorbed in the body was sometimes higher at 3 GHz than at 2.45 GHz for the in-body antenna model because of the frequency shift. The highest power absorbed at 3 GHz was 9.75 mW and it occurred when the antenna was placed on Thigh 2 of the man model.

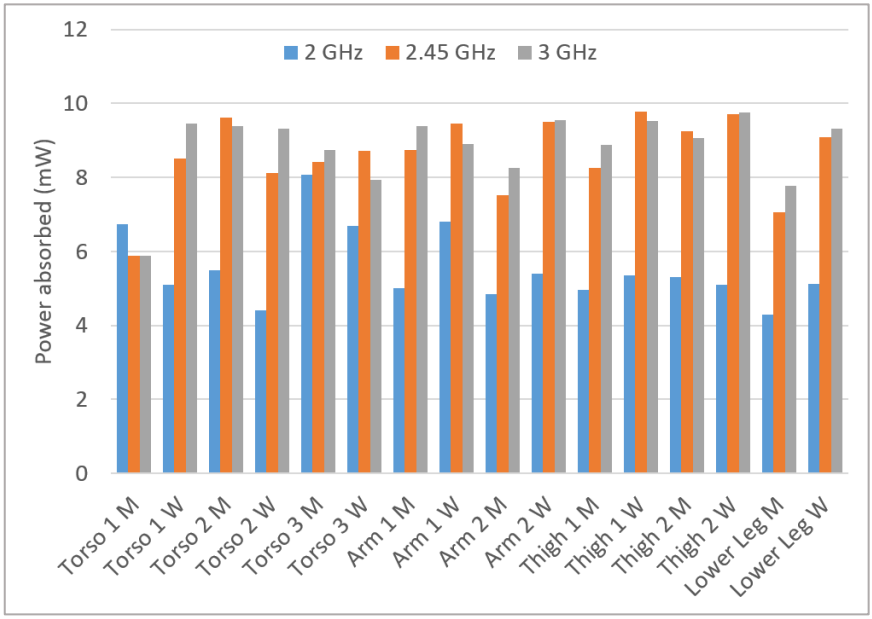

Figure 6.7. Total power absorbed in the woman (W) and in the man (M) voxel models at 2 GHz, 2.45 GHz and 3 GHz for the in-body antenna model.

In order to highlight the most relevant results of the above shown figures, the maximum power levels obtained on the torso, leg and arm at 2.45 GHz, which is the frequency where the most significant results were obtained, are summarized in Table 6.1, detailing the specific location and the body model where these levels were obtained.

Table 6.1.Maximum power absorbed in the different body parts at 2.45 GHz

Body Part	Off-body		In-body	
	P_{abs}(mW)	Location	P_{abs}(mW)	Location
Torso	5.21	Torso 3 Woman	9.62	Torso 2 Man
Arm	3.41	Arm 2 Woman	9.5	Arm 2 Woman
Leg	3.84	Thigh 2 Man	9.78	Thigh 1 Woman

3.3. Power absorbed in the different tissues

The power absorbed in the different tissues was analyzed for each body position at the three frequencies. The following figures show the percentage of power absorbed in each tissue due to the off-body and in-body antennas when placing them on the man (Man Off, Man IN) and woman (Woman Off, Woman IN) models. For both antennas, the highest amount of power was absorbed in the three first layers of the human models (skin, fat and muscle). This is due to the low penetration depth at these frequencies.

The results obtained when placing the antennas on the different positions of the torso are provided in Figure 6.8, Figure 6.9 and Figure 6.10.

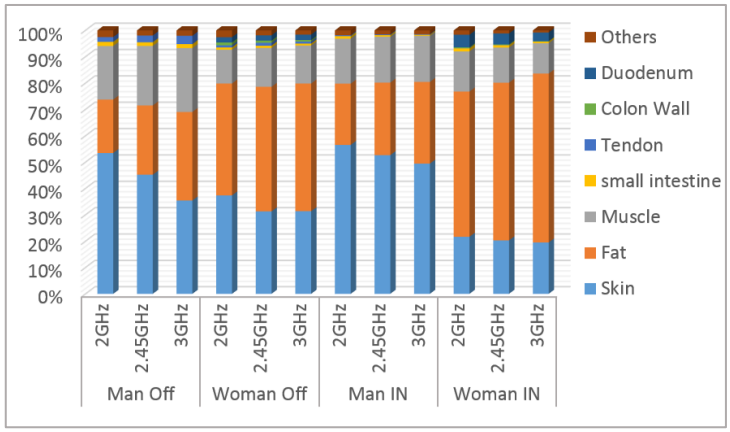

Figure 6.8. Power absorbed in each tissue for the antennas placed on Torso 1.

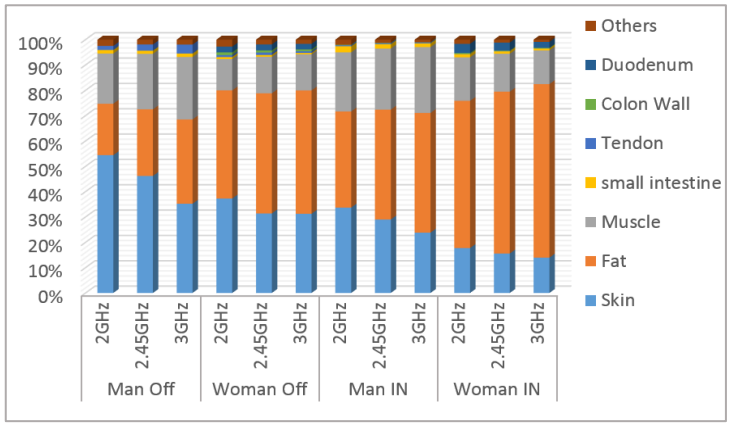

Figure 6.9. Power absorbed in each tissue for the antennas placed on Torso 2.

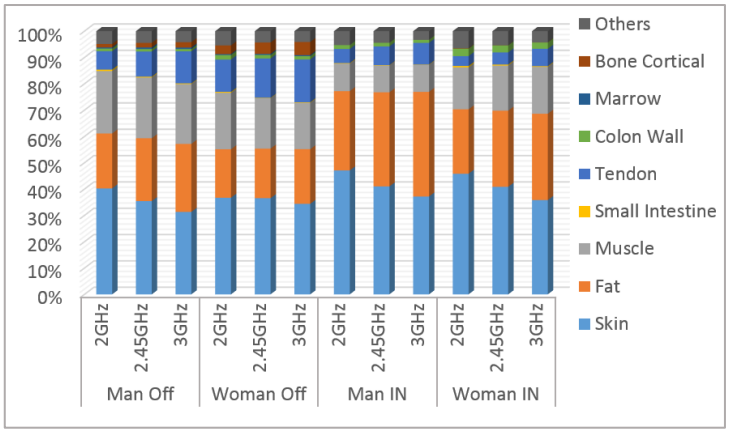

Figure 6.10. Power absorbed in each tissue for the antennas placed on Torso 3.

Overall, when the antenna was on the torso, the skin and fat absorbed more power than the muscle, being the energy absorbed by this latter layer lower than the 26% of the total power absorbed in the body. As shown in Figure 6.10, when placing the antenna on the side of the torso, some radiation was found on the bones, especially when using the antenna intended for off-body communications. This was due to the proximity of the arm to the antenna, as can be seen from Figure 6.11, where the off-body antenna model is placed on Torso 3 position. Finally, some power (less than 7%) was deposited in other body tissues, represented by 'Others' in the graphics, such as in the liver, stomach, nerves or blood vessels.

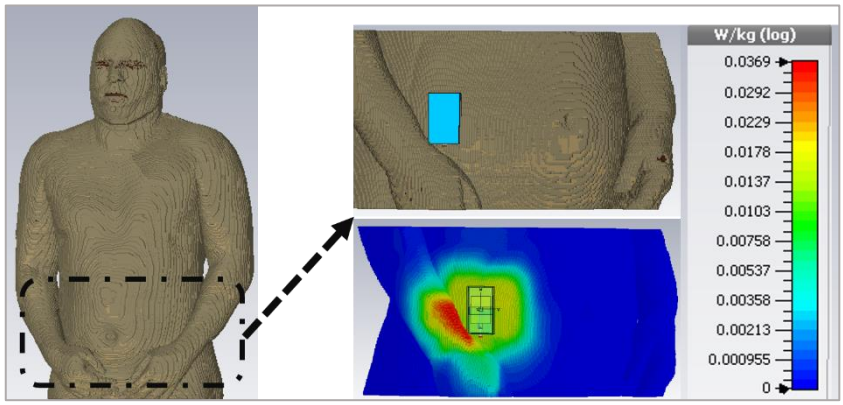

Figure 6.11. (a) Top part of the AustinMan model, (b) antenna placed on Torso 3 position and SAR distribution at 2.45 GHz.

On the arm and on the lower leg, the percentage of radiation absorbed in the fat was lower, since in these parts the fat layer is thinner. Figure 6.12 and Figure 6.13 show the percentage of power absorbed per tissue on the Arm 1 and Arm 2 positions, respectively. As can be seen, the power deposited in the fat layer took values between 3% and 34% on these locations, while the muscle absorbed percentages of power varying between 25% and 71%. On the Arm 2 location, the power deposited in the tendon was also noticeable, taking values between 14% and 16% when placing the in-body antenna on the woman body model.

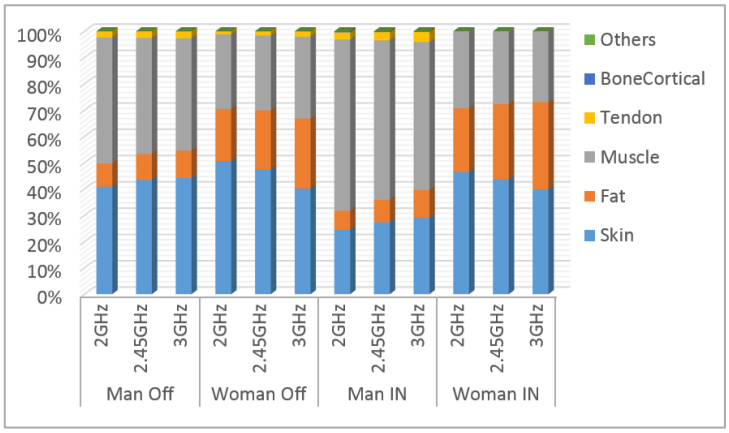

Figure 6.12. Power absorbed in each tissue for the antennas placed on Arm 1.

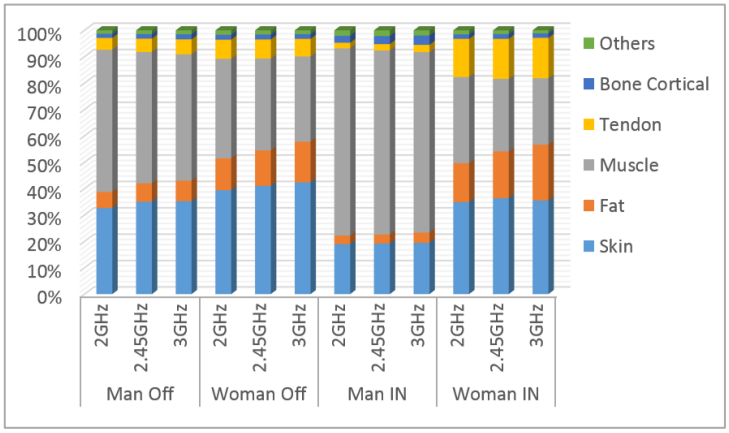

Figure 6.13. Power absorbed in each tissue for the antennas placed on Arm 2.

On the lower leg, the percentage of radiation absorbed in the fat layer ranged between 4% and 20% and in the muscle between 37% and 72%, as can be

observed from Figure 6.14. The power deposited on the tendon was significant in some cases, reaching a value of 17.83% for the in-body antenna on the man model at 3 GHz.

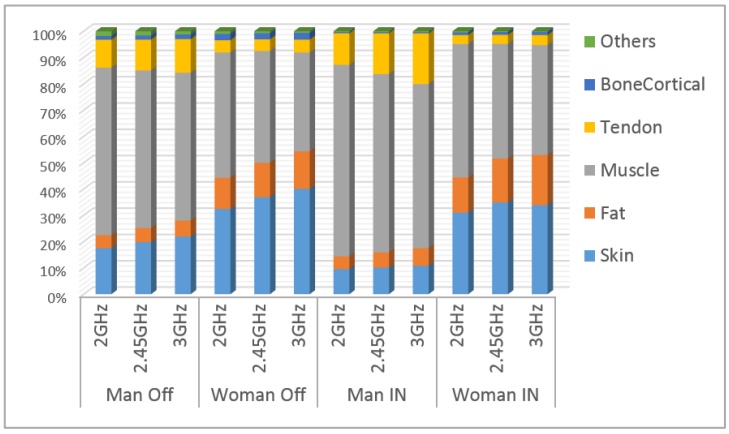

Figure 6.14. Power absorbed in each tissue for the antennas placed on Lower Leg.

Finally, Figure 6.15 and Figure 6.16 show the percentages of energy deposited in different tissues when the antennas were placed on Thigh 1 and Thigh 2 positions, respectively. In these cases, the power absorbed in fat took values between 8% and 51% and the radiation absorbed in the muscle ranged from 18% to 70%.

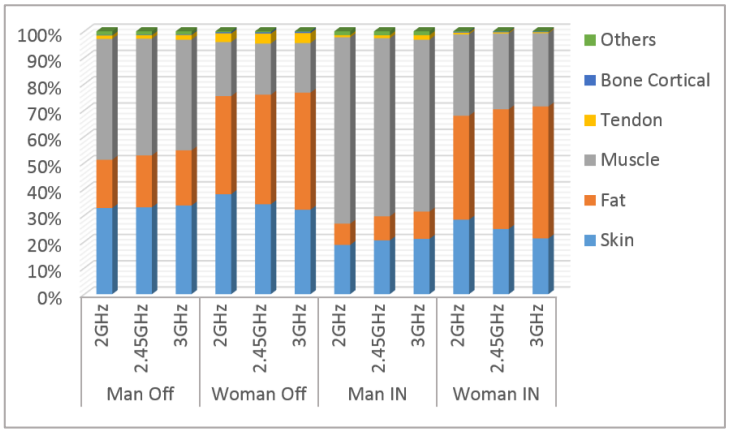

Figure 6.15. Power absorbed in each tissue for the antennas placed on Thigh 1.

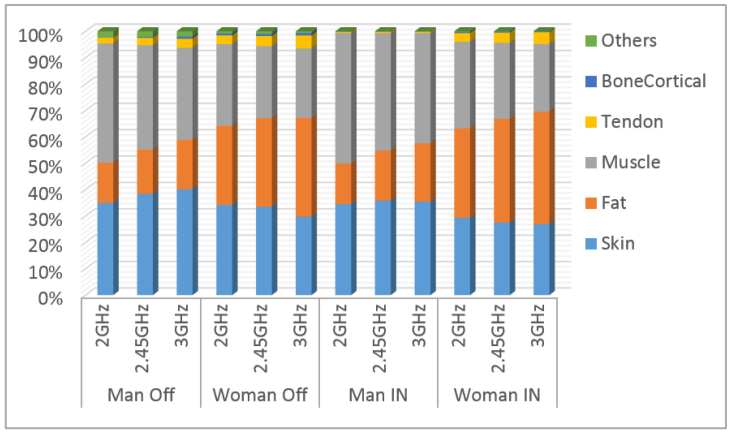

Figure 6.16. Power absorbed in each tissue for the antennas placed on Thigh 2.

4. PERSONAL EXPOSURE FROM ENVIRONMENTAL DATA

As reported by Joseph et al. (2010b), the use of EMF levels together with its equivalent SAR values can be useful in epidemiological studies. In addition, obtaining EMF values in the far field region is much simpler than performing SAR measurements. For this reason, some authors studied different ways of calculating SAR_{WB} levels from electric field measurements. The SAR_{WB} levels are averaged over the mass of the human body.

In this Section, methods developed in different studies were considered for the calculation of the SAR_{WB} values from EMF measurements. Specifically, WiFi signals in the 2.4 GHz frequency band transmitted from access points and user devices were measured using the exposimeter (EME Spy) previously utilized. Three sets of measurements were used. Two new sets of measurements were taken in the two labs described in Chapter 4 (in these labs only the spectrum analyzer was used in that chapter), and the third measurement was selected from the campaigns performed in Chapter 4, choosing the recordings with the highest mean value of electric field. Then, several methods proposed by different authors were used to convert measured electric field data to SAR_{WB} values. A comparison between the results obtained by the different methods was performed.

4.1. EMF Measurements at 2.4 GHz

The detailed description of the three sets of measurements is given below:

- In Lab 1, which is the research lab, measurements were performed in 5 different positions, one in the middle of the room (position 1) and the others close to the corners, leaving a distance of 1.4 m from the walls, as in the previously described measurement campaigns (Chapter 4). The duration of each measurement was equal to 6 hours and data samples in the different positions were recorded during different days in the afternoon and evening.

- The second location was the Lab 2, which is the teaching lab. A measurement of 24-hour duration was performed in the middle of the room to assess the variability of the WiFi signal along the day and night. In this lab, as well as in the previous one, a sample was recorded every 10 seconds.

- The third set of measurements was selected from the campaigns carried out in Chapter 4, and the recordings performed in the position 5 of Classroom 1 were selected, since in that position the highest mean electric field was obtained. As explained in that chapter, these samples were obtained close to the middle of the classroom and a sample per 4 seconds was recorded.

In all the locations, the exposure meter was placed at a height of 1.2 m from the floor, since people usually sit at this level. In the new sets of measurements, a sample every 10 seconds was recorded in order to enable longer battery life, so measurements of 24 hours can be taken without the need of replacing them.

Table 6.2 and Table 6.3 summarize the mean, standard deviation (SD) and maximum values of the measured electric field averaged over 6 minutes. Moreover, the maximum recorded level considering all the samples before average is given. In Lab 1, results per measurement position are given and in Classroom 1 the results obtained in position 5 are provided, both shown in Table 6.2. In Lab 2, the results are calculated for the different periods of the day: morning (from 6:00 to 14:00), afternoon and evening (from 14:00 to 22:00) and night (from 22:00 to 6:00), as shown in Table 6.3. The highest level of the acquired samples was 242 mV/m, from the set of measurements of Chapter 4. In Lab 1, the maximum sample recorded was equal to 127 mV/m, acquired in position 3, and the maximum field level averaged over 6 min was equal to 31.75 mV/m. Regarding the 24-hour measurement, highest levels of the WiFi signal were detected during the day. In general, the WiFi signal levels in Lab 2 were lower than those measured in the research lab (Lab 1). The maximum mean electric field level obtained in the measurements of Chapter 4, is higher than the mean levels of the new sets of recordings.

Table 6.2. Electric field levels (mV/m) measured at the different positions of Lab 1 and in position 5 of Classroom 1

		6 min averaged		
Location	**Position**	**Mean (SD)**	**Max**	**Max sample**
Lab 1	1	26.99 (1.24)	27.96	85.15
	2	30.40 (1.09)	31.75	95.00
	3	13.44 (13.45)	28.16	127.00
	4	26.33 (1.38)	28.06	70.00
	5	23.71 (0.77)	24.85	66.00
Classroom 1	5	109.54 (5.34)	117.16	242.00

Table 6.3. Electric field levels (mV/m) measured during 24 hours in the middle of Lab 2

	6 min averaged		
Period	**Mean (SD)**	**Max**	**Max sample**
Morning	12.65 (2.54)	15.67	42.00
Afternoon & Evening	10.15 (0.63)	11.33	77.00
Night	7.87 (0.35)	8.49	35.00

4.2. Assessing SAR values from Electric Field Measurements

In order to convert measured data to SAR_{WB} values, three methods proposed by different authors were used. The description of each method is presented below, together with the explanation of the conversion developed in this work to get SAR_{WB} values from the WiFi measurements.

- **Method 1**

In (Joseph 2010b) some functions are provided to undertake the conversion for different wireless services and several scenarios. They used different homogeneous spheroid human phantoms at 950 MHz and the results showed that the highest SAR value was obtained for the phantom of lowest weight. For the other services and frequencies, they employed this phantom, the 1- year-old child, whose mass was equal to 10 kg. The dielectric properties for the homogeneous phantoms were selected from (IEC 2005).

In the present work, the function provided for the 1-year-old child at 2.45 GHz is used as the first method to calculate the whole-body SAR. The function provides the 95th percentile of the SAR_{WB} (W/kg) and is given as follows:

$$P_{95}(SAR_{WB}) = a(E)^b \qquad (6.1)$$

The electric field E (V/m) has to be averaged over 6 min and a and b are the parameters to fit the equation to the different phantoms, frequencies and environments. In the selected environment, the urban-indoor new office-standstill, and for the frequency band of 2.4 GHz, the values of a and b are equal to $4.029 \cdot 10^{-5}$ and 2, respectively.

These authors obtained a SAR_{WB} value of 1.19 μW/kg for a measured field level of 170 mV/m in the 2.4 GHz WiFi band, for the same environment and for the same phantom (the 1-year-old child).

- **Method 2**

In (Bamba 2014) a formula is proposed to determine the SAR_{WB}, provided that the incident power densities and the body mass m (kg) are known. This formula is based on the body surface area BSA, since the human body absorption in the GHz region is mainly influenced by it. The BSA estimation formula is given by:

$$BSA = 0.097 \cdot m^{0.6466} \qquad (6.2)$$

In a realistic environment, a person is assumed to be exposed to both line of sight (LOS) plane wave and to diffuse multipath components (DMC) according to the room electromagnetics theory (Andersen 2007). But the DMC cannot be characterized by the specular components due to hardware and software resolution limitations (Poutanen 2011). For this reason, when performing the conversion to SAR levels, usually the DMC is not considered. Bamba et al. (2014) accounted for the DMC using a method that is based on the room EM theory (Andersen 2007), which states that the total power consists of the first specular path (i.e. LOS component) and the DMC. Numerical simulations using the FDTD method were performed to compute the SAR_{WB} and to determine the parameters of the formula. Moreover, they validated the formula on heterogeneous phantoms.

The SAR_{WB} (W/kg) proposed formula due to LOS component considering the BSA above described is provided below:

$$SAR_{WBLOS} = 0.21 \cdot m^{-0.3534} \cdot \eta \cdot k \cdot S_{LOS} \qquad m \geq 10 \qquad (6.3)$$

Where η is the absorption coefficient and at 2.45 it takes a value of 0.54, at that frequency the parameter k is equal to 0.2. S_{LOS} is the incident power density of the LOS component (W/m^2) and m is the person's mass (kg).

The SAR_{WB} due to diffuse fields is given by:

$$SAR_{WBDMC} = 0.21 \cdot m^{-0.3534} \cdot \eta \cdot S_{DMC} \qquad m \geq 10 \qquad (6.4)$$

In the present work, SAR_{WB} values using this method were calculated in two ways, ignoring the DMC and considering it. In the second case, the distance between the receiver and the access point of the lab, which was the main source of WiFi exposure, was considered in order to assess the contribution of the DMC. Based on the work developed in (Poutanen 2011), the DMC contribution should be less than 45%. Moreover, in order to establish the DMC contribution according to the distance between the transmitter and receiver, the work developed by (Bamba 2013) was followed. Considering the maximum values of the 6-min averaged electric fields, and the distance from the closest access point, the DMC contributions were calculated and are shown in Table 6.4. The positions from 1 to 5 are the placements of the personal exposure meter in Lab 1 and Classroom 1 refers to the location where the highest mean electric field was found in the measurement campaign of Chapter 4 (Table 6.2). The periods of the day correspond to the measurements recorded in Lab 2 (Table 6.3). The power density (S) obtained from the maximum averaged electric field levels of these tables are also given in Table 6.4, together with the power densities of the LOS and the DMC components required when considering DMC contributions.

Table 6.4. DMC contribution at each measurement position

Position/ Period	Distance	DMC	Max (6 min averaged)		
			Total S ($\mu W/m^2$)	S_{LOS} ($\mu W/m^2$)	S_{DMC} ($\mu W/m^2$)
1	2 m	13%	2.07	1.80	0.27
2	5 m	35%	2.67	1.74	0.94
3	1 m	5%	2.10	2.00	0.11
4	3 m	25%	2.09	1.57	0.52
5	3.5 m	29%	1.64	1.16	0.48
Classroom 1	2 m	13%	36.41	31.68	4.73
Morning	2 m	13%	0.65	0.57	0.08
Afternoon	2 m	13%	0.34	0.30	0.04
Night	2 m	13%	0.19	0.17	0.02

The equations (6.3) and (6.4) were applied for calculating the SAR_{WB} to two people, the first one with a mass of 10 kg, as the 1-year-old child considered in the previous method, and the second one with a mass of 70 kg, since this was the average mass considered in (Bamba 2014) for the man phantom.

- **Method 3**

Another work that converted electric field strength measurements to exposure in terms of SAR_{WB} values was developed by Ibrani et al. (2014). In this case an empirical formula developed by Piuzzi et al. (2011) was used, which considers the human surface-to-mass ratio $\frac{A}{m}$, the incident power density S and the frequency f, in gigahertz and restricted to 900 MHz-3 GHz frequency range:

$$SAR_{WB} = (0.31 - 0.039 \cdot f)\left(\frac{A}{m}\right)S \quad (6.5)$$

The surface area A (m^2) is calculated from the height (cm) and mass (kg) of the person using the following equation:

$$A = 0.024265 \cdot height^{0.3964} \cdot m^{0.5378} \quad (6.6)$$

In the present work, two human bodies were also considered for these calculations, the one-year-old child of 10 kg of mass and the man with a weight of 70 kg. To apply this method, the heights of the human models are required. The height of the child was chosen as the 50th percentile of the height for a 10 kg boy provided by the WHO (2018), resulting in a value equal to 77.5 cm. Regarding the man, a height of 1.75 m was considered, since it was the height established in (Bamba 2014) for the average man of 70 kg of mass.

Table 6.4 summarizes the three methods used to convert measured electric field levels to SAR_{WB} values. One of the differences between the method 2 and method 3 lies in the way of determining the BSA. In the second methodology, the authors considered an equation that only requires the body mass (Livingston 2001) and then they investigated its correctness by means of numerical simulations. However, a formula that requires the weight and height in order to calculate the BSA was employed in method 3 (Haycock 1978).

Table 6.5. Description of the methods used to convert measurement data to SAR_{WB} values

Method	Description	Input parameters	Ref
Method 1	Function to convert E field to SAR_{WB}	E field	(Joseph 2010b)
Method 2 No DMC	Formula to convert power density (S) to SAR_{WB}	S Body mass	(Bamba 2014)
Method 2 DMC	Calculate DMC contribution Apply formulas to convert: S_{LOS} to SAR_{WBLOS} S_{DMC} to SAR_{WBDMC} $SAR_{WB}=SAR_{WBLOSS}+SAR_{WBDMC}$	S Body mass	(Bamba 2014) (Poutanen 2011) (Bamba 2013)
Method 3	Formula to convert S to SAR_{WB}	S Body mass Height	(Ibrani 2014)

5. SAR_{WB} RESULTS DUE TO WIFI SIGNALS AND WEARABLE ANTENNAS

Table 6.6 shows the results of the SAR_{WB} values obtained for the maximum levels of the electric field levels averaged over 6 minutes included in the third column of Table 6.2 and Table 6.3. As shown in the table, higher values are obtained for the 10 kg child due to the lower mass and, considering method 2, the DMC contributions produce higher results, which makes sense since a more realistic situations is considered adding the emission levels coming from these multipath components.

Moreover, methods 1 and 2 give similar results when the DMC contribution is equal to 13%, this could be explained as follows. When using the method 1 for calculating SAR_{WB}, the parameter a of the equation (6.1) depends, among others, on the scenario. In this work, the parameter value of the urban-indoor new office-standstill scenario was selected and it is probably that the measurements carried out in that scenario for determining the a value were performed in an environment with a DMC contribution close to 13%.

Focusing on the recordings from the measurement campaign of Chapter 4, gives SAR_{WB} results much higher than the other sets of measurements. These samples were selected because gave the highest mean exposure level (position 5 of Classroom 1), so it can be concluded that the SAR_{WB} values calculated for this position give the maximum exposure level at university taking into account the

conditions of the measurement campaigns of this thesis, such as height of measurement.

Regarding the simulations of the wearable antennas, the maximum power absorbed at 2.45 GHz was 5.21 mW for the off-body antenna design and 9.78 mW in the case of the in-body antenna, both obtained on the woman body model. The total masses of the human models are 84.82 kg for the woman and 106.17 kg for the man (Massey 2016). Calculating the SAR_{WB} as the power absorbed divided by the total mass, in these cases considering the woman's mass, gives maximum SAR_{WB} values of 61.42 μW/kg for the off-body antenna and 115.30 μW/kg for the in-body design, as presented in Table 6.6. These levels are two orders of magnitude higher than the levels calculated from the maximum measured electric field (Classroom 1), and around three orders of magnitude higher than the other WiFi measurements.

Table 6.6. SAR_{WB} values (nW/kg) calculated using the three different methods from the electric field measurements obtained in the two labs and in a classroom of the university and those obtained due to the wearable antennas

SAR_{WB} (nW/kg)								
		Converted data from EMF measurements						
		Method 1	**Method 2**				**Method 3**	
	Position	**10 kg**	**10 kg**	**70 kg**	**DMC 10 kg**	**DMC 70 kg**	**10 kg**	**70 kg**
	1	31.49	20.84	9.59	31.68	14.57	21.07	11.84
	2	40.61	26.87	12.36	64.50	29.67	27.17	15.26
Lab 1	3	31.96	21.15	9.73	25.38	11.67	21.38	12.01
	4	31.72	20.99	9.66	41.98	19.31	21.22	11.92
	5	24.88	16.47	7.57	35.57	16.36	16.65	9.35
Classroom1	5	553	366	184	556	280	370	208
	Morning	9.89	6.54	3.01	9.95	4.58	6.62	3.72
Lab 2	Afternoon	5.18	3.42	1.58	5.21	2.39	3.46	1.95
	Night	2.91	1.92	0.88	2.92	1.34	1.94	1.09
Wearable antennas								
Off-Body Max Level		$61.42 \cdot 10^3$						
In-Body Max Level		$115.30 \cdot 10^3$						

The basic restriction for the SAR_{WB} at these frequencies is 0.08 W/kg (ICNIRP 1998), so all the values obtained in this analysis are below the limits.

6. CONCLUSIONS

The evaluation of near field exposure in the 2.4 GHz frequency band was performed using 3 different types of radiation sources. The first two sources were the two wearable slot antennas designed for off-body and in-body communications. As shown in this chapter, it is important to perform the evaluation at different frequencies because of the frequency shift produced from one location to another. The power absorbed at 3 GHz was sometimes higher than at 2.45 GHz. Moreover, when analyzing the power absorbed in different tissues it was concluded that in some cases the results depend on the body posture. For example, when placing the off-body antenna on the side of the torso of the woman body model, part of the power was absorbed in the arm due to its proximity to the antenna and this gave a higher level of exposure.

Regarding the third radiation source, the SAR_{WB} was calculated using the field strength data measured from the WiFi networks. Two new sets of measurements were carried out with the exposimeter. Moreover, the measurements of the highest mean exposure level acquired in the campaign detailed in Chapter 4 were used to calculate the SAR_{WB} levels in that location. These samples were taken in the middle of a classroom with the exposimeter. Although the maximum sample level in such measurement campaign was acquired with the spectrum analyzer in another location, in order to convert measured data to SAR values, the sample levels have to be averaged over 6 min, so taking the recordings with the highest average value is more critical. After averaging the field levels, the maximum values were selected for doing the conversion, obtaining in this way the maximum SAR_{WB} values.

Finally, the exposure levels produced by wearing the antennas were compared with the exposure values calculated from the WiFi signal measurements. The antennas placed on the body gave exposure levels between two and three orders of magnitude higher than the levels calculated from the WiFi signals.

CHAPTER 7: CONTRIBUTIONS & FUTURE WORK

In this chapter, the main contributions of this work are gathered, the obtained results dissemination is presented, and finally, several research lines for future work are described.

1. CONTRIBUTIONS

The driving force for this research work is the willing to contribute to the methods to measure, analyze and assess human exposure to EMFs, as well as provide significant values useful to reinforce the knowledge of exposure levels in both the near and far field regions.

More precisely, the contributions of this work can be described according to the objectives defined in Chapter 1.

1.1. Establish a measurement methodology appropriate for recording accurate and actual WiFi signal levels

The third chapter of this thesis includes the existing difficulties for accurately measuring signals transmitted in the form of pulses or bursts and the need of providing specific methods for recording these signals. In some cases, such as when measuring radio impulsive noise, a procedure for taking samples in the time domain is adequate. Nevertheless, this is not the case of WiFi signals since the power level in a wide range of frequencies has to be measured simultaneously. Therefore, the methodology for acquiring accurate WiFi signal levels is based on a spectrum analyzer configuration in the frequency domain.

As a first step, a procedure for selecting the proper equipment configuration was developed, since as detailed in Chapter 3, the spectrum analyzer settings can have huge influence on the results, especially when working with signals transmitted in the form of pulses. The proposed procedure for finding the optimal setup was described in detail and it consists of three phases:

- Acquisition of reference signal levels.
- Study of the influence of the measurement parameters.
- Identification of the spectrum analyzer optimal configuration.

One of the benefits of this procedure is that it can be applied to identify the optimal equipment configuration to acquire samples of the human exposure levels caused by other signals, such as the WiFi signals transmitted in the 5 GHz frequency band, or even in the case of signals from other RF services, as for example the ones corresponding to 5G mobile communication systems.

The reference levels defined in the first phase of the above mentioned procedure were obtained from time domain measurements. The proposed

configuration for taking signal samples in the time domain was given in Table 3.3 and it is also presented in the following Table.

Table 7.1. Spectrum analyzer configuration in the time domain.

Parameter	Time Domain
fc (MHz)	2412 ± 0.3125·N N= 0, 1, 2, … 32
Span (MHz)	Zero Span
RBW (MHz)	0.3
VBW (MHz)	1
SWT (s)	1
SWP	8001 points
Detector	RMS
Trace Mode	clear/write

The second contribution of this part of the work is the proper measurement configuration for taking WiFi signal samples in one channel and in the whole 2.4 GHz WiFi band. The setups of the spectrum analyzer for these two cases were provided in Table 3.9 and Table 3.10 of this thesis, and both configurations are given in the following Table.

Table 7.2. Configurations of the spectrum analyzer for performing measurements in one channel and in the whole 2.4 GHz WiFi band.

Parameter	Value One channel	Value 2.4 GHz WiFi band
f_c	Central frequency of the channel	2441.75 MHz
Span	20 MHz	83.5 MHz
RBW	0.3 MHz	1 MHz
VBW	1 MHz	3 MHz
SWT	2.5 ms	2.5 ms
SWP	501 points	501 points
Detector	RMS	RMS
Trace Mode	clear/write	clear/write

1.2. Assess human exposure to WiFi signals in public indoor environments

This phase of the work contributes to the study of characteristic RF emissions and its corresponding exposure levels in the evaluated scenarios. These

results are relevant in order to enhance the knowledge in dosimetry and exposure assessment, as reported in the WHO research agenda (WHO 2010). One of the novelties of the measured WiFi signal samples lies in the methodology followed for acquiring them, the one mentioned in the previous subsection, since that is the first measurement configuration for WiFi signal exposure based on accurately defined signal reference levels.

Before presenting the obtained WiFi exposure levels, a discussion of the data analysis and the proper statistics for evaluating this type of exposure was reported in Chapter 4, which can be very useful for future measurement campaigns aimed at reporting spatial or temporal variability of emissions in WLANs. One of the conclusions drawn from this discussion was that the 90th percentile was found to be the most appropriate one for representing WiFi exposure variations based on the nature of these signals. The median value or 50th percentile had fewer variations along the day and between the different studied places. Also, percentiles higher than the 99th, which can have higher variations, were not representative of EMF exposure since they indicated singular occurrences of the signal. However, the mean and median values are important statistics for epidemiological studies and the maximum levels are of interest when checking compliance with regulations.

The statistical discussion and the presentation of the WiFi exposure levels for long-term and 1-hour measurements also contribute to the analysis of EMF exposure data. Regarding the 24-hours measurements, first the signal variability due to the different placements of the receiver within the same location was reported. Then, exposure variability along 24 hours in the same point was shown and finally, average WiFi exposure levels for each place and period of the day were calculated. In the case of the 1-hour measurements, the WiFi signal variability due to the different measurement points within a place was determined and the exposure assessment in each place was also conducted.

Finally, the WiFi exposure levels in the 2.4 GHz frequency band reported in various scientific papers and measured by means of different instrumentation or methodologies were compared. The detailed comparison of the instrumentation and procedures were provided in Chapter 4 and the results from the different measurement campaigns are summarized in Table 4.15 of such chapter, as shown below.

Table 4.15. Electric field levels (V/m) obtained in different measurement campaigns

Ref	*Mean*	*Median*	*Range*	*Description*
(Sagar 2018)	0.01-0.03	-	-	Eme Spy 201 ExpoM-RF
(Joseph 2010a)	0.019-0.082	-	-	Eme Spy 120/ 121
(Joseph 2010c)	0.020	-	0.006-0.1	Weighting factor
(Röösli 2008) ROS	0.05	0.02	NA-0.23	Eme Spy 120
(Röösli 2008) Naïve	0.06	0.05	0.05-0.22	Eme spy 120
(Karipidis 2017)	0.060-0.114	-	-	Radiation Meter
(Tomitsch 2015)	0.077-0.118	0.000-0.013	-	Max-hold
Our work	0.005	0.005*	0.004-0.408	Analyzer 24 h
Our work	0.005	0.005*	0.005*-0.269	Analyzer 1 h
Our work	0.031	0.029	0.005-0.242	Eme Spy 200 1 h

* The calculated values were between 0.0045 and 0.0049 V/m, but when rounding to the nearest third decimal a value of 0.005 V/m was set.

1.3. Design and implementation of wearable devices

In Chapter 5 the design and fabrication of two different wearable antennas was presented. These devices, which are increasingly being demanded, give solution to different applications as explained in the beginning of that chapter. One of the advantages of these antenna models is that the human exposure to RF emissions was considered in the designing process, analyzing in this way several parameters related to the power absorbed in the body.

Some of the remarkable results regarding the absorption in human bodies are described below. One of them was the linear relationship between the antenna radiation efficiency and the power absorbed in body tissues, presented in Figure 5.7. Considering this and that the efficiency of the antenna model proposed for off-body communications was improved with respect to the previous models, the power absorbed in tissues was reduced.

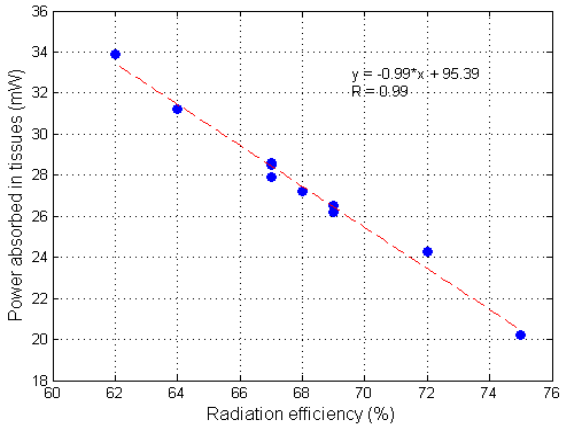

Figure 5.7. Power absorbed in tissues as function of antenna radiation efficiency.

Then, it was checked that SAR and power absorbed in the body are not always correlated. This can be explained because SAR results give information about the maximum absorption averaged over 10 g of body tissue, but this does not allow the evaluation of the power absorbed by the different parts of the body. Risco et al. (2012) demonstrated that two similar values of SAR can be related to very different values of head absorption and in this work, the same effect in other parts of the body was demonstrated.

Finally, the body mass index was found to be not an influential factor on the performance of the antennas.

1.4. Conduct an analysis of the exposure in the near field region

The evaluation of the power absorption in the near field region was described in Chapter 6. First, a comprehensive investigation into exposure due to wearable antennas was presented, contributing to the understanding of dosimetry and exposure assessment in the near field region. SAR and power absorption in human bodies were assessed for two body models, a male and a female, when placing the two different antennas in different locations of the body models. In addition, the percentage of power absorbed by different types of tissues was also reported. These evaluations were performed at three different frequencies in the 2.4 GHz band to consider the frequency shift produced when placing the antennas at different locations.

Another contribution was the review and application of the methods proposed in the literature to convert data measured in the far field region to

SAR_{WB} values. Three different methods proposed by different authors were selected to convert WiFi signal levels measured in the far field region to SAR_{WB} levels. The SAR_{WB} levels calculated from the WiFi measurements and from the wearable antennas were shown in Table 6.6 of that chapter and these results are also included below.

Table 6.6. SAR_{WB} values (nW/kg) calculated using the three different methods from the electric field measurements obtained in the two labs and in a classroom of the university and those obtained due to the wearable antennas

SAR_{WB} (nW/kg)								
		Converted data from EMF measurements						
		Method 1	**Method 2**				**Method 3**	
	Position	**10 kg**	**10 kg**	**70 kg**	**DMC 10 kg**	**DMC 70 kg**	**10 kg**	**70 kg**
Lab 1	1	31.49	20.84	9.59	31.68	14.57	21.07	11.84
	2	40.61	26.87	12.36	64.50	29.67	27.17	15.26
	3	31.96	21.15	9.73	25.38	11.67	21.38	12.01
	4	31.72	20.99	9.66	41.98	19.31	21.22	11.92
	5	24.88	16.47	7.57	35.57	16.36	16.65	9.35
Classroom 1	5	553	366	184	556	280	370	208
Lab 2	Morning	9.89	6.54	3.01	9.95	4.58	6.62	3.72
	Afternoon	5.18	3.42	1.58	5.21	2.39	3.46	1.95
	Night	2.91	1.92	0.88	2.92	1.34	1.94	1.09
Wearable antennas								
Off-Body Max Level		$61.42 \cdot 10^3$						
In-Body Max Level		$115.30 \cdot 10^3$						

2. DISSEMINATION

2.1. International Journals

Title: Wearable slot antenna at 2.45 GHz for off-body radiation: Analysis of efficiency, frequency shift, and body absorption

Authors: Marta Fernandez, Hugo G. Espinosa, David V. Thiel, Amaia Arrinda

Publication: Bioelectromagnetics, vol. 39, n. 1, pp. 25-34

Year: 2017

Contributions: This paper presents the interaction between the human body and an antenna designed for off-body communications. The effect between the body and the antenna is studied by means of simulations and measurements and some conclusions regarding the power absorption are drawn.

Title: An inward directed antenna for gastro-intestinal radio pill tracking at 2.45 GHz

Authors: Marta Fernandez, David V. Thiel, Amaia Arrinda, Hugo G. Espinosa

Publication: Microwave and Optical Technology Letters. Doi:10.1002/mop.31217

Year: 2018 (Accepted in March 2018, it will be published in May 2018)

Contributions: In this paper the procedure for designing, fabricating and validating the in-body antenna model is presented. The antenna performance is tested on different people and simulations are carried out to check its usefulness as a receiver for gastro-intestinal pill.

Title: Measurement methodology for determining the optimal frequency domain configuration to accurately record WiFi exposure levels

Authors: Marta Fernandez, David Guerra, Unai Gil, Ivan Peña, Amaia Arrinda

Publication: IEEE Transactions on instrumentation and measurement

Year: Accepted in May 2018

Contributions: This paper shows the measurement methodology proposed in order to accurately assess WiFi signal levels. The procedure followed in order to define this methodology is explained in detail. The drawbacks of other methods are also presented.

Title: Harmonization of noise measurement methods: Measurements of radio impulsive noise from a specific source

Authors: Marta Fernandez, Iratxe Landa, Amaia Arrinda, Rubén Torre, Manuel M. Vélez

Publication: IEEE Antennas and Propagation magazine, vol. 57, pp. 64-72

Year: 2015

Contributions: This paper describes a procedure for measuring and evaluating radio impulsive noise, which consists of emissions transmitted in the form of short pulses. A methodology for combining the measured impulsive samples to bursts is presented. Once the bursts are defined, the impulsive noise can be characterized.

Title: Measurements of impulsive noise from specific sources in medium wave band

Authors: Marta Fernandez, Iratxe Landa, Amaia Arrinda, Rubén Torre, Manuel M. Vélez

Publication: IEEE Antennas and wireless propagation letters, vol. 13, pp. 1263-1266

Year: 2014

Contributions: This letter presents the results obtained in measurements of impulsive noise in an indoor environment, when there is a main source of noise producing impulses. These results are useful for characterizing noise sources.

Title: Maximum-Entropy-Rate Selection of Features for Classifying Changes in Knee and Ankle Dynamics During running

Authors: Garry A. Einicke, Haider A. Sabti, David Thiel, Marta Fernández

Publication: IEEE Journal of Biomedical and Health Informatics, Early Access

Year: 2017

Contributions: A wearable musculo-skeletal monitoring system, which consists of two wearable sensors, is used to investigate deteriorations in knee and ankle dynamics during running.

Title: Characterisation of exposure to non-ionising electromagnetic fields in the Spanish INMA birth cohort

Authors: Mara Gallastegi, Mònica Guxens, Ana Jiménez-Zabala, Irene Calvente, Marta Fernández, Laura Birks, Benjamin Struchen, Martine Vrijheid, Marisa Estarlich, Mariana F. Fernández, Maties Torrent, Ferrán Ballester, Juan J Aurrekoetxea, Jesús Ibarluzea, David Guerra, Julián González, Martin Röösli, Loreto Santa-Marina

Publication: BMC Public Health, 16:167

Year: 2016

Contributions: This study describes the methodologies used for characterizing exposure of children to EMFs in the INMA (INfancia y Medio Ambiente- Environment and Childhood) Project. Indirect and direct methods are conducted to assess exposure levels, the first ones consist of filling questionnaires, gathering information about the proximity to emission sources and using geospatial propagation models. The direct methods are related to measurements.

Title: Power Absorption in Human Bodies due to Wearable Antennas and RF Signals in the 2.4 GHz Frequency Band

Authors: Marta Fernandez, Hugo G. Espinosa, David Guerra, Ivan Peña, David V. Thiel, Amaia Arrinda

Publication: Bioelectromagnetics

Year: To submit in May 2018

Contributions: This paper presents the evaluation of human exposure to wearable antennas and WiFi signals in the near field region. A comprehensive study of the power absorption in the human tissues due to two different wearable antennas is provided. Furthermore, methods for converting measured WiFi levels to exposure in the near field are studied and applied.

Title: Measurements and analysis of temporal and spatial variability of WiFi exposure levels in the 2.4 GHz frequency band

Authors: Marta Fernandez, David Guerra, Unai Gil, Iván Peña, Amaia Arrinda

Publication: Measurement (Elsevier)

Year: To submit in May 2018

Contributions: This paper presents the evaluation of human exposure to WiFi signals in the 2.4 GHz frequency band. The temporal and spatial variability of these signals is analyzed. Techniques and statistics for analyzing and presenting the obtained values are discussed. Finally, the results obtained in various measurement campaigns are compared and analyzed.

2.2. International Conferences

Title: Slot antenna for wearable applications and SAR evaluation

Authors: Marta Fernandez, Hugo Espinosa, David Thiel

Conference: Australian symposium on Antennas (ASA)

Date: February 2017

Place: Sydney, Australia

Contributions: The design and fabrication of a slot wearable antenna is described, detailing the advantages of the use of these antenna models for wearable applications. Simulations and measurements of the antenna performance in free space and on body are presented.

Title: Analysis of human exposure due to WiFi signals based on a novel measurement methodology

Authors: Marta Fernández, Iván Peña, David Guerra, Amaia Arrinda

Conference: IEEE International conference on electromagnetics in advanced applications (ICEAA)

Date: September 2016

Place: Cairns, Australia

Contributions: In this paper the contribution to the closest access point to the total WiFi exposure in the 2.4 GHz band is assessed. Moreover, some preliminary measurements of the day and night exposure in WLANs are presented, considering only the closest access point in some of the measurements and all the channels in the specified frequency band in the rest of cases.

Title: Characterisation of exposure to non-ionising electromagnetic fields in primary schools belonging to the study area of INMA-Gipuzkoa birth cohort

Authors: Mara Gallastegi, Ana Jiménez-Zabala, Loreto Santa-Marina, Mikel Ayerdi, Juan José Aurrekoetxea, Marta Fernández, Anke Huss, Jesús Ibarluzea

Conference: Annual Conference of the International Society for Environmental Epidemiology (ISEE)

Date: September 2016

Place: Rome, Italy

Contributions: This study assesses the exposure to EMF-NIR (non-ionizing radiation) in 26 primary schools of the INMA-Gipuzkoa study area by direct methods (spot and long-term measurements).

Title: Impulsive noise characterization and its effect on digital audio quality

Authors: Iratxe Landa, Manuel M. Velez, Amaia Arrinda, Rubén Torre y Marta Fernandez

Conference: IEEE International Symposium on Broadband Multimedia Systems and Broadcasting (BMSB)

Date: June 2015

Place: Gent, Belgium

Contributions: This study is focused on the analysis of the effects that the impulsive and Gaussian radio noise have in digital audio broadcasting. The analysis is based on radio noise measurements, which are latter combined with different transmission modes of DRM and the effects in the reception are studied.

2.3. National Conferences

Title: Análisis de equipos de medida de exposición electromagnética en redes WiFi

Title in English: Analysis of measurement instrumentation for measuring exposure to WiFi signals

Authors: Marta Fernández, Iván Peña, David Guerra, Teresa Echevarría , Amaia Arrinda

Conference: Simposium Nacional de la Unión Científica Internacional de Radio (URSI)

Date: September 2015

Place: Pamplona, Spain

Contributions: Results of WiFi signal levels measured by means of a personal exposure meter and a spectrum analyzer are compared in this study.

2.4. More activities related to scientific dissemination

Speaker at the **seminar** 'Antenas de telefonia movil y redes de comunicación inalámbrica y salud' (in English, 'Mobile phone antennas and wireless communication networks, and health')

Title: Campos electromagnéticos de RF. Redes de telefonía móvil, (in English, 'Radiofrequency electromagnetic fields. Mobile communication networks')

Date: November 2015 **Place:** Vitoria, Spain

Organized by: Basque Government

Contribution: A seminar was given on basic concepts about electromagnetic fields in the radiofrequency range and the operation of mobile phone communication networks. Most of the attendees were technicians working in the Basque Government and local councils with competence in health and environmental programs.

Speaker at the talk 'Las ondas electromagnéticas' (in English, 'electromagnetic waves')

Date: June 2016 **Place:** Durango, Spain

Organized by: Bizidun (an association of senior citizens)

Contribution: A talk was given on basic concepts about wireless networks and antennas. The attendees were senior citizens belonging to 'Bizidun' association.

Doctoral Workshops

Title: Contribución a la metodología de medida de exposición electromagnética debida a redes WiFi (in English, 'Contribution to the methodology for measuring human exposure to WiFi networks')

Authors: Marta Fernández, David Guerra, Amaia Arrinda

Date: 2015 **Place:** Murcia, Spain

Contributions: a talk was given about WiFi signal characteristics and the methods used to measure exposure to these signals.

Title: 'Exposición electromagnética a señales WiFi: definición de metodología de medida y obtención de niveles' (in English, 'Human exposure to WiFi signals: description of the measurement methodology and acquisition of exposure levels')

Authors: Marta Fernández, Iñigo Trigo, Iván Peña, David Guerra, Amaia Arrinda

Date: 2016 **Place:** Bilbao, Spain

Contributions: a poster was presented showing some concepts about WiFi signals and the exposure levels obtained in some measurements.

3. FUTURE WORK

The tasks and results of this thesis contribute significantly to improve the assessment and analysis of human exposure to RF fields in the near and far field regions. The following steps should be focused on applying the described techniques to other situations in order to deep in the knowledge of EMF radiation.

More precisely, this research work could be continued as follows:

- Apply the procedure followed to identify the optimal configuration of the spectrum analyzer to measure EMF exposure due to other signals. For example, it could be applied in order to establish the proper setup for measuring WiFi signals in the 5 GHz frequency band or even for measuring signals from other services, such as the ones corresponding to 5G mobile communication systems.

- Conduct the research of WiFi exposure levels in other scenarios, such as outdoor environments.

- Regarding the evaluation of exposure to wearable antennas, the analysis could be replicated for different postures of the body models, since changes in postures can modify the antenna performance and thus, the power absorption.

- Although computational tools are perfectly valid to assess power absorption in the human body, a future line can be focus on performing measurements using phantom models in order to investigate differences due to the two different systems of evaluation.

REFERENCES AND GLOSSARY

References

Abidoye AP, Azeez NA, Adesina AO, Agbele KK, Nyongesa HO. Using wearable sensors for remote healthcare monitoring system. Journal of Sensor Technology, vol. 1, pp. 22-28, 2011.

Access Point Cisco Aironet 1700 series datasheet. [Online]. Available: http://www.cisco.com/. (Updated 2016) Accessed on: March 2018.

Adamson D, Bownds D, Fernandez A, Goodall E. The response of electric field probes to realistic RF environments. IEEE MTT-S International Microwave Symposium Digest (MTT), 2010.

Adepoju F, Arshak K. Mathematical method for tracking ingestible telemetry capsule in real-time. International Journal of Hybrid Information Technology, vol.8, n. 12, pp. 449-468, 2015.

Akcalar S, Turkbey B, Karcaaltincaba M, Akpinar E, Akhan O. Small bowel wall thickening: MDCT evaluation in the emergency room. Emergency Radiology, vol. 18, pp.409-15, 2011.

Alekseev SI, Ziskin MC. Millimeter-Wave absorption by cutaneous blood vessels: a computational study. IEEE Transactions on Biomedical Engineering, vol. 56, n. 10, pp. 2380-2388, 2009.

Andersen JB, Nielsen JO, Pedersen GF, Bauch G, Herdin M. Room electromagnetics. IEEE Antennas and Propagation Magazine, vol. 49, pp. 27–33, 2007.

Anguera J, Andújar A, Picher C, Gonzalez L, Puente C, Kahng S. Behavior of several antenna topologies near the human head at the 2.4–2.5 GHz band. Microw Opt Technol, vol. 54, pp. 1911–1916, 2012.

Anritsu Signal Analyzer MS2840A-044/046 Brochure. [Online]. Available: https://dl.cdn-anritsu.com/en-en/test-measurement/files/Brochures-Datasheets-Catalogs/Brochure/ms2840a-e1300.pdf . Accessed on: March 2018.

Anzaldi G, Silva F, Fernández M, Quílez M, Riu PJ. Initial analysis of SAR from a cell phone inside a vehicle by numerical computation. IEEE Transactions on Biomedical Engineering. vol. 54, n. 5, 2007.

Appleby R, Thiel DV, Maggs M, Spathis A. Locating underground markers. PCT patent PCTAU2013001171, 2015.

Arab P, Heimlich M, Dutkiewicz E. Investigation of radar localization system accuracy for human gastro intestine (GI) tract. IEEE International Symposium on Medical Information and Communcation Technology, 2013.

Armstrong S. Wireless connectivity for health and sports monitoring: A review. British Journal of Sports Medicine, vol. 41, n. 5, pp. 285-289, 2007.

ARPANSA. Radiation Protection Standard. Maximum Exposure Levels to Radiofrequency Fields - 3 kHz to 300 GHz. Radiation protection Series n. 3, 2002.

Arriola A, Sancho JI, Brebels S, Gonzalez M, De Raedt W. Stretchable dipole antenna for body area networks at 2.45 GHz. IET Microw. Antennas Propag., vol. 5, pp. 852–859, 2011.

Balanis C. Antenna Theory Analysis and Design, 2nd ed., Wiley, 2008.

Baltrenas P, Buckus R. Measurements and analysis of the electromagnetic fields of mobile communication antennas. Measurement, vol. 46, pp. 3942–3949, 2013.

Bamba A, Joseph W, Vermeeren G, Tanghe E, Gaillot DP, Andersen JB, Nielsen J, Lienard M, Martens L. Validation of experimental Whole-Body SAR assessment method in a complex indoor environment. Bioelectromagnetics, vol. 34, pp. 122-132, 2013.

Bamba A, Joseph W, Vermeeren G, Thielens A, Tanghe E, Martens L. A formula for human average whole-body SARwb under diffuse fields exposure in the GHz region. Physics in Medicine & Biology, vol 59, pp. 7435-7456, 2014.

Basar MR, Malek F, Juni KM, Idris MS, Iskandar M, Saleh M. Ingestible wireless capsule technology: A review of development and future indications. Int. J. Antennas & Propagation, 2012.

Basar MR, Malek F, Juni KM, Saleh MIM, Idris MS, Mohamed L, Saudin N, Affendi NAM, Ali A. The use of a human body model to determine the variation of path losses in the human body channel in wireless capsule endoscopy. Progress In Electromagnetics Research, vol. 133, pp. 495-513, 2013.

Bechet P, Miclaus S, Bechet AC. Improving the accuracy of exposure assessment to stochastic-like radiofrequency signals. IEEE Trans. Electromag. Comp., vol. 54, pp. 1169–1177, 2012.

Betta G, Capriglione D, Miele G, Rossi L. Reliable measurements of wi-fi™ electromagnetic pollution by means of traditional spectrum analyzers. Conference Record – IEEE Instrumentation and Measurement Technology Conference, pp. 206-211, 2008.

Bhatt CR, Redmayne M, Abramson MJ, Benke G. Instruments to assess and measure personal and environmental radiofrequency-electromagnetic field exposures. Australas Phys Eng Sci Med vol. 39, pp. 29–42, 2016a.

Bhatt CR, Thielens A, Redmayne M, Abramson MJ, Billahc B, Sima MR, Vermeulen R, Martens L, Joseph W, Benke G. Measuring personal exposure from 900 MHz mobile phone base stations in Australia and Belgium using a novel personal distributed exposimeter. Environment International vol. 92, pp. 388–397, 2016b.

Bolte JFB, van der Zande G, Kamer J. Calibration and uncertainties in personal exposure measurements of radiofrequency electromagnetic fields. Bioelectromagnetics, vol. 32, pp. 652-663, 2011.

Bolte JFB. Lessons learnt on biases and uncertainties in personal exposure measurement surveys of radiofrequency electromagnetic fields with exposimeters. Environment Int., vol. 94, pp. 724-735, 2016.

Boulis A, Smith D, Miniutti D, Libman L, Tselishchev Y. Challenges in body area networks for healthcare: The mac. IEEE Commun. Mag. 2012.

Burgi A, Theis G, Siegenthaler A, Roosli M. Exposure modeling of high-frequency electromagnetic fields. J Expo Sci Environ Epidemiol vol. 18, n.2, pp. 183–191, 2008.

Cala P, Bieńkowski P, Zubrzak B. GSM/UMTS base station as a unusual electromagnetic field source – measurements in environment for LOS and NLOS scenarios. IEEE Conference on Microwave Techniques (COMITE), pp 1-4, 2015.

Cansiz M, Abbasov T, Kurt MB, Celik AR. Mobile measurement of radiofrequency electromagnetic field exposure level and statistical analysis. Measurement vol. 86, pp. 159–164, 2016.

Cardis E, Deltour I, Mann S, Moissonnier M, Taki M, Varsier N, Wake K, Wiart J. Distribution of RF energy emitted by mobile phones in anatomical structures of the brain. Phys. Med. Biol. Vol. 53, pp. 2771–2783, 2008.

Cavallari R, Martelli F, Rosini R, Buratti C, Verdone R. A survey on wireless body area networks: technologies and design challenges. IEEE Communications surveys & tutorials, vol. 16, n. 3, pp. 1635-1657, 2014.

CENELEC European Committee for Electrotechnical Standardization. Basic standard on measurement and calculation procedures for human exposure to electric, magnetic and electromagnetic fields (0 Hz – 300 GHz). EN 50413, 2008.

Chen C, Pomalaza-Raez C. Design and evaluation of a wireless body sensor system for smart home health monitoring. IEEE Global Telecommunications Conf. GLOBECOM, pp. 1 –6, 2009.

Chen M, Gonzalez S, Vasilakos A, Cao H, Leung VCM. Body Area Networks: A survey. Mobile Netw Appl vol. 16, pp. 171–193, 2011.

Cheng S, Zhigang W, Hallbjorner P, Hjort K, Rydberg A. Foldable and stretchable liquid metal planar inverted cone antenna. IEEE Trans. Antennas Propag., 57, pp. 3765–3771, 2009.

Cherukuri S, Venkatasubramanian KK, Gupta SKS. Biosec: a biometric based approach for securing communication in wireless networks of biosensors implanted in the human body. International Conference on Parallel Processing Workshops, 2003.

Chu HT. A Ubiquitous Warning System for Asthma-Inducement. IEEE International Conference on Sensor Networks, Ubiquitous, and Trustworthy Computing, Taichung, pp. 186-191, 2006.

Clouch JW. Electromagnetic lateral waves observed by earth-sounding radars. Geophysics, vol. 41, pp 1126-1132, 1976.

Colombi D, Thors B, Persson T, Wirén N, Larsson LE, Törnevik C. Output power distributions of mobile radio base stations based on network measurements. in IOP Conf. Series: Materials Science and Engineering 44, 2013.

Colson RH, Watson BH. Improved techniques in the construction of pH-sensitive radio pills. A handbook on biotelemetry and radio tracking. Pergamon Press, 1979

CST Microwave Studio. Computer Simulation Technology. 2016.

CTE Orden CTE/23/2002. por la que se establecen condiciones para la presentación de determinados estudios y certificaciones por operadores de servicios de radiocomunicaciones. s.l. BOE, 2002.

Darco M, Liccardo A, Pasquino N. ANOVA-based approach for DAC diagnostics. IEEE Transactions on Instrumentation and Measurement, vol. 61, n. 7, pp. 1874 – 1882, 2012.

Davis CC, Balzano Q. The international intercomparison of SAR measurements on cellular telephones. IEEE Transactions on Electromagnetic Compatibility, vol.51, nº 2, pp. 210-216, 2009.

De Francisco R, Huang L, Dolmans G. Coexistence of WBAN and WLAN in medical environments. IEEE Veh. Technol. Conf, pp. 1–5, 2009.

De Santis V, Sill JM, Bourqui J, Elise C. Fear safety assessment of ultra-wideband antennas for microwave breast imaging. Bioelectromagnetics, vol. 33, pp. 215–225, 2012.

De Silva B, Natarajan A, and Motani M. Inter-user interference in body sensor networks: Preliminary investigation and an infrastructure-based solution. IEEE Int. Workshop on Wearable and Implantable Body Sensor Networks, pp. 35–40, 2009.

De Vicq N, Robert F, Penders J, Gyselinckx B, Torfs T. Wireless body area network for sleep staging. IEEE Biomedical Circuits and Systems Conf. (BIOCAS 2007), pp. 163–166, 2007.

Dissanayake T, Yuce MR, Ho C. Design and Evaluation of a Compact Antenna for Implant-to-Air UWB Communication. IEEE Antennas and wireless propagation letters, vol. 8, pp. 153-156, 2009.

Djuric N, Kljajic D, Kasas-lazetic K, Bajovic V. The SEMONT continuous monitoring of daily EMF exposure in an open area environment. Environmental Monitoring and Assessment, vol. 187m n.4, pp. 1-17, 2015.

Domenicali D, Di Benedetto MG. Performance analysis for a body area network composed of IEEE 802.15.4a devices. Workshop on Positioning, Navigation and Communication, pp. 273 –276, 2007.

EC Council Recommendation of 12 July 1999 on the limitation of exposure of the general public to electromagnetic fields (0 Hz to 300 GHz) (1999/519/EC). 1999.

EME Spy 200, Datasheet. [Online]. Available: http://www.mvg-world.com/es/system/files/EMESPY200 Accessed on March 2018.

Emelyanenko T, O'Keefe SG, Espinosa HG, Thiel DV. Surface field measurements from a buried UHF transmitter: Theory, modelling and experimental results. IEEE Trans. Antennas and Propagation, vol. 65, pp. 4389-4393, 2017.

ESM 140 Mobile-phone dosimeter. [Online]. Available: https://www.maschek.de/uk/frameset.php?p=produkte. Accessed on: March 2018.

ESPI SA Operating Manual, Rohde & Schwarz. [Online]. Available: https://www.rohde-schwarz.com. Accessed on: March 2018.

Espinosa HG, Thiel DV, Brindley C. An assessment of simulation methodologies for the analysis of near-field radiation zones related to human exposure. IEEE International Workshop Antenna Technology, 2014.

Estenberg J, Augustsson T. Extensive frequency selective measurements of radiofrequency fields in outdoor environments performed with a novel mobile monitoring system. Bioelectromagnetics, vol. 35, n. 3, pp. 227–230, 2014.

ETS Lindgren. [Online]. Available: http://www.ets-lindgren.com/ Accessed on April 2018.

ETSI. Wideband transmission systems; Data transmission equipment operating in the 2,4 GHz ISM band and using wide band modulation techniques; Harmonised Standard covering the essential requirements of article 3.2 of Directive 2014/53/EU. ETSI EN 300 328, 2016.

EU Directive 2013/35/EU of the European Parliament and of the Council of 26 June 2013 on the minimum health and safety requirements regarding the

exposure of workers to the risks arising from physical agents (electromagnetic fields). 2013.

European Committee for Electrotechnical Standardization (CENELEC). [Online]. Available: https://www.cenelec.eu/ Accessed on April 2018.

European Statistical System (Eurostat). Population structure and ageing. 2017. [Online]. Available:http://ec.europa.eu/eurostat/statistics-explained/index.php/Population_structure_and_ageing Access on: March 2018.

ExpoM-RF. Personal RF exposure meter. [Online]. Available: https://www.fieldsatwork.ch/products/expom-rf/. Accessed on: March 2018.

Fernández-García R, Gil I. Measurement of the environmental broadband electromagnetic waves in a mid-size European city. Environmental Research, vol. 158, pp. 768-772, 2017.

Foster KR, Moulder JE. Wi-Fi and health: review of current status of research. Health Phys., vol. 105, n. 6, pp. 561-575, 2013.

Foster KR. Radiofrequency exposure from wireless LANS utilizing Wi-Fi technology. Health Phys vol. 92, pp. 280-289, 2007.

Frei P, Mohler E, Bürgi A, Fröhlich J, Neubauer G, Braun-Fahrländer C, Röösli M, The QUALIFEX Team. Classification of personal exposure to radio frequency electromagnetic fields (RF-EMF) for epidemiological research: Evaluation of different exposure assessment methods. Environment International vol. 36, pp. 714–720, 2010.

Gabriel C, Gabriel S, Corthout E. The dielectric properties of biological tissues: I. Literature survey. Phys. Med. Biol. Vol. 41, pp. 2231-2249, 1996.

Gabriel C, Gabriel S. Compilation of the dielectric properties of body tissues at RF and microwave frequencies. 1999. [Online]. Available: http://niremf.ifac.cnr.it/docs/DIELECTRIC/Report.html Access on March 2018.

Galehdar A, Thiel DV. Flexible light-weight antenna at 2.4 GHz for athlete clothing. IEEE International Symposium Antennas and Propagation Society, pp. 4160-4163, 2007.

Gallastegi M, Guxens M, Jimenez-Zabala A, Calvente I, Fernandez M, Birks L, et al. Characterisation of exposure to non-ionising electromagnetic fields in the Spanish INMA birth cohort: study protocol. BMC Public Health, 16:167, 2016.

Gao T, Massey T, Selavo L, Crawford D, Chen B, Lorincz K, Shnayder V, Hauenstein L, Dabiri F, Jeng J, Chanmugam A, White D, Sarrafzadeh M, Welsh M. The advanced health and disaster aid network: A light-weight wireless medical system for triage. IEEE Trans. Biomed. Circuits Syst., vol. 1, pp. 203 –216, 2007.

Gil I, Fernández-García R. Study of the exposure to time-varying electric field in the ESEIAAT UPC School. IEEE Progress in Electromagnetic Research Symposium (PIERS), 2016.

Gkonis F, Boursianis A, Samaras T. Assessment of General Public Exposure to LTE signals compared to other Cellular Networks Present in Thessaloniki, Greece. Radiation Protection Dosimetry, vol. 175, n. 3, pp. 388–393, 2017.

Goedhart G, Vrijheid M, Wiart J. Using software modified smartphones to validate self-reported mobile phone use in young people: a pilot study. Bioelectromagnetics, vol. 36, n. 7, pp. 538-43, 2015.

Guxens M, Ballester F, Espada M, Fernandez MF, Grimalt JO, Ibarluzea J, et al. Cohort Profile: the INMA–INfancia y Medio Ambiente–(Environment and Childhood) Project. Int J Epidemiol. vol. 41, pp. 930–940, 2012.

Hadjem A, Conil E, Gati A, Wong M, Wiart J. Analysis of Power Absorbed by Children's Head as a Result of New Usages of Mobile Phone. IEEE Transactions on Electromagnetic Compatibility, vol. 52, n. 4, 2010.

Haycock GB, Schwartz GJ, Wisotsky DH. Geometric method for measuring body surface area: a height-weight formula validated in infants, children and adults. Journal of Pediatrics vol. 93, pp. 62–66, 1978.

Huo H, Xu Y, Bilen C, Zhang H. Coexistence issues of 2.4GHz sensor networks with other RF devices at home. Int. Conf. on Sensor Technol. and Applications, pp. 200–205, 2009.

Hurt WD, Ziriax JM, Mason PA. Variability in EMF permittivity values: implications for SAR calculations. IEEE Transactions on Biomedical Engineering, vol. 47, n. 3, pp. 396-401, 2000.

Hussain I, Salvietti G, Spagnoletti G, Prattichizzo D. The Soft-SixthFinger: a wearable EMG controlled robotic extra-finger for grasp compensation in chronic stroke patients. IEEE Robotics and Automation Letters, pp. 1000-1006, 2016.

Ibrani M, Ahma L, Hamiti E. Assessment of the exposure of children to electromagnetic fields from wireless communication devices in home environments. IET Communications, vol. 8, pp. 2222-2228, 2014.

IEEE 802.15.4 Standard, Part 15.4: Wireless Medium Access Control (MAC) and Physical Layer (PHY) Specifications for Low-Rate Wireless Personal Area Networks (LR-WPANs). Piscataway, New Jersey, 08855-1331: IEEE, 2006.

IEEE Standard 802.11n. Amendment 5: Enhancements for Higher Throughput. New York, 2009.

IEEE standard 802.15.6. IEEE Standard for Local and metropolitan area networks— Part 15.6: Wireless Body Area Networks. New York, 2012.

IEEE Standard for Information technology-Telecommunications and information exchange between systems. Local and metropolitan area networks- Specific requirements. Part 11: Wireless LAN Medium Access Control (MAC) and Physical Layer (PHY) Specifications, IEEE Std. 802.11, 2016.

IEEE Standards. IEEE Recommended Practice for the Measurement of Potentially Hazardous Electromagnetic Fields—RF and Microwave. C95.3, 1991.

IEEE Standards. IEEE Standard for safety levels with respect to human exposure to radiofrequency electromagnetic Fields, 3 kHz to 300 GHz. C95.1, 2005. (Revision of IEEE Std C95.1-1991).

IFAC Institute for Applied Physics, Italian National Research Council. Calculation of the dielectric properties of body tissues. [Online]. Available: http:// niremf.ifac.cnr.it/tissprop/ Accessed on April 2018.

IndexSAR Phantom models from. [Online]. Available: https://indexsar.com/product-category/phantoms/ Accessed on April 2018.

International Agency for Research on Cancer (IARC). World Cancer Report. 2014.

International Commission on Non-Ionizing Radiation Protection (ICNIRP). Guidelines for limiting exposure to time-varying electric, magnetic, and electromagnetic fields (up to 300 GHz). ICNIRP Guidelines, vol. 74, nº 4. April 1998.

International Electrotechnical Commission (IEC). [Online]. Available: http://www.iec.ch/ Accessed on April 2018.

International Electrotechnical Commission (IEC). Human exposure to radio frequency fields from hand-held and body-mounted wireless communication devices–human models, instrumentation, and procedures to determine the specific absorption rate (SAR) for hand-held devices used in close proximity to the ear (frequency range of 300MHz to 3 GHz). International Standard 62 209, 2005.

International Telecommunication Union (ITU). [Online]. Available: https://www.itu.int/ Accessed on April 2018.

International Telecommunication Union (ITU). Man made noise measurements in the HF range. ITU-R Rep. SM.2155, Geneva, Switzerland, 2009.

International Telecommunications Union (ITU). Methods for Measurements of Radio Noise. ITU-R Recommendation Standard SM.1753-2, 2012.

Iskra S, McKenzie RJ, Cosic I. Factors influencing uncertainty in measurement of electric fields close to the body in personal RF dosimetry. Radiat Prot Dosimetry, vol. 140 pp. 25–33, 2010.

ITU-T. Guidance on measurement and numerical prediction of electromagnetic fields for compliance with human exposure limits for telecommunication installations. Recommendation ITU-T K.61, 2008.

ITU-T. Monitoring of electromagnetic field levels. Recommendation ITU-T K.83, 2011.

Jaimes AF, de Sousa FR. A taxonomy for learning, teaching, and assessing wireless body area networks. IEEE Latin American Symposium on Circuits & Systems, 2016.

James DA, Leadbetter RI, Neeli MR, Burkett BJ, Thiel DV, Lee JB. An integrated swimming monitoring system for the biomechanical analysis of swimming strokes. Sports Technol., vol. 4, pp. 141–150, 2013.

Jantunen I, Laine H, Huuskonen P, Trossen D, Ermolov V. Smart sensor architecture for mobile-terminalcentric ambient intelligence. Sens. Actuators A. Phys. Vol. 142, pp. 352–360, 2004.

Joseph W, Frei P, Roosli M, Thuroczy G, Gajsek P, Trcek T, Bolte J, Vermeeren G, Mohler E, Juhasz P, Finta V, Martens L. Comparison of personal radio frequency electromagnetic field exposure in different urban areas across Europe, Environmental Research vol. 110 pp. 658–663, 2010a.

Joseph W, Pareit D, Vermeeren G, Naudts D, Verloock L, Martens L, Moerman I. Determination of the duty cycle of WLAN for realistic radio frequency electromagnetic field exposure assessment. Biophysics and Molecular Biology, vol. 111, pp 30-36, 2013.

Joseph W, Verloock L, Goeminne F, Vermeeren G, Martens L. Assessment of general public exposure to LTE and RF sources present in an urban environment. Bioelectromagnetics, vol. 31, pp. 576-579, 2010c.

Joseph W, Verloock L, Tanghe E, Martens L. In-situ measurement procedures for temporal RF electromagnetic field exposure of the general public. Health Phys. vol. 96, pp. 529-542, 2009.

Joseph W, Vermeeren G, Verloock L, Martens L. Estimation of Whole-Body SAR from electromagnetic fields using personal exposure meters. Bioelectromagnetics, vol. 31, pp. 286-295, 2010b.

Kang E, Im Y, Kim U. Remote control multi-agent system for u-healthcare service. Int. Symp. on Agent and Multi- Agent Systems: Technologies and Applications, Springer-Verlag, pp. 636–644, 2007.

Karipidis K, Henderson S, Wijayasinghe D, Tjong L, Tinker R. Exposure to radiofrequency electromagnetic fields from Wi-Fi in Australian schools. Radiation Protection Dosimetry, vol. 175, pp. 432–439, 2017.

Kaufmann T, Fumeaux C. Wearable textile half-mode substrate-integrated cavity antenna using embroidered vias. IEEE Antennas Wireless Propag. Lett., vol. 12, pp. 805–808, 2013.

Keysight Technologies. ESA-E Series Spectrum Analyzer Data Sheet. [Online]. Available: https://literature.cdn.keysight.com/litweb/pdf/5989-9815EN.pdf?id=1548393. Accessed on: March 2018.

Keysight Technologies. Spectrum Analysis Basics – Application Note 150, 2016.

Khalid M, Mee T, Peyman A, Addison D, Calderon C,Maslanyj M, Mann S. Exposure to radio frequency electromagnetic fields from wireless computer networks: duty factors of Wi-Fi devices operating in schools. Progress in. Biophysics & Molecular Biology, vol. 107, pp. 412-420, 2011.

Khan MM, Shanaz S, Al-Mamun A. Investigation of performance parameters of different wearable narrowband antennas in close proximity to the human body. International conference on computer and information technology, 2012.

Kijewski-Correa T, Haenggi M, Antsaklis P. Wireless sensor networks for structural health monitoring: a multi-scale approach. Analysis & Computational Specialty Conference, 2006.

Kim K, Yun S, Lee S, Nam S, Yoon YJ, Cheon C. A Design of a High-Speed and High-Efficiency Capsule Endoscopy System. IEEE Transactions on biomedical engineering, vol. 59, n. 4, pp. 1005-1011, 2012.

Krayni A, Hadjem A, Vermeeren G, Sibille A, Roblin C, Joseph W, Martens L, Wiart J. Modeling and characterization of the uplink and downlink exposure in wireless networks. International Journal of Antennas and Propagation, 2017.

Kundu AS, Mazumder O, Bhaumik S. Design of wearable, low power, single supply surface EMG extractor unit for wireless monitoring. International Conference on Nanotechnology and Biosensors, Singapore, 2011.

Kunz K S, Luebbers R J. The Finite Difference Time Domain Method for Electromagnetics. CRC Press, 1993.

Kwak KS, Ameen MA, Kwak D, Lee C, Lee H. A study on proposed IEEE 802.15 WBAN MAC protocols. International Symposium on Communications and Information Technology, 2009.

Latré B, Braem B, Moerman I, Blondia C, Demeester P. A survey on wireless body area networks. Wirless Network, vol. 17, pp. 1–18, Jan. 2011.

Lecoutere J, Thiel DV, Puers R. The near field effect of the human body on a flexible resonant dipole antenna. Symposium on Biotelemetry, Leuven, Belgium, 2016.

Lee YD, Chung WY. Wireless sensor network based wearable smart shirt for ubiquitous health and activity monitoring. Sensors and Actuators B: Chemical, vol. 140, pp 390-395, 2009.

Letertre T, Monebhurrun V, Toffano Z. Electromagnetic field measurements of WIMAX systems using isotropic broadband probes. IEEE MTT-S International Microwave Symposium Digest (MTT), 2011.

Leung S, Diao Y, Chan K, Siu Y, Wu Y. Specific absorption rate evaluation for passengers using wireless communication devices inside vehicles with different handedness, passenger counts, and seating locations. IEEE Transactions on biomedical engineering, vol. 59, n. 10, 2012.

Livingston EH, Lee S. Body surface area prediction in normal weight and obese patients. American Journal Physiology Endocrinology and Metabolism, vol. 281, pp. 586 –591, 2001.

Loni Z, Espinosa HG, Thiel DV. Floating monopole antenna on a tethered subsurface sensor at 433 MHz for ocean monitoring applications. IEEE Oceanic Engineering, 2017.

Lunca E, Damian C, Salceanu A. EMF exposure measurements on 4G/LTE mobile communication networks. International Conference and Exposition on Electrical and Power Engineering, Iasi, Romania, 2014.

Lunca E, David V, Salceanu A, Cretescu I. Assessing the Human Exposure due to Wireless Local Area Networks in Office Environments. Environmental Engineering and Management Journal vol. 11, pp. 385-391, 2012.

Ma L, Edwards RM, Bashir S, Khattak MI. A wearable flexible multi-band antenna based on a square slotted printed monopole. Antennas and Propagation Conf., UK, pp. 345–348, 2008.

Malik B, Singh R. A survey of research in WBAN for biomedical and scientific applications. Health and Technology, vol. 3, n. 3, pp. 227–235, 2013.

Martelli F, Verdone R. Coexistence issues for wireless body area networks at 2.45 GHz. European Wireless Conf., pp. 1 –6, 2012.

Martin T, Jovanov E, Raskovic D. Issues in wearable computing for medical monitoring applications: a case study of a wearable ECG monitoring device. Proceedings of ISWC 2000.

Massey JW, Yilmaz AE. AustinMan and AustinWoman: High-fidelity, anatomical voxel models developed from the VHP color images. International Conference of the IEEE Engineering in Medicine and Biology Society (IEEE EMBC), 2016.

McIntosh RL, Anderson V. SAR versus Sinc: What is the appropriate RF exposure metric in the range 1–10 GHz? Part II: Using complex human body models. Bioelectromagnetics, vol. 31, n. 6, pp. 467–478, 2010.

Meyer FJC, Davidson DB, Jakobus U, Stuchly MA. Human exposure assessment in the near field of GSM base-station antennas using a hybrid finite element method of moments technique. IEEE Transactions on Biomedical Engineering, vol. 50, n. 2, 2003.

Miclaus S, Bechet P, Iftode C. The application of a channel-individualized method for assessing long-term, realistic exposure to radiofrequency radiation emitted by mobile communication base station antennas. Measurement, vol. 46, pp. 1355–1362, 2013.

Miclaus S, Bechet P, Stratakis D. Exposure levels due to WLAN devices in indoor environments corrected by a time–amplitude factor of distribution of the quasi-stochastic signals. Radiation Protection Dosimetry, pp. 1–8, 2014.

Mittal I, Anand A. WLAN Architecture. International Journal of Computer Trends and Technology, vol. 8 n. 3, pp. 148-151, 2014.

Movassaghi S, Abolhasan M, Lipman J, Smith D, Jamalipour A. Wireless Body Area Networks: A survey. IEEE Communications Surveys & Tutorials, pp. 1658-1686, 2014.

Nakamura T, Shimizu M, Kimura H, Sato R. Effective permittivity of amorphous mixed materials. Electronics and Communications in Japan, vol. 88, n. 10, pp.1-9, 2005.

Narda Safety test solutions. [Online]. Available: http://www.narda-sts.us/pdf_files/DataSheets/NBM-Probes_DataSheet.pdf Accessed on April 2018.

Nemati E, Jamal Deen M, Mondal T. A Wireless wearable ECG Sensor for long-term applications. IEEE Communications Magazine, vol. 50, Nº 1, pp. 36–43, 2012.

Nordsborg NB, Espinosa HG, Thiel DV. Estimating energy expenditure during front crawl swimming using accelerometers. Procedia Eng. vol. 72, pp. 132–137, 2014.

Otto C, Milenković A, Sanders C, Jovanov E. System architecture of a wireless body area sensor network for ubiquitous health monitoring. Journal of Mobile Multimedia, vol 1, n. 4, pp. 307-326, 2005.

Otto MC, Jovanov E. Wireless sensor networks for personal health monitoring: Issues and an implementation. Computer Communications vol. 29, pp. 2521–2533, 2006.

Ouchi K, Suzuki T. Lifeminder: a wearable healthcare support system using user's context. Conf. on Distributed Computing Systems Workshops, pp. 791 – 792, 2002.

Pachón-García FT, Fernandez-Ortiz K, Paniagua-Sanchez JM. Assessment of Wi-Fi radiation in indoor environments characterizing the time and space-varying electromagnetic fields. Measurement, vol. 63, pp. 309–321, 2015.

Pantelopoulos A, Bourbakis NG. A survey of wearable sensor-based systems for health monitoring and prognosis. IEEE Transactions on Systems, Man, and Cybernetics, Part C, vol. 40, pp. 1-12, 2010.

Pasquino N. Measurement and analysis of human exposure to electromagnetic fields in the GSM band. Measurement, vol. 109, pp. 373-383, 2017.

Patel M, Wang J. Applications, challenges, and prospective in emerging body area networking technologies. IEEE Wirel Commun Mag, vol. 17, pp. 80–88, 2010.

Person C, Le Pennec F, Luc J. Design, modelisation and optimisation of high efficiency miniature E-field probes performed on 3D ceramic prisms for SAR evaluation. Annals of telecommunications, vol. 63, pp 43-53, 2008.

Peyman A, Khalid M, Calderon C, Addison D, Mee T, Maslanyj M, Mann S. Assessment of Exposure to Electromagnetic Fields fromWireless Computer Networks (Wi-Fi) in Schools; Results of Laboratory Measurements. Health Phys, vol. 100, pp. 594-612; 2011.

Peyman A, Rezazadeh A, Gabriel C. Changes in the dielectric properties of rat tissue as a function of age at microwave frequencies. Phys. Med. Biol. vol. 46, pp. 1617–1629, 2001.

Picard D. Advanced dosimetric assessment system. IEEE European Microwave Conference, 2008.

Piuzzi E, Bernardi P, Cavagnaro M, Pisa S, Lin JC. Analysis of adult and child exposure to uniform plane waves at mobile communication systems frequencies (900 MHz–3 GHz). IEEE Transactions on Electromagnetic Compatibility, vol. 53, Nº 1, pp. 38-47, 2011.

Poutanen J, Salmi J, Haneda K, Kolmonen V, Vainikainen P. Angular and shadowing characteristics of dense multipath components in indoor radio channels. IEEE Transactions on antennas and propagation, vol. 59, n 1, pp. 245–253, 2011.

Quirini M, Webster RJ, Menciassi A, Dario P. Design of a pill-sized 12-legged endoscopic capsule robot. IEEE Int. Conf. Robotics and Automation, pp. 1856-1862, 2007.

Ramli SN, Ahmad R, Abdollah MF, Dutkiewicz E. A biometric-based security for data authentication in Wireless Body Area Network (WBAN). International Conference on Advanced Communication Technology, 2013.

Rappaport T S. Wireless Communications Principles and Practice. Prentice-Hall, 2010.

RD Real Decreto 1066/2001 por el que se aprueba el Reglamento que establece las condiciones de protección del dominio público, restricciones a las emisiones radioeléctricas y medidas de protección sanitaria frente a emisiones radioeléctricas. s.l. 2001.

Rhode & Schwarz. Power Measurement on Pulsed Signals with Spectrum Analyzers. Application note, 2003.

Risco S, Anguera J, Andujar A, Picher C, Pajares J. Comparison of a monopole and a PIFA handset antenna in the presence of the human head. Microw Opt Technol Lett, vol. 54, pp. 454–459, 2012.

Rohde & Schwarz. R&S FSC Spectrum analyzer specifications. [Online]. Available: https://www.rohde-schwarz.com. Accessed on: March 2018.

Röösli M, Frei P, Mohler E, Braun-Fahrländer C, Bürgi A, Fröhlich J, Neubauer G, Theis G, Egger M. Statistical Analysis of Personal Radiofrequency Electromagnetic Field Measurements With Nondetects. Bioelectromagnetics vol. 29, pp. 471-478, 2008.

Rosaline SI, Raghavan S. A compact dual band antenna with an Eng SRR cover for SAR reduction. Microw Opt. Technol Lett, vol. 57, pp. 741–747, 2015.

Sabrin S, Rahman MM. Wearable Antenna with Low SAR for 2.45 GHz Wireless medical devices and analysis of the effect of different spacing introduced. IEEE International conference on Electrical Engineering and Information Communication Technology (ICEEICT), Bangladesh, 2015.

Sabti HA, Thiel DV. Node position effect on link reliability for body centric wireless network running applications. IEEE Sensors, vol. 14, pp. 2687–2691, 2014.

Sabti HA, Thiel DV. Self-calibrating body sensor network based on periodic human movements. IEEE Sensors Journal, vol. 15, Nº. 3, pp. 1552-1558, 2015.

Sagar S, Adem SM, Struchen B, Loughran SP, Brunjes ME, Arangua L, Dalvie MA, Croft RJ, Jerrett M, Moskowitz JM, Kuo T, Röösli M. Comparison of radiofrequency electromagnetic field exposure levels in different everyday microenvironments in an international context. Environment International, vol. 114 pp. 297–306, 2018.

Salonen P, Rahmat-Samii Y, Schaffrath M, Kivikoski M. Effect of textile materials on wearable antenna performance: a case study of GPS antennas. IEEE International Symp. Antennas and Propagation Society, USA, pp. 459– 462, 2004.

Sánchez-Montero R, Alén-Cordero C, López-Espí PL, Rigelsford JM, Aguilera-Benavente F, Alpuente-Hermosilla J. Long term variations measurement of electromagnetic field exposures in Alcalá de Henares (Spain). Science of the Total Environment, vol. 598, pp. 657–668, 2017.

Scanlon WG. Analysis of tissue-coupled antennas for UHF intra-body communications. International Conference on Antennas and Propagation, ICAP, 2003.

Schmid G, Preiner P, Lager D, Uberbacher R, Georg R. Exposure of the general public due to wireless LAN applications in public places. Radiat Prot Dosimet 124:48Y52; 2007.

Seyfi L. Measurement of electromagnetic radiation with respect to the hours and days of a week at 100kHz–3GHz frequency band in a Turkish dwelling. Measurement vol. 46, pp. 3002–3009, 2013.

Sheltami T, Mahmoud A, Abu-amara M. Warning and monitoring medical system using sensor networks. National Computer Conf., pp. 63–68, 2006.

Sibille A. Statistical modeling of the radio-electric properties of wireless terminals in their environment. IEEE Antennas and Propagation Magazine, vol. 54, nº 6, pp. 117-129, 2012.

Singh W, Shukla A, Deb S, Majumdar A. Energy efficient acquisition and reconstruction of EEG signals. IEEE Annual International Conference of the Engineering in Medicine and Biology Society, USA, 2014.

Smith GS, King RWP. Antennas in matter: Fundamental, theory and applications, MIT Press, 1981.

Soh PJ, Vandenbosch GAE, Wee FH, van den Bosch A, Martínez- Vázquez M, Schreurs D. Specific absorption rate (SAR) evaluation of textile antennas. IEEE Antenn Propag Mag, vol. 57, pp. 229–240, 2015.

Sridhar T. Wireless LAN Switches — Functions and Deployment. Flextronics, 2006. [Online]. Available: http://www.cisco.com/web/about/ac123/ac147/archived_issues/ipj_9-3/wireless_lan_switches.html Accessed on April 2018.

Takei K, Kuwahara M, Okabe H, Kishida H, Hori K, Imakado Y, Nomura T. Coaxial resonant slot antenna, a method of manufacturing thereof, and a radio terminal. US Patent 5914693, 1999.

Tomitsch J, Dechant E. Exposure to electromagnetic fields in households trends from 2006 to 2012, Bioelectromagnetics, vol. 36, pp. 77-85, 2015.

Trinchero D, Fiorelli B, Stefanelli R, Anglesio L, Benedetto A, Trinchero S, d'Amore G, Borsero GM, Vizio G. Electromagnetic field measurement in presence of radiofrequency wideband digital signals. Proc. URSI Gen. Assem, Chicago, pp. 7–16, 2008.

Troisi F, Boumis M, Grazioso P. The Italian national electromagnetic field monitoring network. Ann. Telecommun. vol. 63, pp. 97–108, 2008.

Ullah S, Khan P, Ullah N, Saleem S, Higgins H, Kwak K. A review of wireless body area networks for medical applications. Int. J. Communications, Network and System Sciences, vol. 2, pp. 797-803, 2009.

Usui H, Takahashi M, Ito K. Radiation characteristics of an implanted cavity slot antenna into the human body. IEEE Antennas and Propagation Society International Symposium, USA, 2006.

Vallejo M, Recas J, García del Valle P, Ayala JL. Accurate Human Tissue Characterization for Energy-Efficient Wireless On-Body Communications. Sensors, vol. 13 pp. 7546–7569, 2013.

Varnoosfaderani MV, Thiel DV, Lu J. A wideband slot antenna in a box for wearable sensor nodes. IEEE Antennas and Wireless Propagation Letters, vol. 14, pp. 1494-1497, 2015b.

Varnoosfaderani MV, Thiel DV, Lu J. External Parasitic Elements on Clothing for Improved Performance of Wearable Antennas. IEEE Sensors J. vol. 15, n.1, pp. 307-316, 2015a.

Verloock L, Joseph W, Goeminne F, Martens L, Verlaek M, Constandt K. Temporal 24-hour assessment of radio frequency exposure in schools and homes. Measurement, vol. 56, pp. 50–57, 2014.

Verloock L, Joseph W, Vermeeren G, Martens L. Procedure for assessment of general public exposure from WLAN in offices and in wireless sensor network testbed. Health Phys., vol. 98, no. 4, pp. 628-638, 2010.

Vermeeren G, Markakis I, Goeminne F, Samaras T, Martens L, Joseph W. Spatial and temporal RF electromagnetic field exposure of children and adults in indoor micro environments in Belgium and Greece. Progress in Biophysics and Molecular Biology 113 vol. 2 pp. 254-263, 2013.

Vitas I, Zrno D, Šimunić D, Prasad R. Innovative RF localization for wireless video capsule endoscopy. IEEE Proceedings of the 2014 ITU Kaleidoscope Academic Conference, 2014.

Wac K, Bargh MS, van Beijnum BF, Bults RGA, Pawar P, Peddemors A. Power- and Delay-Awareness of Health Telemonitoring Services: The MobiHealth

System Case Study. IEEE journal on selected areas in communications, vol. 27, Nº 4, 2009.

Wavecontrol. [Online]. Available: http://www.wavecontrol-rfsafety.com/ Accessed on April 2018.

Wold Health Organization (WHO). The international EMF project. [Online]. Available: http://www.who.int/peh-emf/en/ (Updated 2016) Accessed on April 2018.

World Health Organization (WHO). Child Growth Standards [Online]. Available: http://www.who.int/ childgrowth/standards/en/ Accessed on March 2018.

World Health Organization (WHO). Framework for developing health-based EMF standards. 2006.

World Health Organization (WHO). Global Health Observatory data repository. [Online]. Available: http://apps.who.int/gho/data/node.main.EMF?lang=en (Updated 2017) Accessed on April 2018.

World Health Organization (WHO). Research agenda for radiofrequency fields. 2010.

Wu TT, King RWP. Lateral waves: A new formula and interference patterns. Radio Science, vol. 17, no. 3, pp. 521-531, 1982.

Xia W, Saito K, Takahashi M, Ito K. Performances of an Implanted Cavity Slot Antenna Embedded in the Human Arm. IEEE Transactions on Antennas and Propagation, vol. 57, n. 4, pp. 894-899, 2009.

Yang GZ. Body Sensor Networks. Springer, 2010.

Yang WB and Sayrafian-Pour K. Interference mitigation for body area networks. IEEE Int. Symp. on Personal Indoor and Mobile Radio Communications, pp. 2193–2197, 2011.

Ye Y, Khan U, Alsindi N, Fu R, Pahlavan K. On the accuracy of RF positioning in multi-Capsule endoscopy. IEEE International Symposium on Personal, Indoor and Mobile Radio Communications, 2011.

Yuan W, Wang X, Linnartz JP. A coexistence model of IEEE 802.15.4 and IEEE 802.11b/g. IEEE Symp. Commun. and Veh. Technol., pp. 1–5, 2007.

Zhao Y, Li S, Davidson A, Yang B, Wang Q, Lin Q. A MEMS viscometric sensor for continuous glucose monitoring. Journal of Micromechanics and Microengineering. vol. 17, pp. 2528–2537, 2007.

Zhu SZ, Langley R. Dual-band wearable textile antenna on an EBG substrate. IEEE Trans. Antennas Propag., vol. 57, n. 4, pp. 926–935, 2009.

Glossary

BMI	Body Mass Index
BSA	Body Surface Area
CDF	Cumulative Distribution Function
CENELEC	European Committee for Electrotechnical Standardization
DMC	Diffuse Multipath Components
EMF	Electromagnetic Field
f_c	Center Frequency
FDTD	Finite-Difference Time-Domain
IARC	International Agency for Research on Cancer
ICNIRP	International Commission on Non-Ionizing Radiation Protection
IEC	International Electrotechnical Commission
IEEE	Institute of Electrical and Electronic Engineers
ITU	International Telecommunication Union
LOS	Line of Sight
NLOS	No Line of Sight
RF	Radiofrequency
RMS	Root Mean Square
RWB	Resolution Bandwidth
S	Power Density
SAR	Specific Absorption Rate

SAR_{WB}	Whole Body Specific Absorption Rate
SD	Standard Deviation
SWP	Sweep Points
SWT	Sweep Time
VBW	Video Bandwidth
WBAN	Wireless Body Area Networks
WGN	Gaussian noise
WHO	World Health Organization
WLAN	Wireless Local Area Network